

EXCITATION OF BARYONIC RESONANCES
INDUCED BY NUCLEONS AND LEPTONS

Luis Alvarez Ruso
Departamento de Física Teórica
Universidad de Valencia
1999

Universidad de Valencia
Departamento de Física Teórica



Excitation of baryonic resonances induced by nucleons and leptons

PH. D. THESIS

LUIS ALVAREZ RUSO

1999

Universidad de Valencia
Departamento de Física Teórica



**Excitación de resonancias
bariónicas inducida por
nucleones y leptones**

TESIS DOCTORAL

LUIS ALVAREZ RUSO

1999

Eulogio Oset Báguena, Catedrático del Departamento de Física Teórica de la Universidad de Valencia y **Manuel J. Vicente Vacas**, Profesor Titular del Departamento de Física Teórica de la Universidad de Valencia,

CERTIFICAN: Que la presente Memoria “Excitación de resonancias bariónicas inducida por nucleones y leptones” ha sido realizada bajo su dirección en el Departamento de Física Teórica de la Universidad de Valencia, por **Luis Alvarez Russo** y constituye su Tesis para optar al grado de Doctor en Física.

Y para que así conste, en cumplimiento de la legislación vigente, presentan ante la Facultad de Física Teórica de la Universidad de Valencia la referida Tesis.

Valencia, a 27 de julio de 1999

Fdo: Eulogio Oset Báguena

Manuel J. Vicente Vacas

Ἐν οἴδα, ὅτι οὐδέν οἴδα.

$\Sigma\omega\kappa\rho\acute{\alpha}\tau\eta\varsigma$

Contents

Prefacio	1
Preface	5
I Two-pion production in nucleon-nucleon collisions	9
1 The NN \rightarrow NN$\pi\pi$ reaction	11
1.1 Introduction	11
1.2 Isospin analysis	12
1.3 Experimental status	14
1.4 The cross section	16
1.5 The model	18
1.5.1 Low energy effective Lagrangian	18
1.5.2 Delta resonance terms	23
1.5.3 Roper resonance terms	25
1.5.4 Isovector one boson exchange potential and short range correlations	29
1.5.5 Isoscalar excitation of the Roper resonance	32
1.6 Results and discussion	33
1.6.1 Total cross sections	33
1.6.2 Differential cross sections	40
1.7 Summary	45
2 Final state interaction in pp \rightarrow pp$\pi^+\pi^-$	49
2.1 Introduction	49
2.2 The production amplitude	50
2.3 Nucleon-nucleon 1S_0 wave function from a separable potential	52
2.4 Results and discussion	55
2.5 Summary	58
3 The np \rightarrow d($\pi\pi$)0 reaction	59
3.1 Introduction	59
3.2 The model	61

3.3	Results and discussion	63
3.4	Summary	71
II	Charge changing weak production of the Δ resonance	73
4	Charged current weak electroproduction of Δ resonance	77
4.1	Introduction	77
4.2	Transition currents and cross sections	78
4.2.1	$e^- p \rightarrow \Delta^0 \nu_e$ and $e^+ p \rightarrow \Delta^{++} \bar{\nu}_e$	78
4.2.2	$N - \Delta$ transition form factors	79
4.2.3	$e^- p \rightarrow N^* \nu_e$	82
4.2.4	$N - N^*$ transition form factors	83
4.3	Numerical results	85
4.3.1	$e^- p \rightarrow \Delta^0 \nu_e$	85
4.3.2	$e^+ p \rightarrow \Delta^{++} \bar{\nu}_e$	85
4.3.3	$e^- p \rightarrow N^* \nu_e$	87
4.3.4	Experimental considerations	89
4.4	Summary	91
5	$\nu d \rightarrow \mu^- \Delta^{++} n$ reaction and axial vector $N - \Delta$ coupling	93
5.1	Introduction	93
5.2	Differential cross section	94
5.2.1	Differential cross section for $\nu d \rightarrow \mu^- \Delta^{++} n$	94
5.2.2	Effect of the width of Δ resonance	97
5.3	Axial vector $N - \Delta$ coupling	98
5.3.1	Neutrino scattering experiments	98
5.3.2	Electron scattering experiments	101
5.3.3	Pion photoproduction and electroproduction experiments	102
5.4	Summary	103
6	Conclusions and outlook	105
III	Appendices	109
A	Monte Carlo Quadrature	111
B	Non-relativistic baryon propagators	113
C	Amplitudes for the $pp \rightarrow pp\pi^+\pi^-$ channel	117
D	Integrals for the NN wave function	121

E Deuteron wave functions	125
F Amplitudes for np → d ($\pi\pi$)⁰	127
G Charged current neutrino-nucleon quasielastic scattering	131
Bibliography	133

Prefacio

El objetivo fundamental de la física de interacciones fuertes es la comprensión de la estructura de los hadrones y sus interacciones. El establecimiento de QCD como la teoría fundamental de las interacciones fuertes constituyó un paso decisivo en esta dirección. Dicha teoría puede ser aplicada directamente a la descripción de procesos en la región de altas energías con la ayuda de métodos perturbativos. La situación es distinta a energías bajas e intermedias, donde nuestra incapacidad para resolver QCD en el régimen no perturbativo impide que podamos derivar las propiedades de los hadrones a partir de principios básicos. A bajas energías, la teoría quiral de perturbaciones proporciona un marco teórico que permite un estudio sistemático de las consecuencias de algunas de las simetrías de QCD. Esta línea de trabajo ha sido bastante exitosa en el sector de los bosones de Goldstone (π , K , η). En presencia de bariones aparecen complicaciones adicionales a causa de que la masa de los mismos es comparable con la escala de rotura de la simetría quiral y de la presencia de las resonancias bariónicas como son la $\Delta(1232)$ y la $N^*(1440)$. La contribución de los estados exitados del nucleón a los procesos de baja energía puede ser integrada y sustituida por contratérminos finitos, pero este procedimiento es cuestionable, especialmente en el caso de la Δ que se encuentra tan solo 300 MeV por encima del nucleón y que se acopla fuertemente al sistema πN . La situación es incluso más complicada cuando se tienen dos o más bariones.

A energías intermedias, las resonancias bariónicas son los auténticos protagonistas de la dinámica que gobierna las reacciones inelásticas que ocurren en nucleones y núcleos. Dichas reacciones son un instrumento ideal para profundizar en las propiedades de los estados excitados bariónicos. La riqueza del espectro de bariones constituye una clara muestra de la complejidad de las interacciones fuertes a estas energías. El modelo de quarks permite clasificar de modo sistemático estos estados a partir de los quarks constituyentes. También permite predecir de modo bastante acertado muchas de sus propiedades como son sus masas y modos de desintegración, pero el vínculo de los quarks constituyentes con los quarks y gluones de QCD ha de ser esclarecido.

En este contexto las reacciones de producción de dos piones constituyen una elección atractiva para el trabajo tanto teórico como experimental. La reacción $(\pi, \pi\pi)$ en nucleones y núcleos ha sido ampliamente estudiada. La motivación fundamental para ello está relacionada con el interés por extraer información acerca de la interacción pion-pion de un modo independiente de modelos. A pesar de que esto no ha sido conseguido de un modo satisfactorio, las reacciones $(\pi, \pi\pi)$ han probado ser una herramienta importante para el

estudio de ciertos aspectos de la dinámica de las resonancias, como son la determinación de la constante de acoplamiento del vértice $\pi\Delta\Delta$ o el estudio de los modos de descomposición de la resonancia $N^*(1440)$. Por otra parte, datos recientes obtenidos empleando diferentes blancos nucleares parecen indicar la modificación de los pares de piones de isoespin nulo en su propagación en el medio nuclear. La fotoproducción de pares de piones también ha sido extensamente estudiada. Un análisis reciente de la misma ha conseguido la descripción de las amplitudes $N^*(1520) \rightarrow \Delta\pi$ y su comparación con diferentes cálculos basados en modelos de quarks. Estos estudios han sido extendidos a la región de $q^2 \neq 0$ empleando electrones. Esta cuestión es objeto de investigación experimental en TJNAF como parte del programa de electroexcitación de resonancias.

La primera parte de esta tesis está dedicada al estudio de la producción de dos piones en la dispersión inelástica de nucleones. Este proceso comparte muchos de los atractivos de las otras reacciones de producción de dos piones pero con un nuevo y crucial ingrediente: la interacción nucleón-nucleón. En este caso, al igual que en la producción de piones o mesones más pesados, hay grandes transferencias de momento involucradas, lo cuál implica que se accede a la parte de corto alcance de la interacción nucleón-nucleón.

En el primer capítulo hemos desarrollado el primer modelo microscópico de la reacción $NN \rightarrow NN\pi\pi$, pensado para describir la misma en un amplio rango de energías que va desde el umbral hasta energías cinéticas del proton incidente de unos 1.4 GeV (o sea 800 MeV por encima del umbral) y para todos los canales de isoespin posibles. Los resultados que obtenemos para las secciones eficaces totales y diferenciales son comparados con los datos experimentales disponibles. La información experimental sobre esta reacción crecerá considerablemente en el futuro próximo como resultado de las mediciones realizadas y previstas en el detector WASA de Uppsala. Para construir nuestro modelo nos hemos basado en un modelo previo de la reacción $\pi N \rightarrow \pi\pi N$. Una característica relevante de la misma es la importancia de la resonancia $N^*(1440)$ y su canal de desintegración en $N(\pi\pi)_{S-wave}^{T=0}$. Algo similar se obtiene en nuestro caso, solo que aquí tenemos que considerar la transición $NN \rightarrow NN^*$ acerca de la cuál tenemos un conocimiento limitado, que procede de un reciente análisis de la reacción (α, α') .

Un análisis realista de los resultados experimentales de producción de mesones en colisiones nucleón-nucleón cerca del umbral y que están siendo obtenidos en diferentes laboratorios es impensable si no se tiene correctamente en cuenta la interacción de estado final entre los nucleones. En muchos trabajos se ha asumido que dichos efectos se pueden tener en cuenta a base de agregar un factor que multiplica a la amplitud calculada en la aproximación de Born con ondas planas (esquema de Watson-Migdal). Sin embargo este procedimiento ha sido criticado sobre la base de que con el mismo se obtiene la dependencia correcta en energía de la sección eficaz, pero no necesariamente su tamaño adecuado. En el capítulo 2 hemos estudiado los efectos de la interacción de estado final en el caso de la producción de dos piones. Hemos considerado el canal $pp \rightarrow pp\pi^+\pi^-$ cerca del umbral, de modo que podemos asumir que la amplitud de producción está dominada por la excitación isoscalar de la resonancia Roper, seguida de su desintegración en $N(\pi\pi)_{S-wave}^{T=0}$. Otras de las ventajas que ofrece este caso particular es que la parte fuerte de la interacción de estado final está dominada por el estado 1S_0 . Para obtener la función de onda de dicho

estado hemos resuelto la ecuación de Shrödinger empleando un potencial separable. En nuestros cálculos hemos empleado la aproximación de Born de ondas distorsionadas que comparamos con la aproximación de Watson-Migdal.

En el capítulo 3 nos ocupamos del canal $np \rightarrow d\pi\pi$, que recibió una atención especial en los años 70 en conexión con el llamado efecto ABC. La anomalía ABC es un aumento en el espectro de masas invariantes cerca de los extremos del espectro. Fue observado por primera vez por Abashian, Booth y Crowe en un experimento llevado a cabo para la reacción $pd \rightarrow {}^3HeX$ con haces de protones de energías entre los 624 y los 743 MeV. Estructuras similares se encontraron en $np \rightarrow dX$ y $dd \rightarrow {}^4HeX$. Inicialmente se pensó que se trataba de una nueva partícula, pero experimentos posteriores mostraron que la masa y anchura correspondiente a los picos variaba con las condiciones cinemáticas. Más aun, hay evidencias de que el efecto ABC desaparece a bajas energías, lo que sugiere que los mecanismos involucrados tienen una fuerte dependencia en energías y ángulos. Nosotros mostramos que la estructura que muestran los espectros de la reacción $np \rightarrow d\pi\pi$ a bajas energías puede ser explicada como consecuencia de la interferencia de dos mecanismos que involucran la excitación de la resonancia Roper. A más altas energías nuestros cálculos, aunque no describen los detalles de los espectros, muestran la aparición de los picos del efecto ABC. La presente descripción revela la importancia de la resonancia Roper para la fenomenología de esta reacción y está llamada a tener repercusiones en los análisis de otras reacciones como $dd \rightarrow {}^4He\pi\pi$ y $pd \rightarrow {}^3He\pi\pi$ que están siendo estudiadas cerca del umbral en varios laboratorios.

Como hemos mencionado anteriormente, los estados excitados del nucleón pueden ser estudiados a partir de la interacción fuerte, con haces de nucleones y piones, de la interacción electromagnética, con fotones y electrones y también a partir de la interacción débil, con haces de electrones y neutrinos. La segunda parte de la presente memoria está dedicada a la física de la transición $N - \Delta$ inducida por reacciones débiles de cambio de carga. El estudio de la Δ presenta claras ventajas al estar claramente aislada del resto de resonancias que aparecen a más altas energías, así como por el hecho de que el canal πN de desintegración es claramente dominante, lo cuál facilita su identificación.

La mayor parte de la información de que disponemos acerca de los factores de forma débiles de la transición $N - \Delta$ provienen del análisis de los experimentos llevados a cabo en los laboratorios de Argonne, Brookhaven y CERN con haces de neutrinos cuya distribución de energías no es bien conocida, y empleando detectores de cámaras de burbujas. Con el advenimiento de una nueva generación de aceleradores de electrones con energías del orden de los pocos GeV que permiten alcanzar altas luminosidades, es posible realizar experimentos en la región de las resonancias con buena estadística. En el capítulo 4 estudiamos las reacciones $e^-p \rightarrow \Delta^0\nu_e$ y $e^+p \rightarrow \Delta^{++}\bar{\nu}_e$, para explorar la posibilidad de emplearlas para obtener información acerca de los factores de forma débiles que pueda ser contrastada con las predicciones teóricas existentes.

Habida cuenta de que los factores de forma vectoriales están relacionados con los electromagnéticos, que pueden ser obtenidos a partir de los experimentos de fotoproducción y electroproducción, los experimentos con corrientes débiles permitirían obtener información acerca de los factores de forma axiales para la transición $N - \Delta$. Entre ellos, el domi-

nante es $C_5^A(q^2)$. La determinación de su valor a $q^2 = 0$ es importante porque el valor de $C_5^A(0)$ que se obtiene utilizando la hipótesis de la conservación parcial de la corriente axial (PCAC) es un 30 % mayor que el estimado en la mayoría de los modelos de quarks. Algo similar ocurre en el sector electromagnético donde las amplitudes de transición dipolar magnética y electrica, M_{1+} y E_{1+} respectivamente, que se obtienen en los experimentos de fotoproducción y electroproducción de la Δ son un 30 % mayores que las que predicen los cálculos teóricos. Dicha discrepancia podría ser una manifestación de la violación de la simetría $SU(6)$. En el capítulo 5 estudiamos la reacción $\nu d \rightarrow \mu^- \Delta^{++} n$ para extraer $C_5^A(0)$ de los datos a bajos q^2 obtenido en el BNL, prestando especial atención a los efectos de la estructura del deuterón y de la anchura de la resonancia Δ .

Preface

The ultimate goal of strong interaction physics is to explain the structure and interaction of hadrons. The major progress in this direction came with the establishment of QCD as the fundamental theory of the strong interaction. It can be applied directly to the description of the high energy domain using perturbative methods. The situation is different at low and intermediate energies, where our inability to solve the dynamics of QCD in the non-perturbative regime prevents us from deriving the properties of hadrons from first principles. At low energies, Chiral Perturbation Theory provides a theoretical framework that allows a systematic study of the consequences of some of the QCD symmetries. It has proven to be very successful in the sector of Goldstone bosons (π , K , η). In presence of baryons, additional complications arise due to the large baryon mass, which is comparable to the chiral symmetry breaking scale, and the presence of low lying resonances such as the $\Delta(1232)$ and the $N^*(1440)$. The contribution of nucleon excited states can be integrated out and replaced by finite counterterms, but this procedure is questionable, specially in the case of the Δ , which lies only 300 MeV above the nucleon and couples very strongly to the πN system. The situation is even more involved for processes with two or more baryons.

At intermediate energies, baryonic resonances become an essential ingredient of the underlying dynamics governing many inelastic reactions that take place in both nucleons and nuclei. These reactions are the major instrument to deepen our insight into the properties of the baryonic excited states. The richness of the baryonic spectrum is a clear expression of the complexity of hadronic interactions at these energies. The quark model provides a systematic classification of these states in terms of constituent quarks, and quite successfully predicts many of their properties such as masses and decay modes, but the relationship between these constituent quarks and the fundamental quarks and gluons of QCD must be clarified.

In this context, double-pion production reactions appear as an attractive choice for experimental and theoretical work. The $(\pi, \pi\pi)$ reaction in nucleons and nuclei has been widely studied; the main motivation for studying this reaction was related to the hope to extract model independent information about the $\pi\pi$ interaction. Although this feature has not been fully achieved, $(\pi, \pi\pi)$ has revealed as a useful tool to investigate certain aspects of resonance dynamics like the determination of the $\pi\Delta\Delta$ coupling constant or the study of $N^*(1440)$ decay modes. On the other side, recent data taken with nuclear targets seem to imply an in-medium modification of correlated isospin zero pion pairs. Double-pion

photoproduction has also been extensively studied. A recent theoretical analysis of this reaction brought along a description of the $N^*(1520) \rightarrow \Delta\pi$ amplitudes, which could be contrasted with different quark model calculations. These studies have been extended to the $q^2 \neq 0$ by considering electron probes; this a subject of current experimental research at TJNAF as a part of the program on electroexcitation of resonances.

The first part of this thesis is devoted to the study of two-pion production in nucleon-nucleon scattering. This process shares many attractive issues with the other double pion production reactions since one would again expect the low lying resonances Δ and Roper to play an important role, but there is a new crucial ingredient: the nucleon-nucleon interaction. In this case, as in the production of pions or heavier mesons, large momentum transfers are involved, which implies that the short range part of the NN interaction is acceded.

In the first chapter we develop a microscopic model for the $NN \rightarrow NN\pi\pi$ reaction based on the present phenomenological knowledge of πN and NN interactions in the elastic and inelastic energy domains. Our results for total and differential cross sections are compared with the scarce experimental data available. This information will get considerably enlarged in the near future due to the measurements close to threshold performed and planned at the WASA detector in Uppsala. Yet, any reasonable description of the near threshold data cannot avoid dealing with nucleon-nucleon final state interactions. A proper treatment of this effect would complicate considerably the model from the technical point of view. In Chapter 2 we analyze this problem for the $pp \rightarrow pp\pi^+\pi^-$ channel using a simplified version of the model and within the Distorted Wave Born Approximation. We also compare with a simple and controversial approach to account for final state interactions often used in the recent literature on meson production in NN collisions. In Chapter 3, we focus our attention on the $np \rightarrow d\pi\pi$ channel. It has deserved a great deal of attention in the past, in connection with the ABC effect, an enhancement in the $\pi\pi$ missing mass close to the edges of the spectra. Our description reveals the importance of the Roper resonance in order to understand the low energy phenomenology of this reaction. It is also bound to have repercussions in the analysis of related reactions such as $dd \rightarrow \alpha\pi\pi$ and $pd \rightarrow {}^3He\pi\pi$, which are the subject of experimental research at different facilities.

As we have mentioned, the nucleon excitation spectrum can be probed using strong interactions, with pion and nucleon beams, electromagnetic interactions i.e. with photon and electron beams, and also weak interactions with electrons or neutrino beams. The electroexcitation of resonances represents an important part of the present experimental program at TJNAF. The second part of this thesis is dedicated to the physics of $N - \Delta$ transitions induced by charge changing weak reactions. The Δ is chosen because the fact that it is well separated from the rest of resonances and decays into pion and nucleon facilitates its experimental study.

The bulk of the existing information on weak $N - \Delta$ form factors comes from the analysis of experiments performed with wide band neutrino beams, whose energy distributions are poorly known, and bubble chamber detectors. In Chapter 4 we consider the inverse reactions $e^- p \rightarrow \Delta^0 \nu_e$ and $e^+ p \rightarrow \Delta^{++} \bar{\nu}_e$ in the energy range of Mainz and TJNAF electron accelerators in order to explore the feasibility of studying them experimentally and distin-

guish between the different model predictions for the form factors. Finally, in Chapter 5 we undertake the determination of the most relevant axial vector $N - \Delta$ form factor C_5^A at $q^2 = 0$ from the available data taken at BNL neutrino experiment and contrast it with the different determinations of this magnitude available in the literature.

Part I

Two-pion production in nucleon-nucleon collisions

Chapter 1

The $NN \rightarrow NN\pi\pi$ reaction

1.1 Introduction

Pion production in nucleon-nucleon (NN) collisions is one of the sources of information on the NN interaction, and about nucleon resonance properties. Particularly, the double pion production channel might be especially enlightening in view of the interesting information obtained from the study of analogous reactions with two pions in the final state, such as $\pi N \rightarrow \pi\pi N$ and $\gamma N \rightarrow \pi\pi N$. On the other side, the study of double pion production in the collisions of nucleons and light nuclei has become an active field of experimental research: the $pN \rightarrow NN\pi\pi$ and $pd \rightarrow {}^3He\pi^+\pi^-$ reactions close to threshold are being investigated at the CELSIUS storage ring in Uppsala [1, 2], while for the later one, interesting results have already been obtained for an incident proton energy of 546 MeV by the MOMO collaboration at COSY [3].

We have developed the first microscopic model for the $NN \rightarrow NN\pi\pi$ reaction [4]; it is meant to work at a wide range of energies, from threshold up a kinetic energy of 1.4 GeV for the incoming proton (i.e. 800 MeV above threshold) and for all isospin channels. A direct comparison of our theoretical results with the measured total cross sections and invariant-mass distributions will certainly provide useful information about the mechanisms governing this process. Our model can also provide relevant information towards a better understanding of the so called ABC effect; this will be discussed in detail in Chapter 3. There are also repercussions for the reaction $pp \rightarrow pp\pi^0$, since a possibly relevant mechanism for it can be obtained from $pp \rightarrow pp\pi^0\pi^0$ when one of the π^0 is emitted and the other is absorbed [5].

In order to build the model, we have closely followed the guidelines of a previous model for the $\pi N \rightarrow \pi\pi N$ reaction [6]. A prominent feature of this reaction at threshold is the importance of the N^* (1440) and its decay channel into $N(\pi\pi)_{S-wave}^{T=0}$. This gives us a hint that Roper excitation might also play an important role in the $NN \rightarrow NN\pi\pi$ reaction close to threshold. However, contrary to the case of N^* excitation from πN and γN interactions, which is well known, now we have to deal with the practically unexplored $NN \rightarrow NN^*$ transition.

In Ref. [7], double-pion production in pp collisions was studied following a different approach based on the One Pion Exchange model, and including two mechanisms: one with both pions produced from the same baryon line and another with a single pion produced in each baryon line. The ingredients needed there, $\pi N \rightarrow \pi\pi N$ and $\pi N \rightarrow \pi N$ amplitudes, were taken from experimental cross sections, making several assumptions on how to extrapolate them off shell and summing incoherently the contribution of the two mechanisms. The model was used at higher energies ($T_p \sim 2 - 3$ GeV) than those explored here. Even if phenomenologically one would be considering in Ref. [7] the terms discussed here with explicit models, it would only account for the π exchange in the terms with N^* excitation followed by the $N^* \rightarrow N(\pi\pi)_{S-wave}^{T=0}$ or $N^* \rightarrow \Delta\pi$ decays, while we will show that an isoscalar exchange is the dominant piece in the $NN \rightarrow NN^*$ transition at low energies. It will also be demonstrated that the indirect effect of the short range repulsive NN force weakens the π exchange contribution. Thus, the experience gathered through the years on the NN interaction and the pion nucleon and nuclear interaction, together with the recent findings on isoscalar Roper excitation, makes possible to achieve the detailed model of the present work, clarifying and improving the ideas contained in Ref. [7].

1.2 Isospin analysis

There are eight possible pion pair production reactions, which can occur in the collision of protons with nucleons. They are

$$pp \rightarrow pp\pi^+\pi^- \quad (1.1)$$

$$pp \rightarrow pn\pi^+\pi^0 \quad (1.2)$$

$$pp \rightarrow pp\pi^0\pi^0 \quad (1.3)$$

$$pp \rightarrow nn\pi^+\pi^+ \quad (1.4)$$

$$pn \rightarrow pn\pi^+\pi^- \quad (1.5)$$

$$pn \rightarrow pp\pi^-\pi^0 \quad (1.6)$$

$$pn \rightarrow pn\pi^0\pi^0 \quad (1.7)$$

$$pn \rightarrow nn\pi^+\pi^0 \quad (1.8)$$

In Ref. [8] a systematic isospin analysis of meson pair production in nucleon-nucleon collisions is performed. The amplitudes of these reactions can be decomposed into isospin amplitudes corresponding to the isospin states of the system, classified by the total isospin and the isospin of nucleon and pion pairs ($\pi\pi$) (NN) or pion-nucleon pairs (πN) (πN). In Ref. [8], the ($\pi\pi$) (NN) representation is used. Total cross sections for the different channels can be then expressed in terms of these transition isospin matrix elements $\mathcal{A}_{TT\pi\pi NN}$.

Denoting as Φ the relative phase between the matrix elements \mathcal{A}_{101} and \mathcal{A}_{121} (there is no interference between other amplitudes), one gets

$$\sigma(pp\pi^+\pi^-) = \frac{1}{8}|\mathcal{A}_{111}|^2 + \frac{1}{6}|\mathcal{A}_{101}|^2 + \frac{1}{120}|\mathcal{A}_{121}|^2 + \sqrt{\frac{1}{180}}|\mathcal{A}_{101}||\mathcal{A}_{121}|\cos\Phi \quad (1.9)$$

$$\sigma(pn\pi^+\pi^0) = \frac{3}{40}|\mathcal{A}_{121}|^2 + \frac{1}{8}|\mathcal{A}_{111}|^2 + \frac{1}{4}|\mathcal{A}_{110}|^2 \quad (1.10)$$

$$\sigma(pp\pi^0\pi^0) = \frac{1}{12}|\mathcal{A}_{101}|^2 + \frac{1}{60}|\mathcal{A}_{121}|^2 - \sqrt{\frac{1}{180}}|\mathcal{A}_{101}||\mathcal{A}_{121}|\cos\Phi \quad (1.11)$$

$$\sigma(nn\pi^+\pi^+) = \frac{3}{20}|\mathcal{A}_{121}|^2 \quad (1.12)$$

$$\begin{aligned} \sigma(pn\pi^+\pi^-) = & \frac{1}{8}|\mathcal{A}_{110}|^2 + \frac{1}{24}|\mathcal{A}_{011}|^2 + \frac{1}{12}|\mathcal{A}_{000}|^2 + \frac{1}{12}|\mathcal{A}_{101}|^2 + \frac{1}{60}|\mathcal{A}_{121}|^2 \\ & - \sqrt{\frac{1}{180}}|\mathcal{A}_{101}||\mathcal{A}_{121}|\cos\Phi \end{aligned} \quad (1.13)$$

$$\sigma(pp\pi^-\pi^0) = \frac{3}{80}|\mathcal{A}_{121}|^2 + \frac{1}{16}|\mathcal{A}_{111}|^2 + \frac{1}{24}|\mathcal{A}_{011}|^2 \quad (1.14)$$

$$\begin{aligned} \sigma(pn\pi^0\pi^0) = & \frac{1}{24}|\mathcal{A}_{000}|^2 + \frac{1}{24}|\mathcal{A}_{101}|^2 + \frac{1}{30}|\mathcal{A}_{121}|^2 \\ & + \sqrt{\frac{1}{180}}|\mathcal{A}_{101}||\mathcal{A}_{121}|\cos\Phi \end{aligned} \quad (1.15)$$

$$\sigma(nn\pi^+\pi^0) = \frac{3}{80}|\mathcal{A}_{121}|^2 + \frac{1}{16}|\mathcal{A}_{111}|^2 + \frac{1}{24}|\mathcal{A}_{011}|^2. \quad (1.16)$$

After taking into account the obvious result $\sigma(nn\pi^+\pi^0) = \sigma(pp\pi^-\pi^0)$, one can see that the remaining seven equations are not independent. They lead to the the following identity

$$\begin{aligned} 2\sigma(pp\pi^+\pi^-) - & \sigma(pn\pi^+\pi^0) - 4\sigma(pp\pi^0\pi^0) + 2\sigma(nn\pi^+\pi^+) \\ & + 2\sigma(pn\pi^+\pi^-) - 2\sigma(pp\pi^-\pi^0) - 4\sigma(pn\pi^0\pi^0) \equiv 0. \end{aligned} \quad (1.17)$$

In other words, the eight possible reactions lead to six independent total cross sections.

1.3 Experimental status

In the past, there has been little experimental work devoted to the study of double pion production in nucleon-nucleon collisions at intermediate energies (we restrict ourselves to kinetic energies of the incoming nucleon in the Laboratory frame (LA) $T_p \leq 1.4$ GeV). In spite of this, we have at our disposal 37 data points of total cross sections for different channels and a few invariant mass and angular distributions, all taken from four experimental papers, which we comment briefly below.

D. C. Brunt, M. J. Clayton and B. A. Westwood [9] extracted the total cross sections for the reactions (1.1), (1.5) and (1.6) at incident proton momenta 1.825 GeV/c ($T_p = 1.11$ GeV) and 2.11 GeV/c ($T_p = 1.37$ GeV) from an experiment with a proton beam and a 80 cm bubble chamber filled with deuterium. The total cross sections on free nucleons are obtained after the application of corrections due to the structure of the deuteron target, namely, double scattering. Because of the Fermi momentum of the nucleons inside the deuteron, they represent an average over a center-of-mass (CM) energy distribution with full width 90 MeV, centered on the nominal value obtained from the beam momentum. The paper also provides some angular and invariant mass distributions for the reactions (1.1) and (1.5) at the highest energy, excluding the events with spectator momentum bigger than 150 MeV/c for neutrons and 200 MeV/c for protons. The contamination from double scattering was estimated to vary between 15 and 40 %.

In Ref. [10], the authors undertook the task of providing data on elastic and all the inelastic proton-proton cross sections in the region between the single pion production threshold and $T_p \sim 1$ GeV, which was misrepresented in the literature. Their work is based on the exposure of the KEK 1 m liquid hydrogen bubble chamber to proton beams with 11 momenta in the range 0.9 – 2.0 GeV/c (0.36-1.25 GeV). Double pion production total cross sections were measured for reactions (1.1), (1.2), (1.3) and (1.4) at 6, 5, 4 and 3 different momenta respectively. The events corresponding to the first of these reactions were identified by four-prong events and the others by two-prong ones. If an event whose secondary tracks appeared to be proton and π^+ , and its missing mass was greater than the sum of neutron and π^0 masses, then it was identified as reaction (1.2). If both tracks appeared to be positive pions, and the missing mass was greater than twice the neutron mass, the event was identified as (1.4). If both tracks appeared to be protons and the missing mass was greater than twice the π^0 mass, it was identified as reaction (1.3). These events could be contaminated by three pion production reactions at $T_p > 934$ MeV, but this contamination is expected to be negligible since no $pp\pi^+\pi^-\pi^0$ event was found in the experiment.

The work of L. G. Dakhno et al. [8], which was mentioned above in connection to the isospin classification, is devoted to the measurement of total cross sections for the pion pair production reactions (1.1), (1.5) and (1.6), as well as $pd \rightarrow pd\pi^+\pi^-$ at five energies between 0.7 and 1.0 GeV. The experiment was performed in a 35 cm bubble chamber filled with deuterium and exposed to a proton beam. All three and four-prong events with one negative track were recorded. These events could be initiated by the following reactions: $pd \rightarrow ppp\pi^-$, $\rightarrow pd\pi^+\pi^-$, $\rightarrow ppn\pi^+\pi^-$ and $\rightarrow ppp\pi^-\pi^0$. The three-prong events corre-

sponded to the cases when one of the protons had a momentum less than 80 MeV/c and, therefore, was not visible in the bubble chamber. In the framework of the impulse approximation, when one of the nucleons is assumed to be a spectator, the events of $pd \rightarrow ppn\pi^+\pi^-$ represent the sum of reactions (1.1) and (1.5). For the separation of these processes, the nucleon with the least momentum in the laboratory system was always assumed to be the spectator, as it was done in Ref. [9]. Corrections arising from the deuteron structure were estimated to be of the order of 5 % and, hence, neglected. The authors also claimed that the Fermi motion of the nucleons in the deuteron would lead to an unimportant shift of the incoming energy values, although such shift has been later estimated to be of the order of 30 MeV [11].

The paper of A. Abdivaliev and collaborators [12] analyses the data for the reactions $np \rightarrow d\pi^+\pi^-$ and $np \rightarrow np\pi^+\pi^-$, obtained by irradiation of a 1 m hydrogen bubble chamber with a neutron beam of momenta 1.73 and 2.23 GeV/c ($T_n = 1.03$ and 1.48 GeV). The momentum spread of the beam did not exceed 3 % and the angular spread was around 0.3 mrad. For the later reaction, pion pairs effective mass, pion 3-momentum and angular distributions are shown. These observables can be compared with our model at least for the lowest of the two energies.

Two pion production in proton-proton collisions at CELSIUS

Nowadays, double pion production in pp collisions is being studied at the CELSIUS storage ring using a hydrogen target and the WASA/PROMICE detector [1]. All possible reaction

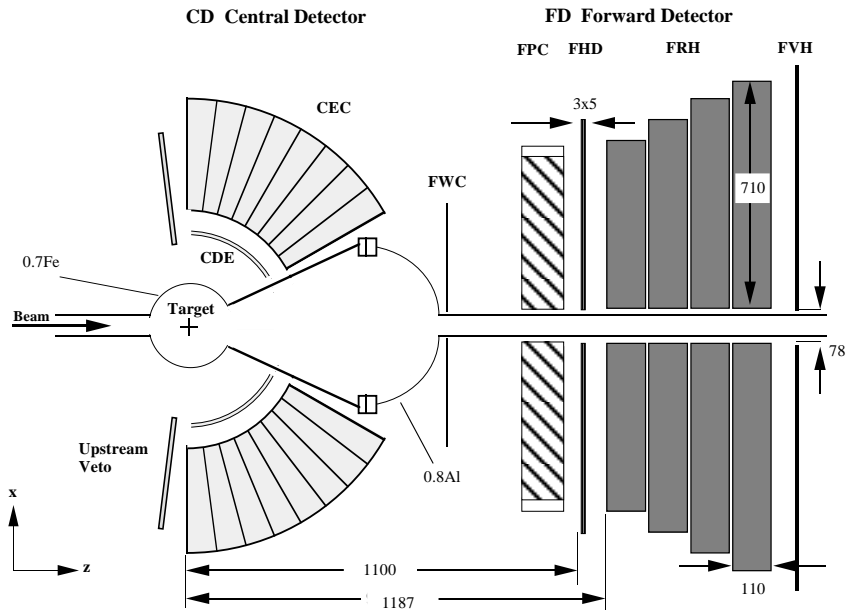


Figure 1.1: The WASA/PROMICE detector at CELSIUS, TSL, Uppsala.

channels except (1.4) have been measured simultaneously at five energies between 650 and 775 MeV. The detector is well suited to measure meson production reactions at threshold. The charged particles are detected in the forward part of the detector (FD), which is a segmented plastic scintillation calorimeter covering the angular range $4^\circ - 21^\circ$. Since this setup does not contain a magnetic field, the delayed pulses from the decays $\pi^+ \rightarrow \mu^+ \nu_\mu$ and $\mu^+ \rightarrow e^+ \nu_e \bar{\nu}_\mu$ have been used for π^+/π^- identification, with an efficiency of about 60 % [1, 13]. Neutral pions can be identified through their decay into two photons that are detected in coincidence in the Central Electromagnetic Calorimeter (CEC). The data is currently under analysis and total cross sections will be obtained. Provided that the kinematics of every event is fully reconstructed, the study of various distributions will be possible if the statistics is good enough.

1.4 The cross section

Let us consider the process $N(p_1)N(p_2) \rightarrow N(p_3)N(p_4)\pi(p_5)\pi(p_6)$ with $p_i = (E_i, \mathbf{p}_i)$, ($i = 1 - 4$) the four-momenta of the particles. The differential cross section can be written as [14]

$$d\sigma = \frac{1}{S} \frac{1}{(2\pi)^8} \frac{(2M)^4}{4E_1 E_2 v_{rel}} \prod_{i=3}^6 \frac{d\mathbf{p}_i}{2E_i} \overline{\sum} |\mathcal{M}|^2 \delta^{(4)}(p_3 + p_4 + p_5 + p_6 - p_1 - p_2), \quad (1.18)$$

where M is the nucleon mass and

$$E_1 E_2 v_{rel} = [(p_1 p_2)^2 - M^4]^{1/2} = 2(2MT + T^2)^{1/2} (M + T); \quad (1.19)$$

$\overline{\sum} |\mathcal{M}|^2$ stands for the amplitude squared, summed and averaged over the final and initial polarization states respectively. T is the kinetic energy of the incoming nucleon in LA. Finally, S is the symmetry factor

$$S = \prod_l k_l! \quad (1.20)$$

for k_l identical particles of species l in the final state. In our case, S can be 1, 2 or 4 depending on the isospin channel.

From the previous expression, all possible distributions can be obtained. Here I will derive explicitly a formula for the total cross section. Choosing the center-of-mass frame and integrating over \mathbf{p}_5 one obtains

$$\begin{aligned} \sigma(T) = & \frac{1}{S} \frac{1}{2^3} \frac{1}{(2\pi)^8} \frac{M^4}{(2MT + T^2)^{1/2} (M + T)} \times \\ & \int \frac{d\mathbf{p}_3 d\mathbf{p}_4 d\mathbf{p}_6}{E_3 E_4 E_5 E_6} \delta(2E_0 - E_3 - E_4 - E_5 - E_6) \overline{\sum} |\mathcal{M}|^2, \end{aligned} \quad (1.21)$$

where $E_5 = [m_\pi^2 + (\mathbf{p}_3 + \mathbf{p}_4 + \mathbf{p}_6)^2]^{1/2}$ with m_π the pion mass; E_0 is the energy of each of the initial nucleons in CM. In order to integrate out the remaining δ -function, let us perform the rotation $\mathbf{p}_6^R = \hat{\mathcal{R}}\mathbf{p}_6$, where $\hat{\mathcal{R}}$ is chosen in such a way that the vector $\hat{\mathcal{R}}(\mathbf{p}_3 + \mathbf{p}_4)$ is directed along the z direction, which is identified with the direction of the incoming beam in LA. Then,

$$\int \frac{d\mathbf{p}_6}{E_5 E_6} \delta(\dots) \overline{\sum} |\mathcal{M}|^2 = \int \frac{d\mathbf{p}_6^R}{E_5 E_6} \delta(2E_0 - E_3 - E_4 - E_5 - E_6) \overline{\sum} |\mathcal{M}|^2(\hat{\mathcal{R}}^{-1}\mathbf{p}_6^R) \quad (1.22)$$

with

$$\begin{aligned} E_5 &= \left[m_\pi^2 + \left(\mathbf{p}_3 + \mathbf{p}_4 + \hat{\mathcal{R}}^{-1}\mathbf{p}_6^R \right)^2 \right]^{1/2} \\ &= \left[m_\pi^2 + \left(\hat{\mathcal{R}}(\mathbf{p}_3 + \mathbf{p}_4) + \mathbf{p}_6^R \right)^2 \right]^{1/2} \\ &= [E_6^2 + (\mathbf{p}_3 + \mathbf{p}_4)^2 + 2|\mathbf{p}_3 + \mathbf{p}_4||\mathbf{p}_6| \cos \theta_6^R]^{1/2}. \end{aligned} \quad (1.23)$$

In these variables, the integration over $\cos \theta_6^R$ can be easily performed leading, after some algebraic manipulation, to our final expression for the total cross section

$$\begin{aligned} \sigma(T) = & \frac{1}{S} \frac{1}{2^3} \frac{1}{(2\pi)^8} \frac{M^4}{(2MT + T^2)^{1/2} (M + T)} \int dE_3 d\Omega_3 dE_4 d\Omega_4 dE_6 d\varphi_6^R \times \\ & \left. \frac{|\mathbf{p}_3| |\mathbf{p}_4|}{|\mathbf{p}_3 + \mathbf{p}_4|} \Theta(1 - |\cos \theta_6^0|) \overline{\sum} |\mathcal{M}|^2(\hat{\mathcal{R}}^{-1}\mathbf{p}_6^R) \right|_{\cos \theta_6^R = \cos \theta_6^0}. \end{aligned} \quad (1.24)$$

where

$$\cos \theta_6^0 = \frac{(2E_0 - E_3 - E_4 - E_6)^2 - E_6^2 - (\mathbf{p}_3 + \mathbf{p}_4)^2}{2|\mathbf{p}_3 + \mathbf{p}_4||\mathbf{p}_6|}. \quad (1.25)$$

The step function $\Theta(x)$ guarantees that $\cos \theta_6^0$ is always between -1 and 1. The rotation $\hat{\mathcal{R}}^{-1}$ is not unique; a possible choice for it is

$$\hat{\mathcal{R}}^{-1} = \begin{pmatrix} \cos \theta \cos \varphi & -\sin \varphi & \sin \theta \cos \varphi \\ \cos \theta \sin \varphi & \cos \varphi & \sin \theta \sin \varphi \\ -\sin \theta & 0 & \cos \theta \end{pmatrix} \quad (1.26)$$

with

$$\begin{aligned}\cos \theta &= \frac{(\mathbf{p}_3 + \mathbf{p}_4)_3}{|\mathbf{p}_3 + \mathbf{p}_4|} & \sin \theta &= \sqrt{1 - \cos^2 \theta} \\ \cos \varphi &= \frac{(\mathbf{p}_3 + \mathbf{p}_4)_1}{\sin \theta |\mathbf{p}_3 + \mathbf{p}_4|} & \sin \varphi &= \frac{(\mathbf{p}_3 + \mathbf{p}_4)_2}{\sin \theta |\mathbf{p}_3 + \mathbf{p}_4|}.\end{aligned}\tag{1.27}$$

The eight-dimensional integral of Eq. (1.24) can be most efficiently evaluated using the Monte Carlo method. Another advantage of the Monte Carlo integration is that all needed differential cross section can be obtained at the same time; further details about the integration procedure can be found in Appendix A.

1.5 The model

The complete set of Feynman diagrams of the present model is shown in Fig. 1.2. It includes the contribution from the effective pion-nucleon Lagrangian at its lowest order, as well as the explicit excitation of $N^*(1440)$ and $\Delta(1232)$ resonances. Below, I describe in detail all the ingredients needed for our calculation.

1.5.1 Low energy effective Lagrangian

The amplitudes (1), (2) and (3) of Fig. 1.2 can be derived from the low energy effective field theory for strong interactions, with the inclusion of baryons [15, 16, 17]. Here we restrict ourselves to the non-strange sector. To leading order $\mathcal{O}(q)$ in an expansion in external momenta and meson (quark) masses, the effective SU(2) Lagrangian is the following

$$\mathcal{L} = \mathcal{L}_{\pi\pi}^{(2)} + \mathcal{L}_{\pi N}^{(1)},\tag{1.28}$$

where $\mathcal{L}_{\pi\pi}^{(2)}$ describes $\pi - \pi$ interactions and $\mathcal{L}_{\pi N}^{(1)}$ the interactions of one nucleon with one or more pions

$$\mathcal{L}_{\pi\pi}^{(2)} = \frac{f^2}{4} \langle \partial_\mu U^\dagger \partial^\mu U + \chi(U + U^\dagger) \rangle\tag{1.29}$$

$$\mathcal{L}_{\pi N}^{(1)} = \bar{\Psi} (i\gamma^\mu \mathcal{D}_\mu - M + \frac{g_A}{2} \gamma^\mu \gamma_5 u_\mu) \Psi.\tag{1.30}$$

Here, U is a 2×2 unitary matrix that gives a convenient parameterization of the pion field

$$U(\Phi) = u(\Phi)^2 = \exp \left\{ i\sqrt{2}\Phi/f \right\}\tag{1.31}$$

$$\Phi(x) \equiv \frac{1}{\sqrt{2}} \boldsymbol{\tau} \boldsymbol{\phi} = \begin{pmatrix} \frac{1}{\sqrt{2}}\pi^0 & \pi^+ \\ \pi^- & -\frac{1}{\sqrt{2}}\pi^0 \end{pmatrix},\tag{1.32}$$

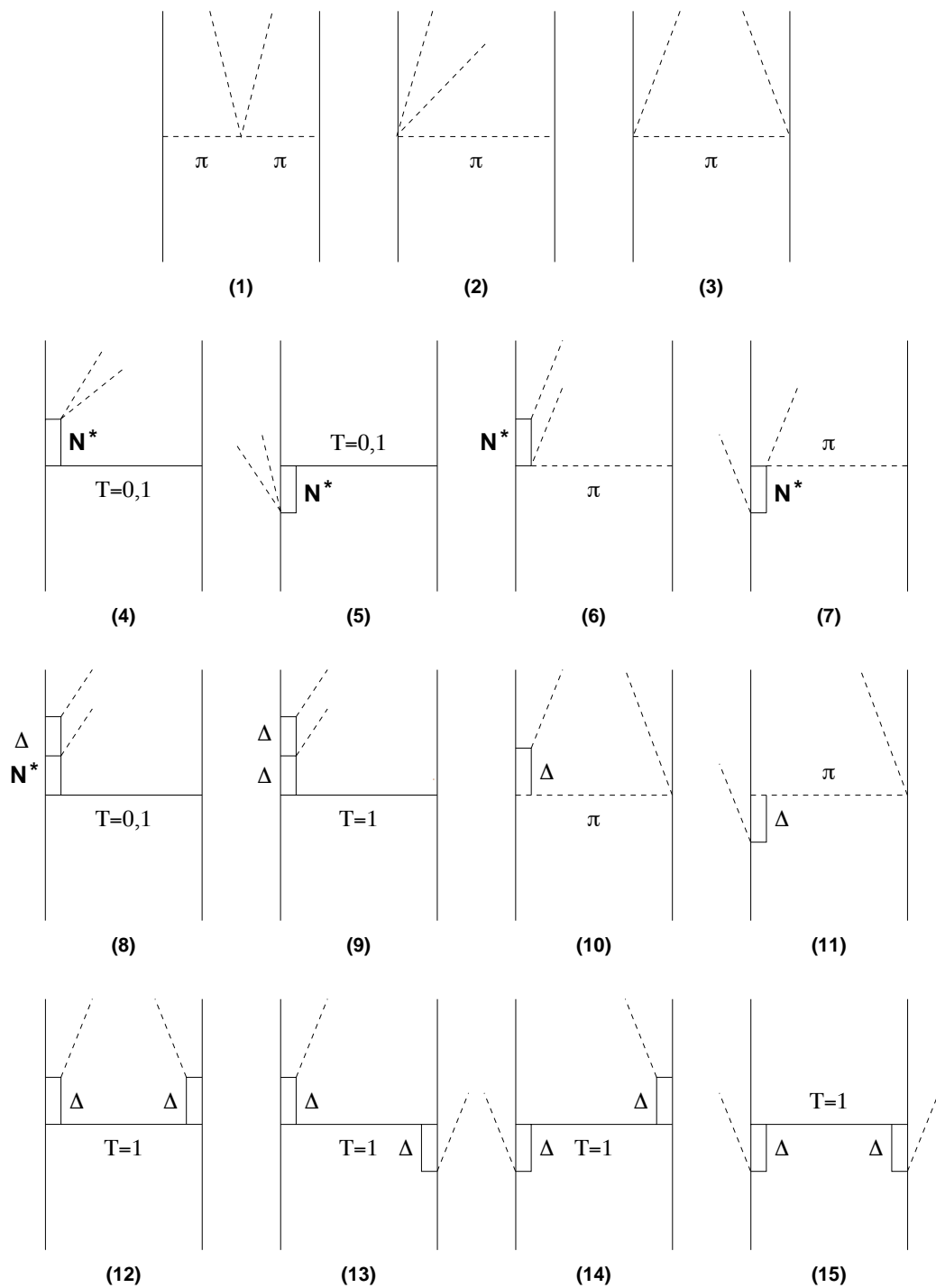


Figure 1.2: Complete set of Feynman diagrams of the model.

where τ_i are the Pauli matrices; the symbol $\langle \rangle$ denotes flavor trace. For the matrix χ , responsible for the explicit chiral symmetry breaking, in the case of isospin symmetry ($m_u = m_d = m$), one finds

$$\chi = 2B_0 \begin{pmatrix} m_u & 0 \\ 0 & m_d \end{pmatrix} = \begin{pmatrix} m_\pi^2 & 0 \\ 0 & m_\pi^2 \end{pmatrix}, \quad (1.33)$$

where B_0 is related to the quark condensate

$$B_0 f^2 = \langle 0 | \bar{q}q | 0 \rangle. \quad (1.34)$$

The proton and neutron fields are combined in an isospinor Ψ

$$\Psi = \begin{pmatrix} p \\ n \end{pmatrix}, \quad (1.35)$$

and the covariant derivative of the nucleon field in the absence of external sources is given by

$$\mathcal{D}_\mu \Psi = \partial_\mu \Psi + \Gamma_\mu \Psi, \quad \Gamma_\mu = \frac{1}{2} (u^\dagger \partial_\mu u + u \partial_\mu u^\dagger), \quad u_\mu = iu^\dagger \partial_\mu U u^\dagger. \quad (1.36)$$

Finally, in the quiral limit (i.e. $m \rightarrow 0$), f can be identified with the pion decay constant, which is determined experimentally from the charged pion weak decay $\pi^+ \rightarrow \mu^+ + \nu_\mu$ [18]

$$f_\pi = f(1 + \mathcal{O}(m)) = 92.4 \text{ MeV}. \quad (1.37)$$

In the same limit, M is the nucleon mass and g_A the axial-vector strength measured in low energy neutron β decay ($g_A \approx 1.26$). It is related to the pion nucleon coupling ($f_{\pi NN}/m_\pi$) by the Goldberger-Treiman relation [19]

$$\frac{f_{\pi NN}}{m_\pi} = \frac{g_A}{2f_\pi} \quad (1.38)$$

By expanding the matrix U in powers of Φ and keeping the terms with up to four pion fields in $\mathcal{L}_{\pi\pi}^{(2)}$ and up to three in $\mathcal{L}_{\pi N}^{(1)}$ we obtain the following set of Lagrangians

$$\mathcal{L}_{\pi\pi\pi\pi} = \frac{1}{6f_\pi^2} \left[(\partial_\mu \phi \phi)^2 - \phi^2 (\partial_\mu \phi)^2 + \frac{1}{4} m_\pi^2 \phi^4 \right], \quad (1.39)$$

$$\mathcal{L}_{NN\pi} = -\frac{f_{\pi NN}}{m_\pi} \bar{\Psi} \gamma^\mu \gamma_5 \partial_\mu \phi \tau \Psi, \quad (1.40)$$

$$\mathcal{L}_{NN\pi\pi\pi} = \frac{1}{6f_\pi^2} \frac{f_{\pi NN}}{m_\pi} \bar{\Psi} \gamma^\mu \gamma_5 [(\partial_\mu \phi \tau) \phi^2 - (\phi \tau) (\partial_\mu \phi \phi)] \Psi, \quad (1.41)$$

$$\mathcal{L}_{NN\pi\pi} = -\frac{1}{4f_\pi^2} \bar{\Psi} \gamma^\mu \tau (\phi \times \partial_\mu \phi) \Psi. \quad (1.42)$$

Historically, different forms of the Lagrangians (1.39)-(1.41) have been used in the literature [15, 20]. It can be shown that they all emerge from the Lagrangians (1.29, 1.30) by choosing different representations for the pion field $U(\Phi)$. Although it has been shown explicitly for specific cases that these sets produce the same physical amplitudes for specific processes like $(\pi, 2\pi)$ [20] or Double Charge Exchange $A(\pi^\pm, \pi^\mp)B$ [21], this equivalence is a consequence of a theorem, which states that experimental observables do not depend on the representation [22]. It was also common to include in the Lagrangians a parameter ξ to describe the pattern of chiral symmetry breaking [23, 20, 24]; now we know that only $\xi = 0$ is consistent with QCD [25].

Let us now discuss whether we should include terms appearing at next order in the q expansion, i.e. $\mathcal{L}_{\pi N}^{(2)}$ [16]. The terms of the dimension two effective relativistic pion-nucleon Lagrangian relevant to our calculation are [26]

$$\begin{aligned} \mathcal{L}_{\pi N}^{(2)} = & c_1 \bar{\Psi} \Psi \langle \chi_+ \rangle + i \frac{c'_2}{4M} \bar{\Psi} \gamma_\mu \overset{\leftrightarrow}{\mathcal{D}}_\nu \Psi \langle u^\mu u^\nu \rangle - \frac{c''_2}{8M^2} \bar{\Psi} \overset{\leftrightarrow}{\mathcal{D}}_\mu \overset{\leftrightarrow}{\mathcal{D}}_\nu \Psi \langle u^\mu u^\nu \rangle \\ & + c_3 \bar{\Psi} u_\mu u^\mu \Psi + i c_4 \frac{1}{4} \bar{\Psi} \sigma_{\mu\nu} [u^\mu, u^\nu] \Psi, \end{aligned} \quad (1.43)$$

with

$$\chi_+ = u^\dagger \chi u^\dagger + u \chi^\dagger u. \quad (1.44)$$

This Lagrangian will contribute to the πN elastic scattering and thus, to the $NN\pi\pi$ vertex. In fact, expanding $\mathcal{L}_{\pi N}^{(2)}$, one gets

$$\begin{aligned} \mathcal{L}_{NN\pi\pi} = & -2 \frac{m_\pi^2}{f_\pi^2} c_1 \bar{\Psi} \phi^2 \Psi + i \frac{c'_2}{2f_\pi^2 M} \bar{\Psi} \gamma_\mu \overset{\leftrightarrow}{\partial}_\nu \Psi (\partial^\mu \phi \partial^\nu \phi) - \frac{c''_2}{4f_\pi^2 M^2} \bar{\Psi} \overset{\leftrightarrow}{\partial}_\nu \overset{\leftrightarrow}{\partial}_\mu \Psi (\partial^\mu \phi \partial^\nu \phi) \\ & + c_3 \frac{1}{f_\pi^2} \bar{\Psi} (\partial_\mu \phi)^2 \Psi - c_4 \frac{1}{2f_\pi^2} \bar{\Psi} \sigma_{\mu\nu} \tau (\partial^\mu \phi \times \partial^\nu \phi) \Psi. \end{aligned} \quad (1.45)$$

In Ref. [27] the couplings c_i ($c_2 = c'_2 + c''_2$) are determined from a best fit to different πN observables. Then, it is shown that they can be understood from resonance exchange. Assuming that c_1 is saturated completely by scalar meson exchange, the values for c_2 , c_3 and c_4 can be explained as a combination of Δ , ρ , Roper (R) and scalar meson exchange:

$$\begin{aligned} c_1 & \approx c_1^S \\ c_2 & \approx c_2^\Delta + c_2^R \\ c_3 & \approx c_3^\Delta + c_3^R + c_3^S \\ c_4 & \approx c_4^\Delta + c_4^R + c_4^\rho. \end{aligned} \quad (1.46)$$

Our model is intended to describe the data over a wide range of energies. For this reason, we include the resonances Δ , $N^*(1440)$ explicitly (we neglect the contribution of the ρ)

and, therefore, do not include the c_i parameters related to these resonances, in order to avoid double counting. At this stage, we are left with c_1^S and c_3^S . If we take the values $c_1^S = -0.93 \text{ GeV}^{-1}$, $c_3^S = -1.40 \text{ GeV}^{-1}$ from the estimations of Ref. [27], we see that their contribution to the isoscalar s-wave πN scattering length is

$$a^{(+)}(S) = -\frac{1}{2\pi} \left(1 + \frac{m_\pi}{M}\right)^{-1} \frac{m_\pi^2}{f_\pi^2} (-2c_1^S + c_3^S) = 0.024 \text{ fm}, \quad (1.47)$$

which is around five times smaller than the isovector scattering length

$$a^{(-)}(S) = \frac{1}{8\pi} \left(1 + \frac{m_\pi}{M}\right)^{-1} \frac{m_\pi}{f_\pi^2} = 0.113 \text{ fm} \quad (1.48)$$

arising from the Lagrangian of Eq. (1.42) (and in good agreement with the experimental value $a_{exp}^{(-)} = 0.129 \pm 0.003 \text{ fm}$ [28]). Since, as will be shown, the contribution of the diagram (3) of Fig. 1.2, calculated with $\mathcal{L}_{NN\pi\pi}$, is very small, it makes sense to neglect the amplitude coming from the even smaller isoscalar $NN\pi\pi$ vertex. The conclusion of this discussion is that we will drop the terms of order $\mathcal{O}(q^2)$ from the calculation.

Our next step is to make a non-relativistic approximation. For this purpose, we use the results of Appendix 6(b) of Ref. [29]. The Dirac tensor matrix elements are given as

$$\bar{u}(p', s') \Gamma u(p, s) = \chi_{s'}^\dagger M(p', p) \chi_s, \quad (1.49)$$

where u and χ are four-component and two-component spinors respectively, while Γ stands for a particular combination of Dirac matrices; $M(p', p)$ has values according to Table A6.1 of Ref. [29]. Neglecting terms proportional to $|\mathbf{p}|/M$, $|\mathbf{p}'|/M$, one obtains

Γ	γ_μ	$\gamma_\mu \gamma_5$
M	$(1, \mathbf{0})$	$(0, \boldsymbol{\sigma})$

and hence, the Lagrangians (1.40)-(1.42) can be rewritten as

$$\mathcal{L}_{NN\pi} = \frac{f_{NN\pi}}{m_\pi} \psi_N^\dagger \sigma_i \partial_i \boldsymbol{\phi} \boldsymbol{\tau} \psi_N, \quad (1.50)$$

$$\mathcal{L}_{NN\pi\pi\pi} = -\frac{1}{6f_\pi^2} \frac{f_{NN\pi}}{m_\pi} \psi_N^\dagger \sigma_i [(\partial_i \boldsymbol{\phi} \boldsymbol{\tau}) \boldsymbol{\phi}^2 - (\boldsymbol{\phi} \boldsymbol{\tau})(\partial_i \boldsymbol{\phi} \boldsymbol{\phi})] \psi_N, \quad (1.51)$$

$$\mathcal{L}_{NN\pi\pi} = -\frac{1}{4f_\pi^2} \psi_N^\dagger \boldsymbol{\tau} (\boldsymbol{\phi} \times \partial_0 \boldsymbol{\phi}) \psi_N. \quad (1.52)$$

With these Lagrangians, $\mathcal{L}_{\pi\pi\pi\pi}$ of Eq. (1.39) and the pion propagator, given by the standard expression for meson fields

$$D_\pi(q) = \frac{1}{q^2 - m_\pi^2}, \quad (1.53)$$

we calculate the amplitudes corresponding to diagrams (1)-(3) of Fig. 1.2. Since the vertices are off-shell one should introduce form factors. For those vertices involving pions and nucleons, we take the widely used monopole form

$$F_\pi = \frac{\Lambda_\pi^2 - m_\pi^2}{\Lambda_\pi^2 - q^2} \quad (1.54)$$

assuming the same $\Lambda = 1.2$ GeV, consistent with the Bonn model [30]. In the case of the $\pi\pi$ scattering vertex we have neglected the form factor based on the fact that its monopole cutoff has been estimated to be larger than 2 GeV [31], at least in the context of a dynamical One Boson Exchange (OBE) model of the $\pi\pi$ interaction[32]. Detailed expressions for the obtained amplitudes in the $pp \rightarrow pp\pi^+\pi^-$ channel are presented in Eqs. (C.2), (C.3) of Appendix C. We will see that, in spite of the fact that these amplitudes do not vanish at threshold, their contribution to the total cross section is very small, even at low energies, in most channels.

1.5.2 Delta resonance terms

The $\Delta(1232)$ is the most important resonance observed in the πN interacting system, driven by the strong p-wave attraction. In the spirit of the intermediate energy Δ -isobar model [33, 34], we consider the $\Delta(1232)$ as a separate baryon. It is present in diagrams (8)-(15) of Fig. 1.2, mostly coupled to πN . The relativistic effective Lagrangian for this coupling is given by [35, 36]

$$\mathcal{L}_{\Delta N\pi} = \frac{f^*}{m_\pi} \bar{\Psi}_\Delta^\mu \mathbf{T}^\dagger [g_{\mu\nu} - z\gamma_\mu\gamma_\nu] \partial_\nu \boldsymbol{\phi} \Psi_N + h.c., \quad (1.55)$$

where $\bar{\Psi}_\Delta^\mu$ is the Rarita-Schwinger field for a spin 3/2 particle and z is a parameter that characterizes the off-shell behavior of Ψ_Δ^μ . The value of z has been extensively studied [36] but is irrelevant for our purposes since the leading order non-relativistic $\Delta N\pi$ Lagrangian does not contain it and can be written as

$$\mathcal{L}_{\Delta N\pi} = \frac{f^*}{m_\pi} \psi_\Delta^\dagger S_i^\dagger (\partial_i \boldsymbol{\phi}) \mathbf{T}^\dagger \psi_N + h.c., \quad (1.56)$$

with $\psi_{\Delta(N)}^\dagger$ being two-component spinor fields; \mathbf{S}^\dagger (\mathbf{T}^\dagger) are the spin (isospin) $1/2 \rightarrow 3/2$ transition operators, defined such that their matrix elements simply become Clebsh-Gordan coefficients

$$\langle \frac{3}{2}s' | S_\lambda^\dagger | \frac{1}{2}s \rangle = (\frac{1}{2}s 1\lambda | \frac{3}{2}s') \quad (1.57)$$

and follow the closure sum

$$\sum_s S_i | \frac{3}{2}s \rangle \langle \frac{3}{2}s | S_j^\dagger = \frac{2}{3} \delta_{ij} - \frac{i}{3} \epsilon_{ijk} \sigma_k. \quad (1.58)$$

Analogous relations hold for \mathbf{T}^\dagger . The coupling constant f^* can be extracted from the partial decay width $\Delta \rightarrow N\pi$, which is taken to be $\Gamma_{N\pi} = 120$ MeV (the Breit-Wigner full width is from 115 to 125 MeV and the branching ratio to $N\pi$ is larger than 99%). These resonance properties correspond to the estimates made by the Particle Data Group [18], based on earlier partial wave analyses of πN total, elastic, charge exchange, inelastic ($\pi N \rightarrow N\pi\pi$, $\pi N \rightarrow N\eta$) and pion photoproduction (see for instance [37, 38, 39] and references therein); this will also be the case with the Roper resonance. From Eq. (1.56) one obtains the following expression for the partial decay width

$$\Gamma_\Delta(W) = \frac{1}{6\pi} \left(\frac{f^*}{m_\pi} \right)^2 \frac{M}{W} |\mathbf{q}_{\text{cm}}|^3 \Theta(W - M - m_\pi). \quad (1.59)$$

The step function Θ denotes the fact that the width is zero for invariant masses below the $N\pi$ threshold; W is the Δ invariant mass and \mathbf{q}_{cm} the pion momentum in the rest frame of the resonance

$$|\mathbf{q}_{\text{cm}}| = \frac{\sqrt{(W^2 - m_\pi^2 - M^2)^2 - 4m_\pi^2 M^2}}{2W}. \quad (1.60)$$

Setting $W = M_\Delta = 1232$ MeV (on-shell Δ) and using the above mentioned value of $\Gamma(M_\Delta)$ one gets $f^* \approx 2.13$. It is interesting to notice that this value is in remarkable agreement with the $SU(4)$ quark model relation $f^* = 3/\sqrt{2}f_{NN\pi}$, which gives $f^* = 2.12$.

Apart from the pion, the ρ meson is also present in the T=1 exchange channel of the nucleon-nucleon interaction. Taking into account that the ρ has spin one, the phenomenological Lagrangian for the $\Delta N\rho$ coupling can be written in the same fashion as the one for $\Delta N\pi$

$$\mathcal{L}_{\Delta N\rho} = \sqrt{C_\rho} \frac{f^*}{m_\pi} \psi_\Delta^\dagger \epsilon_{ijk} S_i^\dagger (\partial_j \boldsymbol{\rho}_k) \mathbf{T}^\dagger \psi_N + h.c., \quad (1.61)$$

where we simply introduce a scaling factor defined as

$$\sqrt{C_\rho} = \left(\frac{f_{\Delta N\rho}}{m_\rho} \right) / \left(\frac{f^*}{m_\pi} \right). \quad (1.62)$$

The static $SU(2) \times SU(2)$ quark model gives the ratio $f_{\Delta N\rho}/f_{NN\rho} = f^*/f_{NN\pi}$, which implies that $C_\rho \approx 2$ [34]. We take $C_\rho = 3.94$, which is consistent with the Bonn model [30]. This value is, however, tied to the use of a monopole form factor like the one of Eq. (1.54) with m_ρ instead of m_π and $\Lambda_\rho = 1.4$ GeV, which effectively reduces the strength of the coupling at $q^2 = 0$. The interplay between π and ρ exchange will be discussed in detail in Sec. 1.5.4.

Diagram (9) of Fig. 1.2 requires the inclusion of a new Lagrangian for the $\Delta\Delta\pi$ vertex

$$\mathcal{L}_{\Delta\Delta\pi} = \frac{f_\Delta}{m_\pi} \psi_\Delta^\dagger S_{\Delta i} (\partial_i \boldsymbol{\phi}) \mathbf{T}_\Delta \psi_\Delta. \quad (1.63)$$

For the coupling we adopt the quark model value of $f_\Delta = 4/5f_{NN\pi}$ [40]; this number is similar to those provided by other theoretical estimations [24]. However, one should bear

in mind that experimental analysis performed for the $(\pi, \pi\pi)$ reaction obtain best fit values for this coupling of about 3 times smaller [24, 41]. $\mathbf{S}_\Delta(\mathbf{T}_\Delta)$ is the spin (isospin) 3/2 operator. Using the Wigner-Eckart theorem one obtains

$$\langle \frac{3}{2} s' | S_{\Delta\lambda} | \frac{3}{2} s \rangle = \frac{1}{\sqrt{2(3/2) + 1}} (\frac{3}{2} s \mathbf{1} \lambda | \frac{3}{2} s' \rangle \langle \frac{3}{2} \| S_\Delta \| \frac{3}{2} \rangle) \quad (1.64)$$

with

$$\frac{1}{\sqrt{2(3/2) + 1}} \langle \frac{3}{2} \| S_\Delta \| \frac{3}{2} \rangle = \sqrt{\frac{3}{2} \left(\frac{3}{2} + 1 \right)} = \frac{\sqrt{15}}{2}. \quad (1.65)$$

When summing over polarizations of the intermediate Δ states, it is useful to implement the following closure relationship [6, 42]

$$\sum_{s, s'} S_i | \frac{3}{2} s' \rangle \langle \frac{3}{2} s' | S_{\Delta, j} | \frac{3}{2} s \rangle \langle \frac{3}{2} s | S_k^\dagger = \frac{5}{6} i \epsilon_{ijk} - \frac{1}{6} \delta_{ij} \sigma_k + \frac{2}{3} \delta_{ik} \sigma_j - \frac{1}{6} \delta_{jk} \sigma_i. \quad (1.66)$$

We shall also need the Δ propagator; it can be written as

$$D_\Delta(p) = \frac{1}{\sqrt{p^2} - M_\Delta + \frac{1}{2} i \Gamma_\Delta(p)} \quad (1.67)$$

with $p = (p_0, \mathbf{p})$ the momentum of the resonance and $\Gamma_\Delta(p)$, its total width, which can be taken to be approximately equal to the partial $\Delta \rightarrow N\pi$ given in Eq. (1.59). A derivation of this formula is given in Appendix B. Finally, we shall implement form factors of the type of Eq. (1.54) for $\Delta N\pi$, $\Delta N\rho$ off-shell vertices. The cut-off masses Λ , by their inverse, are related to the range over which the vertices extend. Therefore, it makes sense to use the value of $\Lambda_\pi = 1.2$ GeV for both $NN\pi$ and $\Delta N\pi$ as well as for other vertices where an off-shell pion is absorbed by a baryon. For the ρ , as we have already mentioned, we take $\Lambda_\rho = 1.4$ GeV [30] and replace m_π by m_ρ .

1.5.3 Roper resonance terms

The $N^*(1440)$ plays a crucial role in our model. It is heavier than the Δ and couples to the πN system with a weak strength compared to the Δ . For this reason it is not relevant for most applications in pion nuclear and hadronic physics. In fact, its contribution to diagrams like (10)-(15) of Fig. 1.2 but with $N^*(1440)$ in the intermediate states is negligible. Its relevance arises mainly from the decay channel $N^*(1440) \rightarrow N(\pi\pi)_{S-wave}^{T=0}$, which is small $\Gamma_{N\pi\pi(s)}/\Gamma_{tot} = 5 - 10\%$ at the resonance peak [18] but will give a non-vanishing important contribution to double pion production reactions at threshold. This has been found to be the case for the $\pi N \rightarrow \pi\pi N$ reaction [6, 43]. As we shall see, the situation here is similar but more involved since one has to deal with the $NN \rightarrow NN^*$ transition, for which a recent experiment [44] has brought some novel information. Let us now discuss the

phenomenological Lagrangians that are relevant for our purposes. For the $N^*N\pi$ vertex we have

$$\mathcal{L}_{N^*N\pi} = -\frac{\tilde{f}}{m_\pi} \bar{\Psi}_{N^*} \gamma^\mu \gamma_5 \partial_\mu \boldsymbol{\phi} \boldsymbol{\tau} \Psi_N + h.c., \quad (1.68)$$

which is obviously very similar to the $NN\pi$ Lagrangian of Eq. (1.40). Its non-relativistic reduction is then

$$\mathcal{L}_{N^*N\pi} = \frac{\tilde{f}}{m_\pi} \psi_{N^*}^\dagger \sigma_i \partial_i \boldsymbol{\phi} \boldsymbol{\tau} \psi_N + h.c.. \quad (1.69)$$

The coupling constant can be obtained from the partial decay width

$$\Gamma_{N\pi}(W) = \frac{3}{2\pi} \left(\frac{\tilde{f}}{m_\pi} \right)^2 \frac{M}{W} |\mathbf{q}_{\text{cm}}|^3 \Theta(W - M - m_\pi), \quad (1.70)$$

where $|\mathbf{q}_{\text{cm}}|$ is given by Eq. (1.60). Unfortunately, the experimental uncertainties of the Roper width are not small. Taking $\Gamma_{\text{tot}}(M^*) = 350$ MeV and a branching ratio for the $N^* \rightarrow N\pi$ equal to 65 % and W equal to the N^* mass M^* one gets $\tilde{f} = 0.477$. As for the Δ, ρ meson exchange in the T=1 channel should be considered. The Lagrangian is

$$\mathcal{L}_{N^*N\rho} = \sqrt{C_\rho} \frac{\tilde{f}}{m_\pi} \psi_{N^*}^\dagger \epsilon_{ijk} \sigma_i (\partial_j \boldsymbol{\rho}_k) \boldsymbol{\tau} \psi_N + h.c., \quad (1.71)$$

where the same scaling factor C_ρ as in the case of the Δ is assumed.

The diagram (8) of Fig. 1.2 requires to take also into account the $N^*\Delta\pi$ vertex. Due to the relatively large $N^* \rightarrow \Delta\pi$ branching ratio (20 – 30 % [18]) one expect its contribution to be important, especially in the kinematic region where the Roper is on-shell. The Lagrangian for this vertex reads

$$\mathcal{L}_{N^*\Delta\pi} = \frac{g_{N^*\Delta\pi}}{m_\pi} \psi_\Delta^\dagger S_i^\dagger (\partial_i \boldsymbol{\phi}) \mathbf{T}^\dagger \psi_{N^*} + h.c.. \quad (1.72)$$

In order to be accurate in the evaluation of the $N^* \rightarrow \Delta\pi$ decay width we should take into account the width of the Δ resonance. The fact that the Δ width is not small compared to the mass difference between the Roper and the Delta makes this correction advisable [45]. The width is then expressed as

$$\Gamma_{\Delta\pi}(W) = \frac{1}{3\pi^2} \left(\frac{g_{N^*\Delta\pi}}{m_\pi} \right)^2 \int_0^{p_{\text{max}}} dp \frac{p^4}{\sqrt{p^2 + m_\pi^2}} |D_\Delta(W_\Delta)|^2 \Gamma_\Delta(W_\Delta), \quad (1.73)$$

with

$$W_\Delta^2 = W^2 - 2W(\sqrt{p^2 + m_\pi^2}) + m_\pi^2, \quad (1.74)$$

and

$$p_{max} = \left[\left(\frac{W^2 - M^2 - 2Mm_\pi}{2W} \right)^2 - m_\pi^2 \right]^{1/2}; \quad (1.75)$$

D_Δ and Γ_Δ are given by Eqs. (1.67) and (1.59) respectively. Using a branching ratio of 25 % one obtains $g_{N^*\Delta\pi} = 2.07$. The signs of both \tilde{f} and $g_{N^*\Delta\pi}$ correspond to those provided in earlier analyses of the $(\pi, \pi\pi)$ reactions [37, 46, 47, 6].

The structure of the Lagrangian for the $N^*(1440) \rightarrow N(\pi\pi)_{S-wave}^{T=0}$ decay has been studied in Ref. [48]. To order $\mathcal{O}(q^2)$ it contains at least two terms

$$\mathcal{L}_{N^*N\pi\pi} = c_1^* \bar{\Psi}_{N^*} \chi_+ \Psi_N - \frac{c_2^*}{M^{*2}} (\partial_\mu \partial_\nu \bar{\Psi}_{N^*}) u^\mu u^\nu \Psi_N + h.c.. \quad (1.76)$$

The second term is not unique (for a different choice see Ref. [43]), but all inequivalent forms lead to the same expressions in the non-relativistic limit. Expanding up to the second order in pion fields, and making use of the definitions of Eqs. (1.36) and (1.44) we find

$$\mathcal{L}_{N^*N\pi\pi} = -c_1^* \frac{m_\pi^2}{f_\pi^2} \bar{\psi}_{N^*} \boldsymbol{\phi}^2 \psi_N - c_2^* \frac{1}{f_\pi^2} \bar{\psi}_{N^*} (\boldsymbol{\tau} \partial_0 \boldsymbol{\phi}) (\boldsymbol{\tau} \partial_0 \boldsymbol{\phi}) \psi_N + h.c., \quad (1.77)$$

where we have neglected terms of order $\mathcal{O}(vp^2/M^{*2})$. In this case, the free parameters c_1^* and c_2^* can not be both obtained from the partial decay width. They can just be constrained to an ellipse [48]. In fact

$$\Gamma_{N^*\pi\pi} = [\alpha(c_1^*)^2 + \beta(c_2^*)^2 + \gamma c_1^* c_2^*], \quad (1.78)$$

with

$$\begin{aligned} \alpha &= \kappa m_\pi^4 \int_{z^2 < 1} d\omega_1 d\omega_2 (M^* + M - \omega_1 - \omega_2) = 0.497 \times 10^{-3} \text{ GeV}^3 \\ \beta &= \kappa \int_{z^2 < 1} d\omega_1 d\omega_2 (M^* + M - \omega_1 - \omega_2) \omega_1^2 \omega_2^2 = 3.66 \times 10^{-3} \text{ GeV}^3 \\ \gamma &= 2\kappa m_\pi^2 \int_{z^2 < 1} d\omega_1 d\omega_2 (M^* + M - \omega_1 - \omega_2) \omega_1 \omega_2 = 2.69 \times 10^{-3} \text{ GeV}^3, \end{aligned} \quad (1.79)$$

where

$$z = \frac{\omega_1 \omega_2 - M^* (\omega_1 + \omega_2) + m_\pi^2 + (M^{*2} - M^2)/2}{\sqrt{(\omega_1^2 - m_\pi^2)(\omega_2^2 - m_\pi^2)}}, \quad \kappa = \frac{3}{16\pi^3 f_\pi^4}. \quad (1.80)$$

The fact that $(\alpha\beta - \gamma^2/4) > 0$ implies that Eq. (1.78) describes an ellipse. Therefore, c_1^* and c_2^* can be parametrized in the following way

$$\begin{aligned} c_1^* &= \sqrt{\Gamma_{\Delta\pi}} (a \cos \delta \cos t + b \sin \delta \sin t) \\ c_2^* &= \sqrt{\Gamma_{\Delta\pi}} (-a \sin \delta \cos t + b \cos \delta \sin t), \end{aligned} \quad (1.81)$$

with

$$\frac{1}{b^2(a^2)} = \frac{(\alpha + \beta) \pm \sqrt{(\alpha - \beta)^2 + \gamma^2}}{2}, \quad \delta = \frac{1}{2} \arctan \left(\frac{\gamma}{\beta - \alpha} \right) \quad (1.82)$$

and $t \in [0, 2\pi]$. Assuming a 7.5 % branching ratio for the $N^*(1440) \rightarrow N(\pi\pi)_{S-wave}^{T=0}$ decay width, one finds the rather elongated ellipse plotted in Fig. 1.3 (a). In order to further constrain the parameters, we use the model of Ref. [6] for the reaction $\pi^- p \rightarrow \pi^+ \pi^- n$. The cross section shows a strong sensitivity to the values of c_1^* , c_2^* and spans about two orders of magnitude when the values of these parameters are varied along the ellipse, as shown in Fig. 1.3. The best agreement with the experiment is obtained with the traditional value of $c_2^* = 0$, which corresponds to $c_1^* = -7.27 \text{ GeV}^{-1}$ (point 5 in Fig. 1.3 (a)). However, the experimental errors are compatible with the use of $c_1^* = -12.7 \text{ GeV}^{-1}$, $c_2^* = 1.98 \text{ GeV}^{-1}$ (point 4) and intermediate values in the ellipse. Throughout this work, these two sets of c^* parameters will be used. It can be also noticed that the region in the vicinity of point 9 also produces reasonable results but, as argued in Ref. [48], in analogy to the equivalent $c_{1(2)}$ nucleon couplings (see Eq. (1.45)), one would expect $c_1^* < 0$ and $c_2^* > 0$. For this reason we do not use point 9 in our calculations.

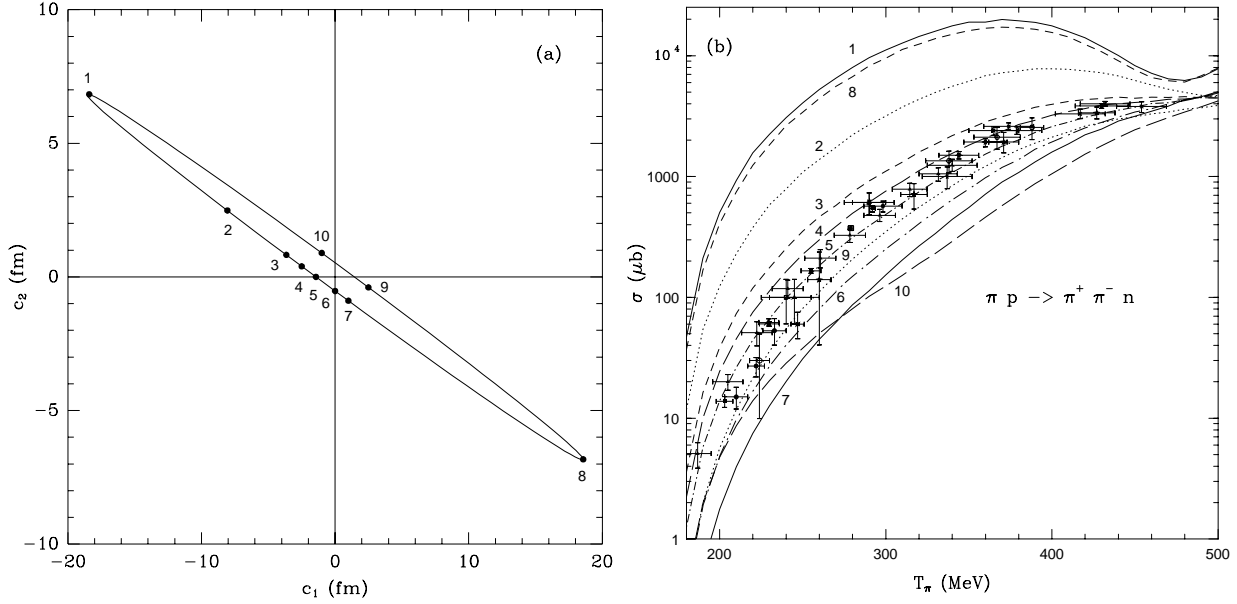


Figure 1.3: Set of allowed values of c_1^* and c_2^* for a fixed width, and $\pi^- p \rightarrow \pi^+ \pi^- n$ total cross sections as a function of the pion kinetic energy in LA (T_π), plotted for different choices of the c^* parameters. The data include all total cross sections values, measured at $T_\pi < 500$ MeV published before May 1993 [49].

A best fit to the different $\pi N \rightarrow \pi\pi N$ channels is done in Ref. [43]. Although the data would roughly be compatible with the use of $c_2^* = 0$, they obtain a best fit with other set of parameters. However, this work contains some small differences with respect to the model of Ref. [6], like the relativistic treatment, the use of an N^* width assuming phase space for πN decay only, and the neglect of the isoscalar πN amplitude and intermediate $\Delta\Delta$

states (which are included in Ref. [6]). These are small differences, but they have some influence in the c_1^* and c_2^* parameters. For the sake of consistency with our input, we take the values of c_1^* and c_2^* from our own analysis.

Finally, the expression for the N^* propagator that we are going to use is derived in Appendix B

$$D_{N^*}(p) = \frac{1}{\sqrt{p^2} - M^* + \frac{1}{2}i\Gamma^*(p)} \quad (1.83)$$

where we take $\Gamma^* = \Gamma_{N\pi} + \Gamma_{\Delta\pi}$, given by Eqs. (1.70), (1.73), which properly accounts for approximately 90 % of the total Roper width at the resonance peak. With these ingredients, and the off-shell form factors, one can produce the $T = 1$ amplitudes of diagrams (4)-(8) of Fig. 1.2. Furthermore, in the case of diagrams (4),(5), (8),(9), as well as (12)-(15), it is crucial to take into account the effect of short range correlations; this issue is studied in detail below. On the other side, while isospin conservation forbids a $T=0$ exchange for $NN \rightarrow N\Delta$ and $NN \rightarrow \Delta\Delta$ transitions, it is not the case with the $NN \rightarrow NN^*$ one; Such $T=0$ exchange potential is discussed in Subsection 1.5.5.

1.5.4 Isovector one boson exchange potential and short range correlations

Let us consider the $T=1$ potential for the nucleon-nucleon interaction

$$V(q) = \left(\frac{f_{NN\pi}}{m_\pi} \right)^2 \mathcal{V}_{ij}(q) \sigma_1^i \sigma_2^j (\boldsymbol{\tau}_1 \boldsymbol{\tau}_2) \quad (1.84)$$

with

$$\mathcal{V}_{ij}(q) = V_L(q) \hat{q}_i \hat{q}_j + V_T(q) (\delta_{ij} - \hat{q}_i \hat{q}_j). \quad (1.85)$$

The longitudinal and transversal pieces correspond to pion and rho exchanges respectively

$$V_L(q) = V_\pi(q) = \mathbf{q}^2 D_\pi(q) F_\pi^2(q), \quad V_T(q) = V_\rho(q) = \mathbf{q}^2 D_\rho(q) F_\rho^2(q) C_\rho, \quad (1.86)$$

where $F_{\pi,\rho}$ are the monopole type form factors introduced earlier; $D_\rho(q)$ is the ρ propagator

$$D_\rho(q) = \frac{1}{q^2 - m_\rho^2}, \quad (1.87)$$

where the imaginary part is not shown because it vanishes at $q^2 < 0$, which is the case here. Although the situation might be different if initial or final state interactions were taken into account, this imaginary part would give a negligible contribution in the range of energies considered here. The pion propagator $D_\pi(q)$ is given in Eq. (1.53). In the case of transition potentials such as $NN \rightarrow \Delta N$, $NN \rightarrow \Delta\Delta$ or $NN \rightarrow N^*N$, the spin and isospin operators in Eq. (1.84) as well as the coupling constants should be modified accordingly, but \mathcal{V}_{ij} remains the same. This assumption is by no means trivial but is supported, at least

in the case of Δ isobars, by the experimental evidence of quenching in the Gamow-Teller and magnetic multipole transitions (see Ref. [34] and references therein).

However, this interaction potential is still incomplete; an adequate treatment of the short range correlations generated by the strong repulsion of nuclear forces at short distances is required. In order to illustrate the importance of these correlations, let us notice that the longitudinal part of the potential can be written as a sum of scalar and tensor pieces, by means of the separation

$$\hat{q}_i \hat{q}_j = \frac{1}{3} \delta_{ij} + \frac{1}{3} S_{ij}, \quad S_{ij} = 3 \hat{q}_i \hat{q}_j - \delta_{ij}. \quad (1.88)$$

Then, for the scalar part, in the static limit ($q_0^2 \ll \mathbf{q}^2$) and dropping the form factors for the sake of simplicity one gets

$$\mathcal{V}_{ij}^{(s)}(\mathbf{q}) = -\frac{1}{3} \frac{\mathbf{q}^2}{\mathbf{q}^2 + m_\pi^2} \delta_{ij}, \quad (1.89)$$

which in coordinate space reads

$$\begin{aligned} \mathcal{V}_{ij}^{(s)}(\mathbf{r}) &= \int \frac{d\mathbf{q}}{(2\pi)^3} \mathcal{V}_{ij}^{(s)}(\mathbf{q}) e^{-i\mathbf{qr}} \\ &= -\frac{1}{3} \left[\delta(\mathbf{r}) - \frac{m_\pi^2}{4\pi} \frac{e^{-m_\pi r}}{r} \right] \delta_{ij}. \end{aligned} \quad (1.90)$$

The $\delta(\mathbf{r})$ is incorrect from the physical point of view since it is a consequence of taking point-like particles. Nuclear correlations forbid the nucleons to be close to each other. At such small distances, the OBE model is no longer appropriate and should be corrected. This fact motivated the introduction of the term

$$\mathcal{V}_{ij}^{LL}(\mathbf{q}) = g' \delta_{ij} \quad (1.91)$$

known as Lorentz-Lorenz correction [50]. In coordinate space

$$\mathcal{V}_{ij}^{LL}(\mathbf{r}) = g' \delta(\mathbf{r}) \delta_{ij}. \quad (1.92)$$

Therefore, if $g' = 1/3$, the correction exactly cancels the singularity. Phenomenological determinations of this magnitude lead to the value $g'(q=0) \approx 0.6$ [51]. The static quark model supports the idea of a universal g' value, but there are indications that its value could be smaller in the case of $NN \rightarrow N\Delta$ and $NN \rightarrow \Delta\Delta$ processes, and closer to the classical value [52].

For large values of $|\mathbf{q}|$, the assumption of a constant g' should be improved. A more realistic way to account for the short-range corrections is to consider a correlated potential in coordinate space

$$V(\mathbf{r}) = [V_\pi(\mathbf{r}) + V_\rho(\mathbf{r})] \Omega(\mathbf{r}), \quad (1.93)$$

where the correlation function $\Omega(\mathbf{r})$ is such that $\Omega(0) = 0$ and $\Omega(\mathbf{r}) \approx 1$ for $|\mathbf{r}| \geq r_c$, with r_c being the correlation length, which should be of the order of the repulsive part of NN interaction. A good analytic approximation for the correlation function is

$$\Omega(\mathbf{r}) = 1 - j_0(q_c r) \quad (1.94)$$

with $q_c = r_c^{-1}$. In momentum space we have

$$\Omega(\mathbf{k}) = \int d\mathbf{r} \Omega(\mathbf{r}) e^{i\mathbf{kr}} = (2\pi)^3 \delta(\mathbf{k}) - \frac{2\pi^2}{q_c^2} \delta(q_c - |\mathbf{k}|). \quad (1.95)$$

Hence,

$$\begin{aligned} \mathcal{V}'_{ij}(\mathbf{q}) &= \int d\mathbf{r} \mathcal{V}_{ij}(\mathbf{r}) \Omega(\mathbf{r}) e^{i\mathbf{qr}} \\ &= \int \frac{d\mathbf{k}}{(2\pi)^3} \mathcal{V}_{ij}(q_0, \mathbf{q} - \mathbf{k}) \Omega(\mathbf{k}) \\ &= \mathcal{V}_{ij}(\mathbf{q}) - \frac{1}{4\pi} \int d\Omega_{\mathbf{a}} \mathcal{V}_{ij}(\mathbf{q} + \mathbf{a}) \quad |\mathbf{a}| = q_c; \end{aligned} \quad (1.96)$$

substituting \mathcal{V}_{ij} from Eq. (1.85) one gets

$$\mathcal{V}'_{ij}(q) = V'_L(q) \hat{q}_i \hat{q}_j + V'_T(q) (\delta_{ij} - \hat{q}_i \hat{q}_j), \quad (1.97)$$

where

$$\begin{aligned} V'_L(q) &= V_L(q) - \left(\mathbf{q}^2 \mathcal{I}_0 + \mathcal{I}_1 + \frac{1}{\mathbf{q}^2} \mathcal{I}_2 \right) \\ V'_T(q) &= V_T(q) - \left(\frac{1}{2} q_c^2 \mathcal{I}_0 - \frac{1}{2} \frac{1}{\mathbf{q}^2} \mathcal{I}_2 + \mathcal{I}_T \right) \end{aligned} \quad (1.98)$$

with \mathcal{I}_n defined as

$$\mathcal{I}_n = \frac{1}{4\pi} \int d\Omega_{\mathbf{a}} [V_L(q_0, \mathbf{q} + \mathbf{a}) - V_T(q_0, \mathbf{q} + \mathbf{a})] (\mathbf{q} \cdot \mathbf{a})^n, \quad (1.99)$$

and

$$\mathcal{I}_T = \frac{1}{4\pi} \int d\Omega_{\mathbf{a}} V_T(q_0, \mathbf{q} + \mathbf{a}) (\mathbf{q} + \mathbf{a})^2. \quad (1.100)$$

The following approximations

$$F_{\pi(\rho)}(\mathbf{q} + \mathbf{a}) = \frac{\Lambda_{\pi(\rho)}^2 - m_{\pi(\rho)}^2}{\Lambda_{\pi(\rho)}^2 - q_0^2 + \mathbf{q}^2 + q_c^2 + 2\mathbf{q} \cdot \mathbf{a}} \approx \frac{\Lambda_{\pi(\rho)}^2 - m_{\pi(\rho)}^2}{\Lambda_{\pi(\rho)}^2 - q_0^2 + \mathbf{q}^2 + q_c^2} \equiv \tilde{F}_{\pi(\rho)}(q) \quad (1.101)$$

$$D_{\pi(\rho)}(\mathbf{q} + \mathbf{a}) = \frac{1}{q_0^2 - \mathbf{q}^2 - q_c^2 - 2\mathbf{q}\cdot\mathbf{a} - m_{\pi(\rho)}^2} \approx \frac{1}{q_0^2 - \mathbf{q}^2 - q_c^2 - m_{\pi(\rho)}^2} \equiv \tilde{D}_{\pi(\rho)}(q) \quad (1.102)$$

allow us to solve the integrals (1.99) and (1.100) analytically. After some straightforward manipulation one obtains

$$\begin{aligned} V'_L(q) &= V_L(q) + g'_L(q) \\ V'_T(q) &= V_T(q) + g'_T(q) \\ g'_L(q) &= -(\mathbf{q}^2 + \frac{1}{3}q_c^2)\tilde{F}_\pi^2\tilde{D}_\pi - \frac{2}{3}q_c^2\tilde{F}_\rho^2\tilde{D}_\rho C_\rho \\ g'_T(q) &= -\frac{1}{3}q_c^2\tilde{F}_\pi^2\tilde{D}_\pi - (\mathbf{q}^2 + \frac{2}{3}q_c^2)\tilde{F}_\rho^2\tilde{D}_\rho C_\rho. \end{aligned} \quad (1.103)$$

Setting the correlation length to be approximately equal to the inverse of the omega meson mass i.e. $q_c = 780$ MeV a $g'(0) = 0.6$ [53] is obtained.

Once the T=1 spin-isospin effective interaction is given, the amplitudes for mechanisms (9), (12)-(15) as well as the T=1 part of (4), (5) and (8) of Fig. 1.2 can be calculated. Explicit expressions for these amplitudes in the case of the $pp \rightarrow pp\pi^+\pi^-$ channel are presented in Appendix C.

1.5.5 Isoscalar excitation of the Roper resonance

Diagrams (4), (5) and (8) of Fig. 1.2 require, apart from the effective T=1 interaction studied above, to take into account the T=0 channel for the transition $NN \rightarrow NN^*$. The strength of the isoscalar excitation of the Roper resonance has been extracted in Ref. [54], where a theoretical analysis of the (α, α') reaction on proton target was performed. This reaction is particularly useful to obtain new information about the properties of the Roper resonance because the fact that the α particle has isospin zero causes a reduction of mechanisms that can contribute. In particular, the fact that Δ excitation in the target is forbidden by isospin conservation, makes possible to assess the Roper excitation in the target. The model of Ref. [54] included the following processes:

- Δ excitation in the projectile
- N^* excitation in the target
- N^* excitation in the projectile
- Double Δ excitation

but it was found that the first two are clearly dominant. The experiment [44] could, therefore, be interpreted in base of the mechanisms shown in Fig. 1.4 and used to extract the unknown strength of the $NN \rightarrow NN^*$ isoscalar transition.

Since the 4He beam has $T = 0$ the N^* excitation in the (α, α') reaction requires the exchange of an isoscalar object. In meson exchange pictures it could be σ or ω exchange. However, the experiment has not enough information to provide the separate strength of

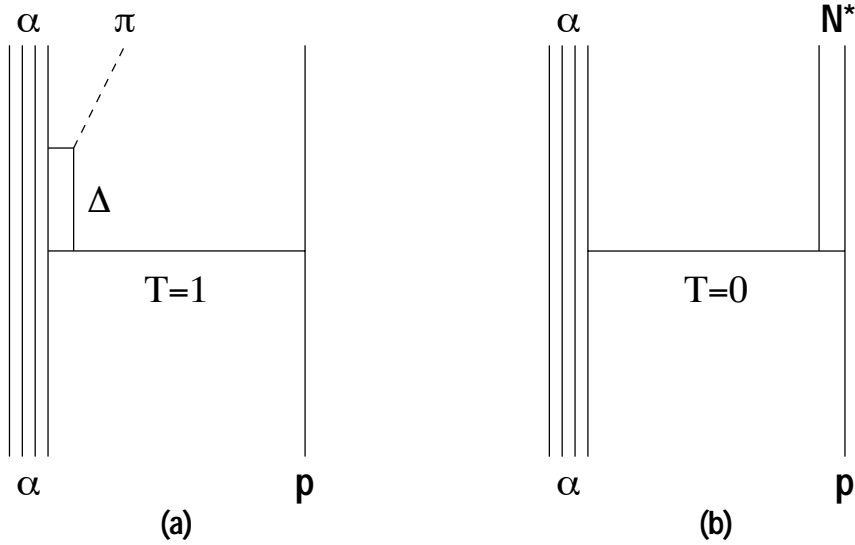


Figure 1.4: Dominant mechanisms in the analysis of (α, α') performed in Ref. [54]; (a) Δ excitation in the projectile, (b) Roper excitation in the target.

both ingredients. For this reason, the transition amplitude was parameterized in terms of an effective “ σ ”, which couples to NN as the σ meson of the Bonn model [30]

$$\mathcal{L}_{NN\sigma} = g_{NN\sigma} \bar{\psi} \phi \psi \quad g_{NN\sigma}^2 / 4\pi = 5.69 \quad (1.104)$$

and couples to NN^*

$$\mathcal{L}_{N^*N\sigma} = g_{N^*N\sigma} \bar{\psi}_{N^*} \phi \psi + h.c. \quad (1.105)$$

with an unknown strength provided by a best fit to the data. Using a form factor of the monopole type with $\Lambda_\sigma = 1.7$ GeV, a value of $g_{N^*N\sigma}^2 / 4\pi = 1.33$ was obtained. Fig. 1.5 is taken from Ref. [54] and illustrates how this model compares to the data of Ref. [44]. The fact that the interference between the leading mechanisms is important allowed to determine the relative sign between $g_{NN\sigma}$ and $g_{N^*N\sigma}$. Choosing the same sign for both couplings leads to a destructive interference; a constructive one would produce a cross section in large disagreement with the data.

The “ σ ” exchange described above is a useful and intuitive parameterization of the effective interaction in the $T=0$ channel. It is an essential ingredient of our model. In particular, its contribution to diagram (4) of Fig. 1.2 will be the dominant one at threshold.

1.6 Results and discussion

1.6.1 Total cross sections

Let us first look at the reaction $pp \rightarrow pp\pi^+\pi^-$. The total cross section as a function of the kinetic energy of the incoming particle in LA is shown in Fig. 1.6. We have separated

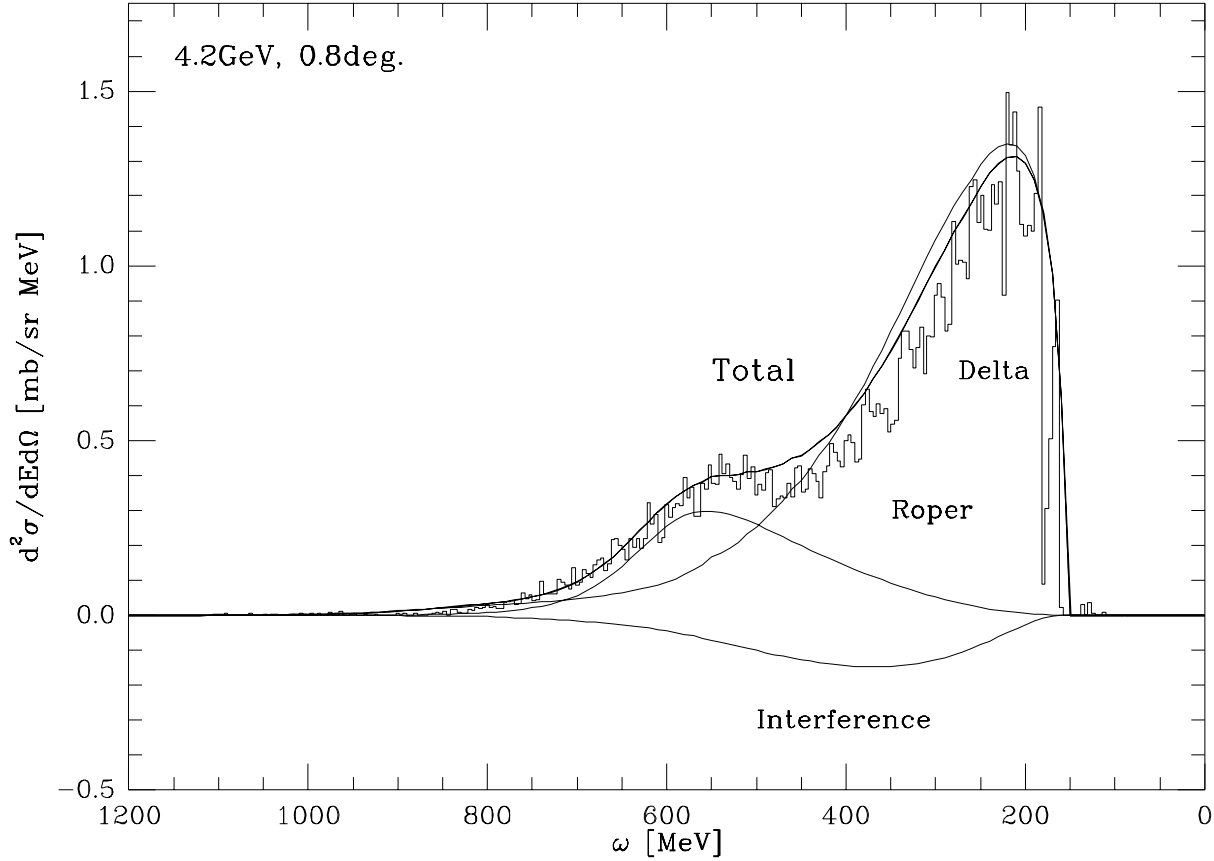


Figure 1.5: Double differential cross section for the (α, α') reaction on proton target as obtained in Ref. [54]; ω stands for the α particle energy transfer.

the contribution of several blocks of diagrams in the figure. They have been calculated using $c_1^* = -7.27 \text{ GeV}^{-1}$ and $c_2^* = 0$ (point 5 in the ellipse of Fig. 1.3, but the total contribution is given for both points 4 and 5 (solid lines) in order to give an idea of the theoretical uncertainties. Although the sum of amplitudes is done coherently, there is in fact little interference in the total cross section. The short-dashed curve corresponds to chiral terms: diagrams (1)-(3) of Fig. 1.2. As we can see, this contribution is negligible in this channel. The dash-dotted curve corresponds to the diagrams (9)-(15) involving only Δ excitations. We see that this contribution is much larger than the former one. At low energies it gives a negligible contribution to the cross section but it rises steeply as a function of the energy and becomes dominant at large energies. In Fig. 1.7 (a), the relative importance of the different double- Δ mechanisms for this channel is given. It is clearly seen that the $\Delta\Delta$ excitation mechanism of diagrams (12)-(15), especially diagram (12), are the most important above $T_p = 1 \text{ GeV}$. The cross section corresponding to the excitation of successive Δ 's, diagram (9), is the one that decreases slower with energy and becomes bigger than the others as one approaches threshold. In Fig. 1.6, the long-dashed

curve stands for diagram (8) exciting N^* and Δ consecutively. We can see that this term is more relevant than the set of Δ terms at low energies. Finally, we show in the long-short

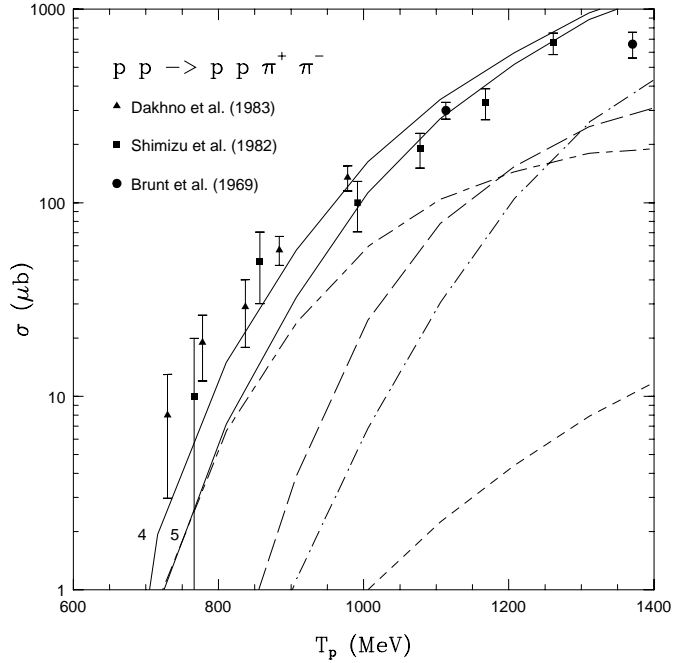


Figure 1.6: Total cross section for reaction (1.1) channel as a function of the incoming proton kinetic energy in the laboratory frame. Solid line, total (the labels 4 and 5 correspond to the choice of points 4 and 5 in the ellipse of parameters c_1^* and c_2^* given in Fig. 1.3); long-short-dashed line, $N^* \rightarrow N(\pi\pi)_{S-wave}^{T=0}$; long-dashed line, $N^* \rightarrow \Delta\pi$; dash-dotted line, Δ excitation mechanisms; short-dashed line, non-resonant terms from diagrams (1)-(3). All partial contributions are calculated with $c_1^* = -7.27 \text{ GeV}^{-1}$, $c_2^* = 0$ (point 5). Experimental data are taken from Refs. [8, 9, 10].

dashed line the contribution of the set of diagrams involving one N^* excitation followed by a two-pion decay in s-wave: diagrams (4)-(7). We can see in the figure that this gives by far the largest contribution at low energies. The sum of all contributions is given by the solid lines. These lines, corresponding to the two acceptable sets of c_1^* , c_2^* parameters, differ by about a factor two at low energies and about 30 % at $T_p \sim 1 \text{ GeV}$. This sets the level of the theoretical uncertainties in this reaction. Another reading of these results is that the $pp \rightarrow pp\pi^+\pi^-$ reaction is a more sensitive tool to assess the $N^* \rightarrow N(\pi\pi)_{S-wave}^{T=0}$ couplings than the $\pi N \rightarrow \pi\pi N$ reaction, and could be used to put stronger constraints on them. In any case, these results have to be seen with the perspective that by omitting the N^* terms the disagreement at energies below $T_p = 900 \text{ MeV}$ is larger than two orders of magnitude.

In order to show the relevance of the findings of the isoscalar excitation of the Roper resonance, we show in Fig. 1.7 (b) the contribution of the N^* terms (diagrams (4) and

(5). It is clear that the $T=1$ amplitude is strongly damped by the effect of the short range repulsion, leading to a one order of magnitude smaller cross section. In view of this, the $T=0$ part becomes the dominant contribution, about one order of magnitude bigger than the one obtained with the correlated $\pi + \rho$ exchange. It is, therefore, the most important ingredient of our model, at least in the channels where pion pairs can be in an isospin zero state.

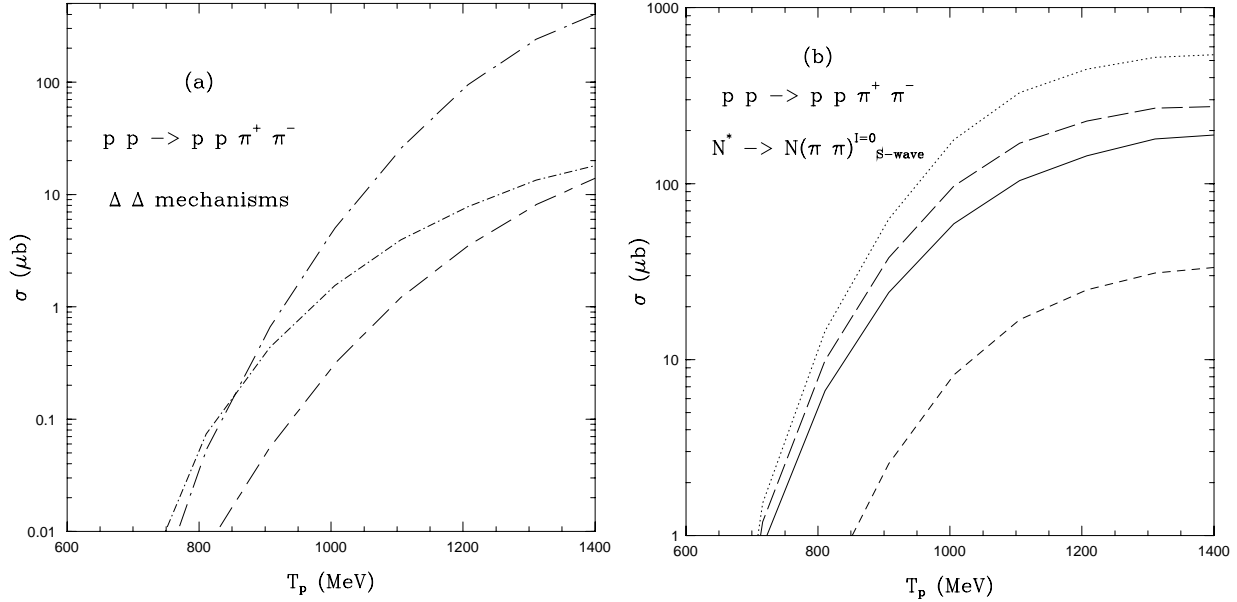


Figure 1.7: Contribution of different mechanisms to the total cross section for channel 1.1. In (a) the long-dash-dotted line stands for diagrams (12)-(15) of Fig. 1.2; the short-dash-dotted line, for diagram (9) and the long-short-dashed on, for (10) and (11). In (b), the contribution of the $N^* \rightarrow N(\pi\pi)^{T=0}_{S-wave}$ mechanisms (solid line) is split into correlated $\pi + \rho$ exchange (short-dashed line) and effective σ exchange (long-dashed line); the dotted line represents the $T=1$ amplitude without correlations.

In Fig. 1.8 we show the results for the $pn \rightarrow pn\pi^+\pi^-$ channel, with the same meaning as in Fig. 1.6 and similar results, although with a larger discrepancy than in the previous case.

In Fig. 1.9 we show the results for the $pp \rightarrow pn\pi^+\pi^0$ reaction. This channel is interesting because the mechanism of N^* excitation and subsequent decay into $N(\pi\pi)^{T=0}_{S-wave}$ shown in diagrams (4) and (5) of Fig. 1.2, which was dominant in the case of the channels considered above, does not contribute now. Diagrams (6) and (7) still contribute, but they are very small because they involve one $N^*N\pi$ p-wave coupling, which vanishes at threshold and also because $T=0$ exchange is not allowed. Indeed, the $\pi^+\pi^0$ system can only be in $T = 1, 2$ but not in $T = 0$. Hence, the mechanism that was dominant in the previous cases is not present here. In spite of that, the agreement with the data is of the

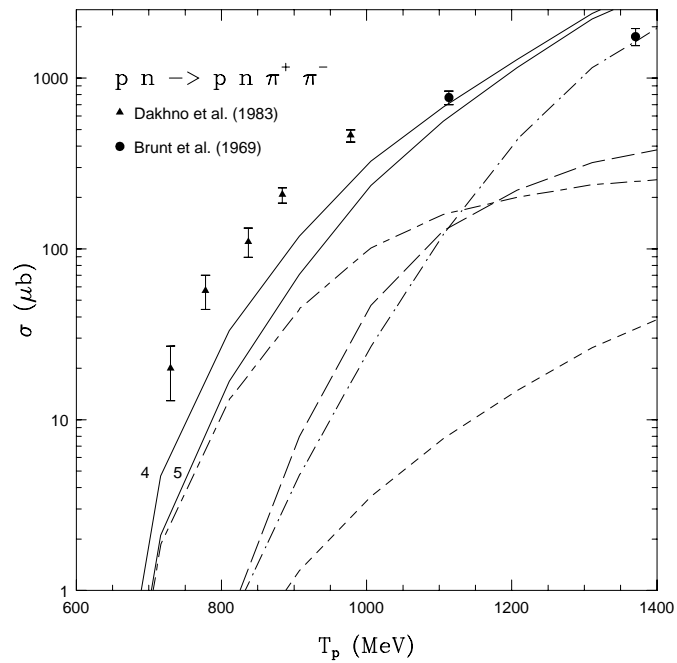


Figure 1.8: Same as Fig. 1.6 for reaction (1.5).

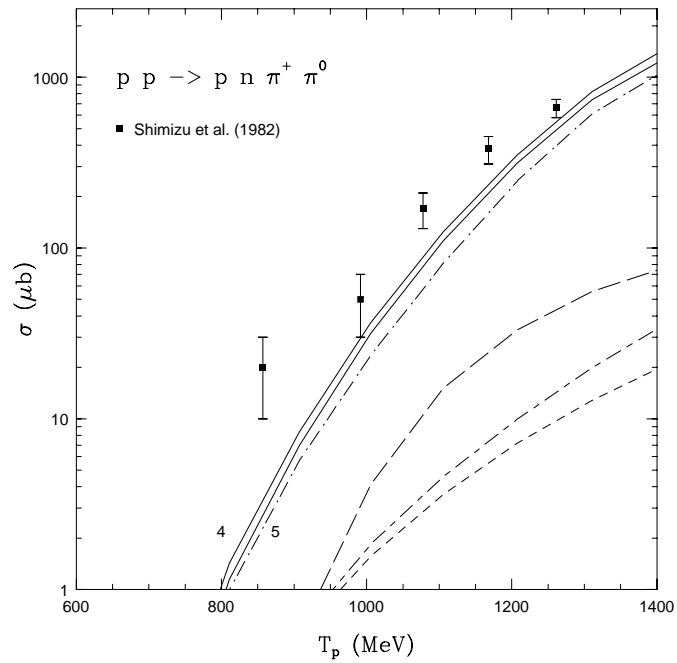


Figure 1.9: Same as Fig. 1.6 for reaction (1.2).

same quality as the one found before for the $pp \rightarrow pp\pi^+\pi^-$ reaction. Now the dominant terms are those exciting Δ 's.

In Fig. 1.10 we show results for the $pn \rightarrow pp\pi^-\pi^0$ reaction. The features are qualitatively similar to those of the previous channel but the discrepancies are considerably bigger. We note that the strength of diagram (8) is now comparatively bigger with respect to Δ excitation terms than in the previous case.

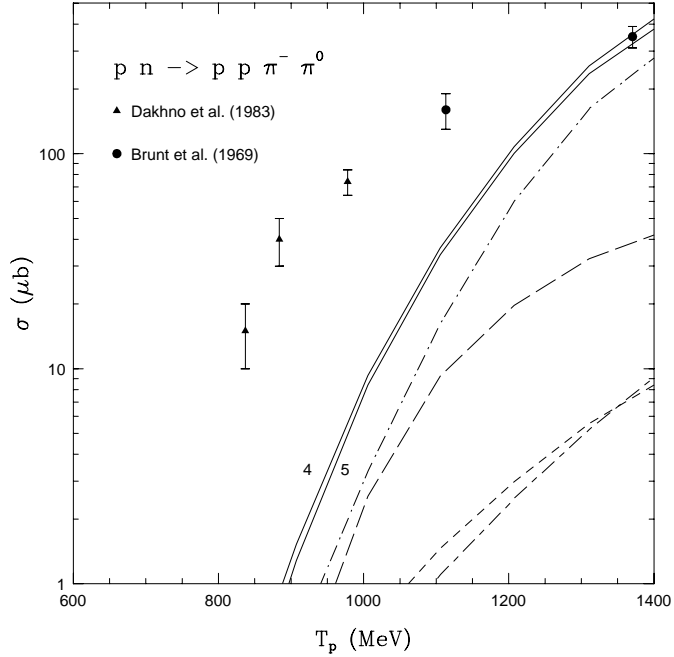


Figure 1.10: Same as Fig. 1.6 for reaction (1.6).

In Fig. 1.11 the results for the $pp \rightarrow nn\pi^+\pi^+$ reaction are shown. Here, at high energies, Δ terms are still dominant, but below 1 GeV chiral terms dominate the amplitudes. This is the only case where these terms are relatively important.

In Fig. 1.12 we show cross sections for the $pp \rightarrow pp\pi^0\pi^0$ channel. This is again a channel where the diagrams (4) and (5) are dominant at low energies, like in the case of reactions (1.1) and (1.5). Chiral terms are not drawn since they are below the scale of the figure. In this case we overestimate the experimental results by about a factor 2-3 although the quality of the data is not as good as in former cases.

With these results we exhaust the experimental data on total cross sections and the isospin independent channels. We have also calculated the $pn \rightarrow pn\pi^0\pi^0$ cross section with our model in order to perform a consistency check using Eq. (1.17).

The model presented here contains only tree level diagrams. Unitarity is not strictly fulfilled. Actually, imposing unitarity with four particles in the final state is less than trivial, as evidenced by the enormous difficulties in the case of three body final state [55]. However, one should bear in mind that as far as we have dominance of a resonant term,

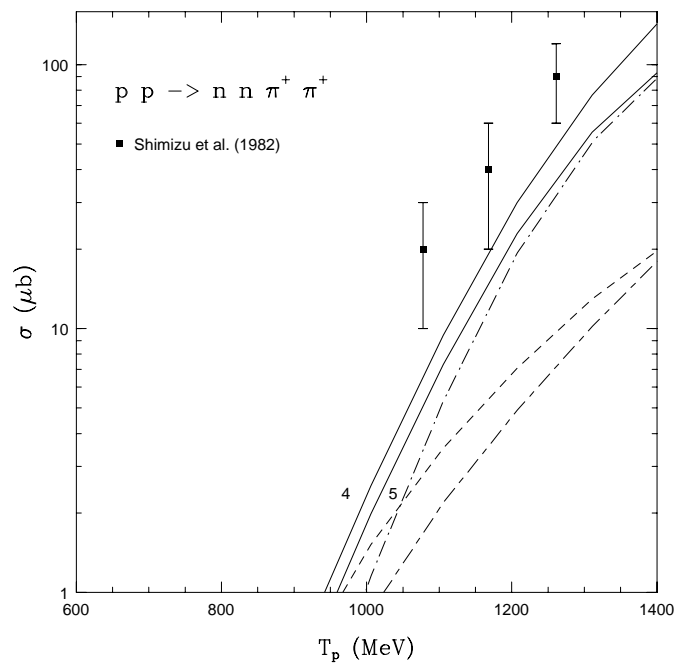


Figure 1.11: Same as Fig. 1.6 for reaction (1.4).

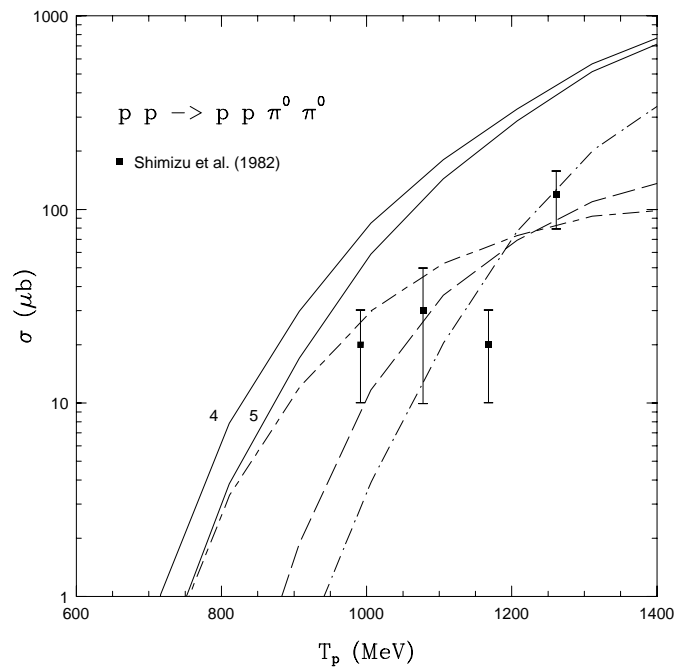


Figure 1.12: Same as Fig. 1.6 for reaction (1.3).

the important aspects of unitarity are included if the proper resonance width is used in the resonance propagator, as we do. Partial unitarization can be accomplished by the introduction of loops, as done for instance in the $\pi N \rightarrow \pi\pi N$ reaction for the chiral terms in Ref. [48]. However, we saw that this sector plays a minor role in the present reaction in view of the dominant contribution of resonant terms. Unitarization schemes, as the one of Olsson [56], have proved to be successful in the two body final state when a resonant term is dominant and there is a small background. One multiplies the resonant term by a phase $e^{i\phi}$, with ϕ small in principle, and demands that the resulting amplitude satisfies Watson's theorem, with the global phase of the amplitude in a particular channel equal to the one of the final state. The angles ϕ needed in the problem of $\gamma N \rightarrow \pi N$ are of the order of 10° [57]. In order to have a feeling for what could be the effect of imposing unitarity in our model, we took the $pp \rightarrow pp\pi^+\pi^-$ channel and multiplied the dominant N^* term by $e^{i\phi}$. We see that for values of ϕ up to 20° the cross section changes at the level of 1 %. Rough as the procedure appears to be, it gives hints that unitarity is not a thing to worry much about in the energy domain studied here.

1.6.2 Differential cross sections

Here, we confront model calculations with the experimental invariant mass, momentum and angular distributions of Refs. [9, 12]. Unfortunately these data do not include a normalization and one can, therefore, compare only the shape, but never the strength. The fact that the data of Ref. [9] come from deuterium also makes the analysis far not straightforward.

In Fig. 1.13, invariant mass plots for the $pp \rightarrow pp\pi^+\pi^-$ reaction channel at $T_p = 1370$ MeV are presented, together with the equivalent experimental plots of $n_s pp\pi^+\pi^-$ (n_s denotes a neutron, which is assumed to be spectator). The $M(p\pi^+)$ and $M(p\pi^-)$ spectra show the presence of the $\Delta(1232)$, which can be interpreted as a sign of the dominance of the double- Δ mechanism, as predicted by the model at this energy (see Fig. 1.1). On the other side, the N^* mechanisms are important because they provide the strength at low invariant masses. The $M(p\pi^+\pi^-)$ shows, however, a discrepancy between data and model predictions; the data have a peak around 1.35 GeV while the model favors higher invariant masses. From this distribution one can clearly notice an inconsistency in the experimental data, which exhibit events at values of $M(p\pi^+\pi^-)$ below its threshold of 1.2 GeV.

Next, we show in Fig. 1.14 how the model predictions compare to several angular distributions for the same reaction and energy considered above. The results agree well with the experiment except for the distribution of angles between pions in CM, where the model shows an enhancement of back to back emission of pions that is not confirmed experimentally. We also compare the angular distributions of protons in the CM system with the data of Brunt et al. at two different energies $T_p = 1113$ and 1370 MeV (Fig. 1.15). Unfortunately, the data at the lower energy should be looked with special care since the small number of events precluded any selection of spectator momentum. Notice that the double- Δ mechanisms gives a rather flat histogram; it is appreciably smaller than the other two dominant mechanisms at $T_p = 1113$ MeV and becomes the largest at $T_p = 1370$ MeV. At both energies the tendency of theory and experiment is to favor the emission of protons

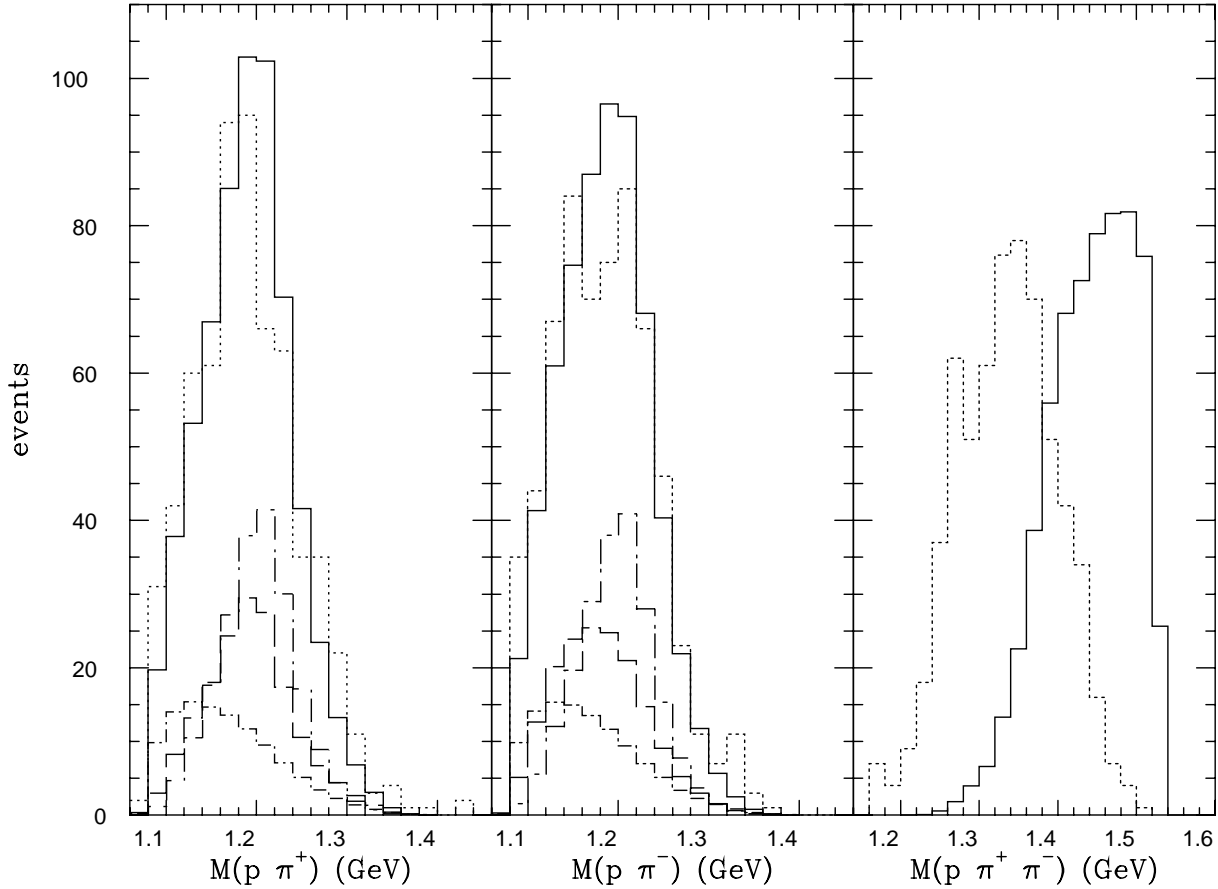


Figure 1.13: Invariant mass plots for the reaction $pp \rightarrow pp\pi^+\pi^-$ at $T_p = 1370$ MeV. The different curves represent the three dominant contributions at this energy: double- Δ mechanisms (long-dash-dotted line), $N^* \rightarrow \Delta\pi$ (long-dashed line) and $N^* \rightarrow N(\pi\pi)_{S-wave}^{T=0}$ (short-dash-dotted line). The solid line stands for the total contribution. The theoretical curves are normalized to the data (dotted line), which correspond to the $n_s pp\pi^+\pi^-$ events with spectator momentum less than 150 MeV from Ref. [9].

in forward and backward directions. In Fig. 1.16, a similar observable is given for the reaction $pn \rightarrow pn\pi^+\pi^-$, now with proton and neutron angular distributions combined in the same plots. Here, the features are basically the same as in the previous case. A possible interpretation of the results of Figs. 1.15 and 1.16 might be that the double- Δ amplitude should be slightly larger with respect to the others at around 1 GeV.

In the following two figures, various invariant mass plots corresponding to the $pn \rightarrow pn\pi^+\pi^-$ channel are presented. In Fig. 1.17, the presence of the Delta resonance is clear in both theoretical and experimental distributions; it is specially prominent in the case of $M(p\pi^+)$ and $M(p\pi^-)$ as expected from the Clebsh-Gordan coefficients. On the other side, Fig. 1.18 shows a discrepancy between our model and the data; both $M(p\pi^+\pi^-)$ and

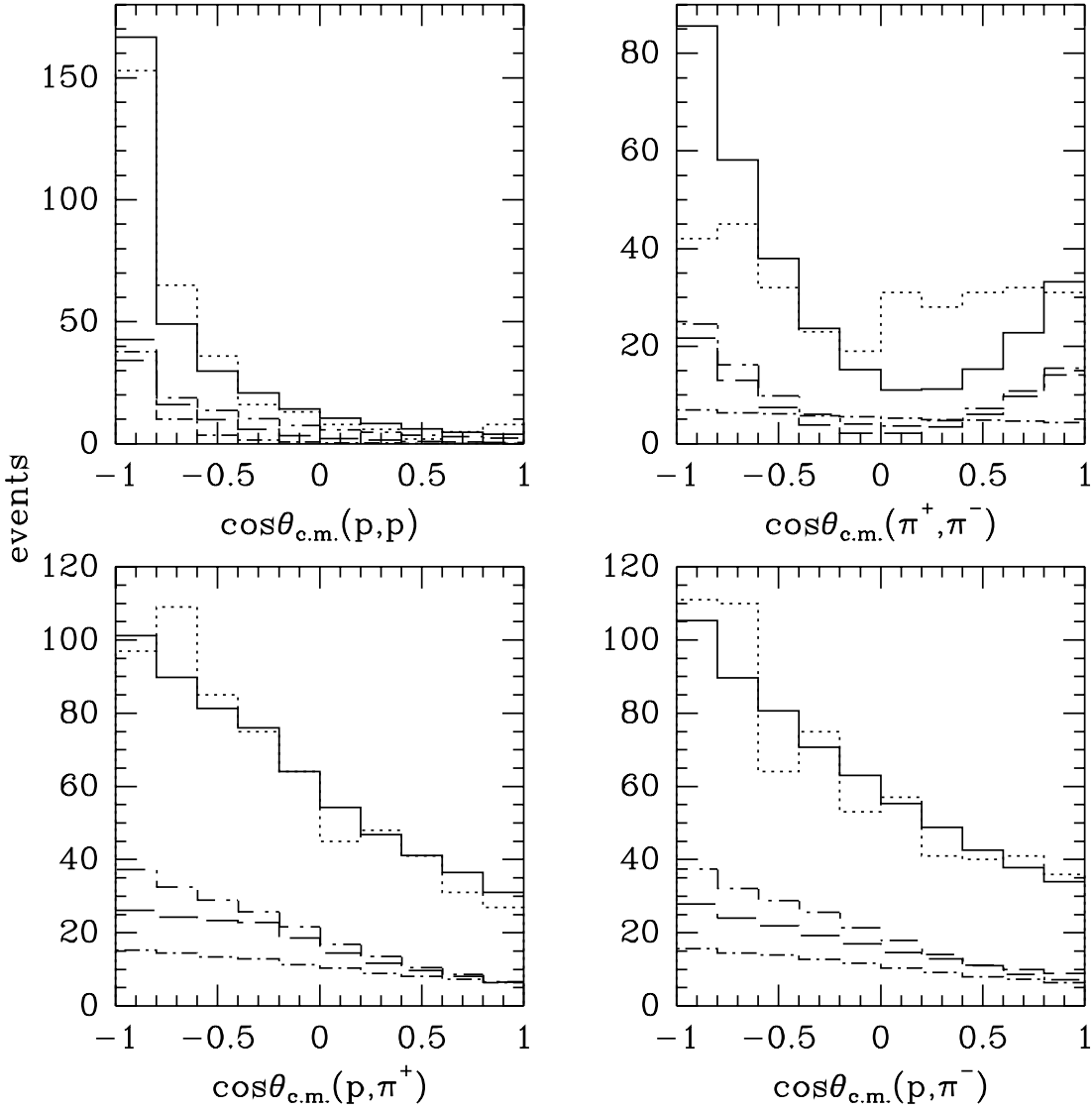


Figure 1.14: Histograms of angles between particles in the $pp\pi^+\pi^-$ CM system at $T_p = 1370$ MeV. The line styles have the same meanings as in Fig. 1.13.

$M(n\pi^+\pi^-)$ theoretical distributions peak at higher invariant masses than the experiment of Brunt et al. [9]. This is basically the same effect observed in Fig. 1.13 although the data are somewhat contradictory since they do not exhibit the same thresholds in spite of coming from the same measurements. The reason of such contradiction might be related with the ambiguity of the definition of the spectator nucleon.

Finally, let us compare our model with the spectra measured by Abdivaliev and collaborators [12]. In Fig. 1.19, $M(\pi^+, \pi^-)$ invariant mass spectrum as well as combined π^+, π^- momentum and angular distributions in the $pn\pi^+\pi^-$ CM system at $T_n = 1029$ MeV are

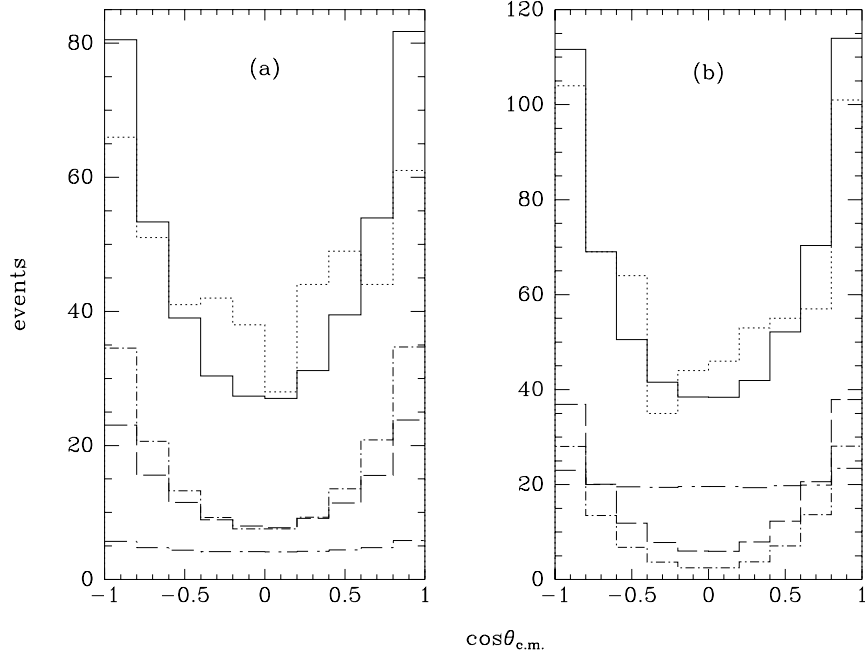


Figure 1.15: Angular distribution of protons in the CM system; (a): $T_p = 1113$ MeV, the experimental plot includes all $n_s pp\pi^+\pi^-$ events; (b): $T_p = 1370$ MeV and spectator momentum < 150 MeV [9]. The line styles have the same meanings as in Fig. 1.13.

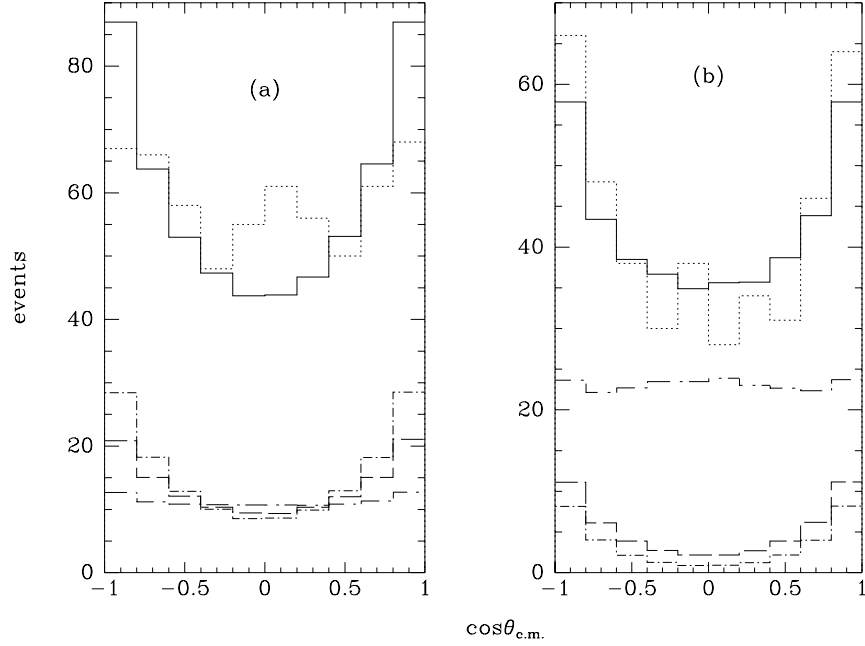


Figure 1.16: Combined plot of proton and neutron angles in the $pn\pi^+\pi^-$ CM system. (a): $T_p = 1113$ MeV, the experimental plot includes all $p_s np\pi^+\pi^-$ events; (b): $T_p = 1370$ MeV and spectator momentum < 200 MeV [9]. The line styles represent the same as in Fig. 1.13.

presented. At this energy, the model predicts that the $N^*(1440)$ mechanisms are the largest ones. Our predictions for 3-momenta and angular distribution of pions are in good agree-

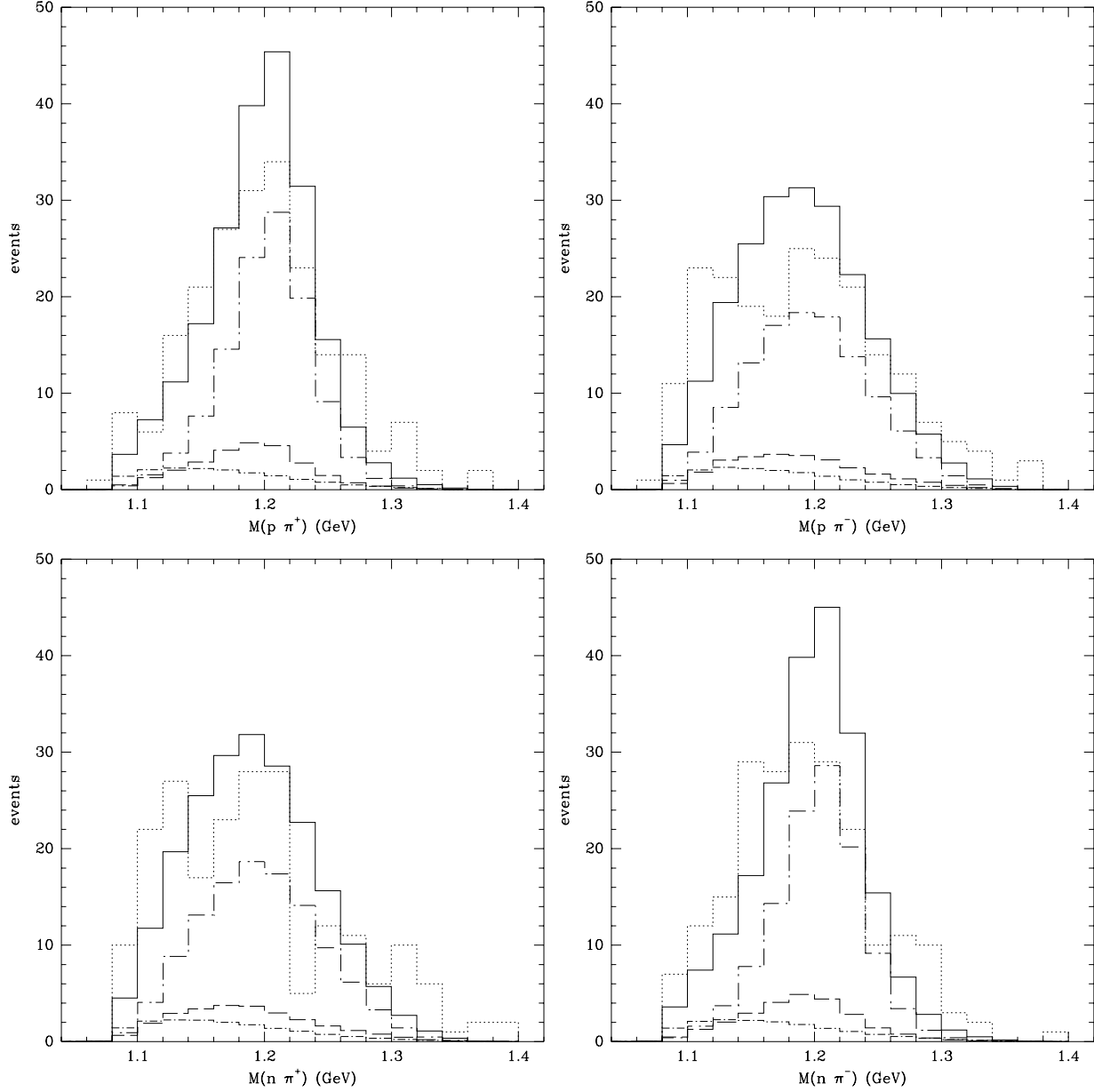


Figure 1.17: Invariant mass plots for the reaction $pn \rightarrow pn\pi^+\pi^-$ at $T_p = 1370$ MeV. The experimental distributions are taken from Brunt et al. [9] and correspond to $p_s p n \pi^+ \pi^-$ events with spectator momentum < 200 MeV. The line styles have the same meanings as in Fig. 1.13.

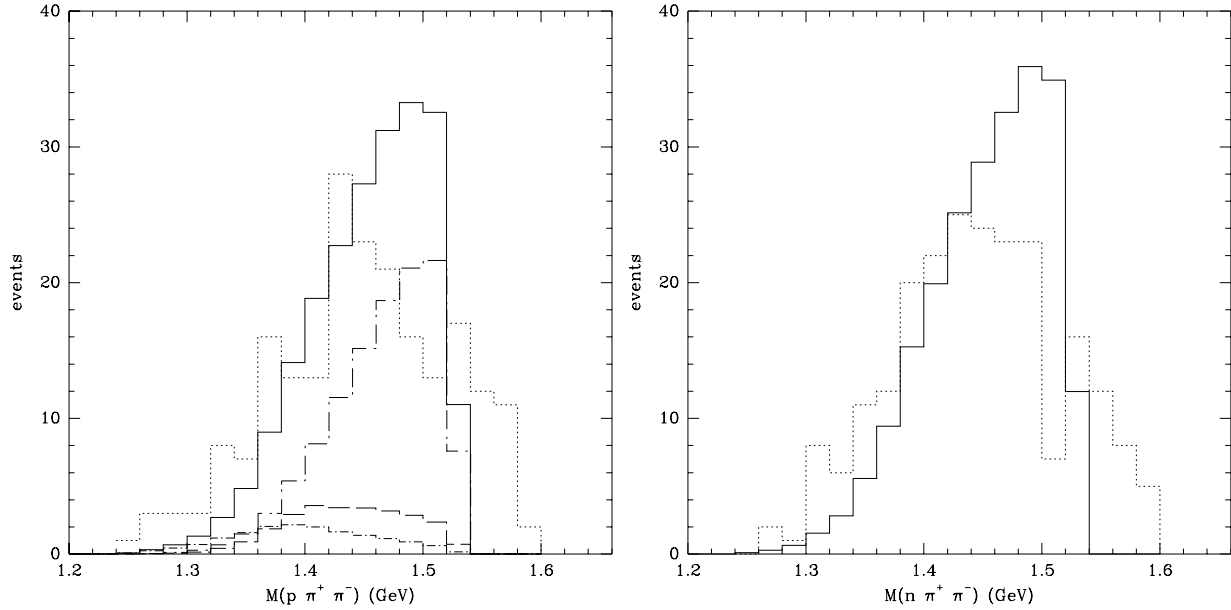


Figure 1.18: Continuation of Fig. 1.17.

ment with the experiment. In the case of the $M(\pi^+, \pi^-)$ spectrum, however, we obtain a maximum at $M(\pi^+, \pi^-) \sim 380 - 400$ MeV while the experiment exhibits it maximum at lower masses. It is interesting to notice that the $N^* \rightarrow N(\pi\pi)_{S-wave}^{T=0}$ mechanism shows the same trend as the experiment. The peak at higher (π^+, π^-) masses seems to be a result of a constructive interference between the dominant mechanisms. Such constructive interference, as will be shown, allows us to explain the data for the $np \rightarrow d\pi\pi$ at a lower energy. This discrepancy is probably an indication of the importance of relativistic corrections.

1.7 Summary

We have constructed a microscopic model for the $NN \rightarrow \pi\pi NN$ reaction consisting of the terms emerging from chiral Lagrangians with nucleons and pions, plus terms involving the excitation of Δ and $N^*(1440)$ resonances. Recent experimental findings about isoscalar N^* excitation in the (α, α') reaction on proton target are used here, leading to the conclusion that in the channels where the two pions can be in a $T = 0$ state ($\pi^+ \pi^-$ and $\pi^0 \pi^0$), the $NN \rightarrow NN^*$ transition, driven by the isoscalar “ σ ” exchange followed by the $N^* \rightarrow N(\pi\pi)_{S-wave}^{T=0}$ decay largely dominates the cross section at low energies. As the energy increases, the $N^* \rightarrow \Delta\pi$ decay channel takes also a share of the cross section and so does the excitation of a Δ in each of the nucleons, which becomes dominant at energies $T_p > 1300$ MeV; this conclusion is evidently supported by the available πN invariant mass plots. Other terms are found to play a minor role. In those reaction channels, where the

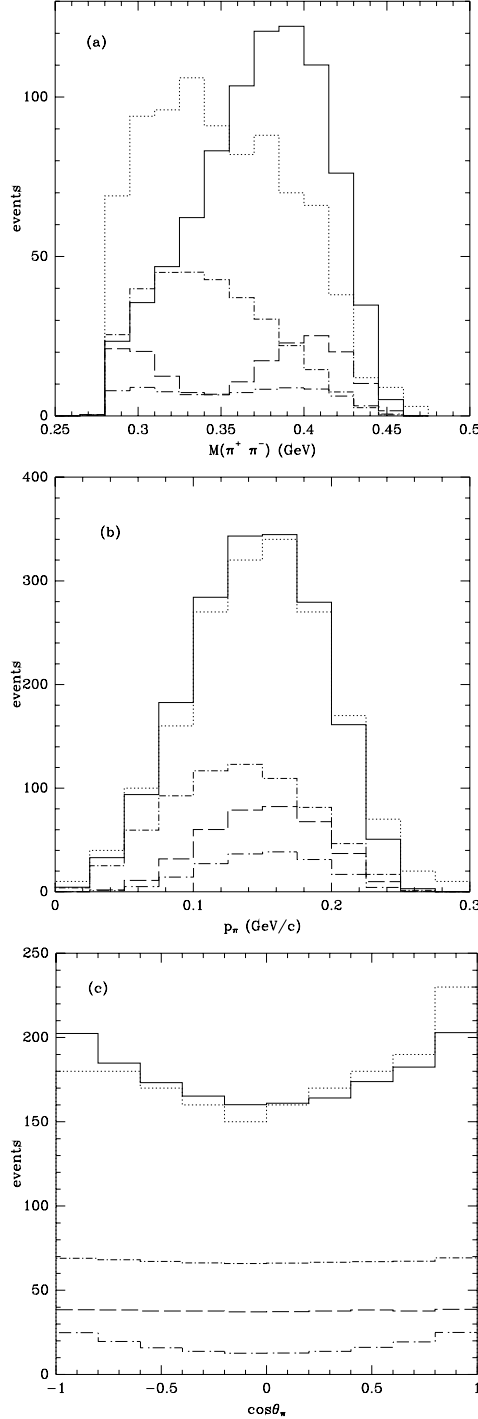


Figure 1.19: Theoretical histograms of the $np \rightarrow np\pi^+\pi^-$ reaction at $T_n = 1029$ MeV compared to the experimental ones of Abdivaliev et al. [12]; (a): $M(\pi^+, \pi^-)$ invariant mass, (b) π^\pm momentum distributions in CM, (c): angular distributions for π^\pm in CM. The line styles represent the same as in Fig. 1.13.

pions cannot have $T=0$ the successive excitation of two Δ on the same nucleon, the Δ excitation on each nucleon, the N^* excitation followed by $\Delta\pi$ decay and even the chiral terms (at low energies) share the strength of the reaction, and one obtains a qualitative agreement with experiment.

Further comparison of our calculation with the data from CELSIUS that are going to be available in the near future, will certainly provide useful information about the properties of resonances and the nucleon-nucleon interaction above the two pion production threshold. The present model is also bound to have repercussions in the study of other double pion production reactions such as $Np \rightarrow d\pi\pi$, $pd \rightarrow {}^3He\pi\pi$ and $dd \rightarrow {}^4He\pi\pi$ that are currently the subject of experimental research in several Laboratories and were actively studied in the past in connection with the still unsolved problem of the ABC effect.

Chapter 2

Final state interaction in $pp \rightarrow pp\pi^+\pi^-$

2.1 Introduction

The study of nucleon-nucleon inelastic collisions provides a powerful tool to deepen our insight into the properties of nucleon-nucleon interactions and baryonic resonances. A large amount of theoretical work on threshold meson production has been performed over the last years [58], stimulated by the precise data obtained at IUCF, CELSIUS and COSY [59]. The extraction of the relevant dynamical mechanisms governing these reactions is, however, not straightforward, due to the presence of nucleon-nucleon interaction effects that should be properly taken into account, specially the NN final state interactions (FSI), which could be strong close to threshold. In many works, it is assumed that the effect of FSI can be factorized from the transition matrix element, and the latter is calculated using plane wave Born approximation [60, 61, 62] (Watson-Migdal scheme). However, this procedure has been criticized by other authors [63, 64]. They argue that the Watson-Migdal procedure gives the correct energy dependence of the total cross section, but not necessarily provides the right strength of the production mechanism.

Our aim here is to study nucleon-nucleon FSI effects in the case of two-pion production. We will consider the reaction channel $pp \rightarrow pp\pi^+\pi^-$ close to threshold, so that we can assume that the production amplitude is dominated by isoscalar excitation of the Roper resonance and its subsequent decay into nucleon and two pions in s-wave, as shown in the previous chapter. This channel has also the advantage that, close to threshold, the strong FSI between protons is completely dominated by the singlet 1S_0 state (the fact that $T + S + L$ must be odd, and $T = 1$ for proton pairs, together with the assumption that $L=0$ imply that $S=1$, i.e. the triplet state is not allowed). On the other side, the electromagnetic repulsion will be another source of distortions. Finally, since the energy of the incoming nucleons has to be high enough to produce two pions, we will neglect initial state interaction effects. This scenario is appreciably interesting provided that the new data from CELSIUS have been measured close to threshold, where FSI effects may be

important.

2.2 The production amplitude

Our production amplitude is described by the diagram of Fig. 2.1. In order to derive it, let

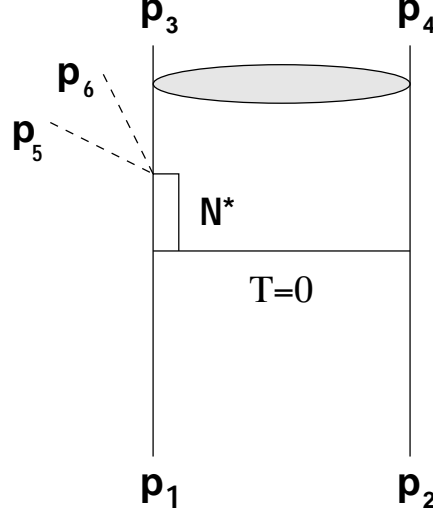


Figure 2.1: Dominant mechanism for $pp \rightarrow pp\pi^+\pi^-$ at low energies with FSI included.

us first consider the case with plane waves in the final state. Excluding trivial kinematical factors, the t matrix is given by

$$\begin{aligned} \langle f | t | i \rangle_{r_3 r_4 r_1 r_2} &\propto -i 2 g_{NN\sigma} g_{N^* N \sigma} \frac{m_\pi^2}{f_\pi^2} \left(c_1^* + \frac{p_5^0 p_6^0}{m_\pi^2} c_2^* \right) \delta_{r_3 r_1} \delta_{r_4 r_2} \\ &\times \int dx_1 dx_2 \frac{dq}{(2\pi)^3} \frac{e^{iq(x_1-x_2)}}{q^2 - m_\sigma^2} F_\sigma^2(q) D_{N^*}(p_{N^*}) e^{-ip_1 x_1} e^{-ip_2 x_2} e^{ip_3 x_1} e^{ip_4 x_2} e^{i(p_5+p_6)x_1} \end{aligned} \quad (2.1)$$

Next we express $\mathbf{x}_1, \mathbf{x}_2$ in terms of the CM and relative coordinates \mathbf{r} and \mathbf{R} respectively

$$\begin{aligned} \mathbf{R} &= \frac{1}{2}(\mathbf{x}_1 + \mathbf{x}_2) \\ \mathbf{r} &= \mathbf{x}_1 - \mathbf{x}_2. \end{aligned} \quad (2.2)$$

Then, after performing the integrals over x_1^0, x_2^0 and \mathbf{R} , which lead to the delta of energy and momentum conservation, one obtains the following expression for the amplitude

$$\begin{aligned} \mathcal{M}_{r_3 r_4 r_1 r_2}(p_3, p_4, p_1, p_2) &= -i 2 g_{NN\sigma} g_{N^* N\sigma} \frac{m_\pi^2}{f_\pi^2} \left(c_1^* + \frac{p_5^0 p_6^0}{m_\pi^2} c_2^* \right) \delta_{r_3 r_1} \delta_{r_4 r_2} \\ &\times \int d\mathbf{r} \frac{d\mathbf{q}}{(2\pi)^3} \frac{1}{q^2 - m_\sigma^2} F_\sigma^2(q) D_{N^*}(p_{N^*}) e^{-i\frac{(\mathbf{p}_3 - \mathbf{p}_4)}{2}\mathbf{r}} e^{-i\mathbf{P}\mathbf{r}} \end{aligned} \quad (2.3)$$

where

$$q^0 = p_4^0 - p_2^0, \quad \mathbf{P} = \mathbf{q} + \frac{1}{2}(\mathbf{p}_5 + \mathbf{p}_6 + \mathbf{p}_2 - \mathbf{p}_1), \quad p_{N^*} = p_1 - q. \quad (2.4)$$

In the spirit of the DWBA, we substitute

$$e^{-i\frac{(\mathbf{p}_3 - \mathbf{p}_4)}{2}\mathbf{r}} \rightarrow \varphi_{\mathbf{k}}(\mathbf{r}), \quad \mathbf{k} = \frac{\mathbf{p}_4 - \mathbf{p}_3}{2} \quad (2.5)$$

and define

$$\tilde{\varphi}_{\mathbf{k}}(\mathbf{P}) = \int d\mathbf{r} \varphi_{\mathbf{k}}(\mathbf{r}) e^{-i\mathbf{P}\mathbf{r}} \quad (2.6)$$

as the pp wave function in momentum space, obtaining

$$\begin{aligned} \mathcal{M}_{r_3 r_4 r_1 r_2}^{fsi}(p_3, p_4, p_1, p_2) &= -i 2 g_{NN\sigma} g_{N^* N\sigma} \frac{m_\pi^2}{f_\pi^2} \left(c_1^* + \frac{p_5^0 p_6^0}{m_\pi^2} c_2^* \right) \delta_{r_3 r_1} \delta_{r_4 r_2} D_{N^*}(p_5 + p_6 + p_3) \\ &\times \int \frac{d\mathbf{q}}{(2\pi)^3} \frac{1}{q^2 - m_\sigma^2} F_\sigma^2(q) \tilde{\varphi}_{\mathbf{k}}(\mathbf{P}), \end{aligned} \quad (2.7)$$

where the 4-momentum of the N^* propagator has been approximately taken to be equal to the sum of the pion momenta and the asymptotic nucleon momentum ($p_3 + p_5 + p_6$) and taken out of the integral, instead of using $p_{N^*} = p_1 - q$; this approximation, whose accuracy has been numerically found to be good ($\leq 1\%$), simplifies the calculation.

From Eq. (2.3), one can easily derive the expression for the amplitude within the Watson-Migdal approximation [65]. If the interaction takes place at very small distances, much smaller than the typical values of k^{-1} , then the precise \mathbf{r} dependence of $\varphi_{\mathbf{k}}(\mathbf{r})$ should be unimportant and one could perform the following substitution in Eq. (2.3)

$$e^{-i\frac{(\mathbf{p}_3 - \mathbf{p}_4)}{2}\mathbf{r}} \rightarrow \varphi_{\mathbf{k}}(\mathbf{r}) \approx \frac{1}{J_0(k)} e^{-i\frac{(\mathbf{p}_3 - \mathbf{p}_4)}{2}\mathbf{r}}, \quad (2.8)$$

where $J_0(k)$ is the s-wave Jost function. The approximation written above is exact in the limit of $\mathbf{r} \rightarrow 0$. The amplitude then reads

$$\mathcal{M}_{r_3 r_4 r_1 r_2}^{fsi}(p_3, p_4, p_1, p_2) = \frac{1}{J_0(k)} \mathcal{M}_{r_3 r_4 r_1 r_2}^{free}(p_3, p_4, p_1, p_2). \quad (2.9)$$

In the effective range approximation for the s-wave scattering phase shifts

$$kcot\delta_S(k) \approx -\frac{1}{a_0} + \frac{1}{2}r_0k^2 \quad (2.10)$$

the inverse of the Jost function is given by [62]

$$\frac{1}{J_0(k)} = \frac{(k^2 + \alpha^2)(r_0/2)}{-1/a_0 + (r_0/2)k^2 - ik} \quad (2.11)$$

where

$$\alpha = \frac{1}{r_0} \left(1 + \sqrt{1 - \frac{2r_0}{a_0}} \right) \quad (2.12)$$

Notice that the inverse of the Jost function has the required property that it goes to unity for large values of k , where FSI should disappear [65]. Here we shall compare the results evaluated with this approximation to those found with the more accurate formula of Eq. (2.7).

2.3 Nucleon-nucleon 1S_0 wave function from a separable potential

At this stage, we should find an appropriate wave function to evaluate the amplitude. The optimal choice would be to use the 1S_0 wave function that arises directly from the solution of the Schrödinger equation with a realistic potential like Bonn or Paris potentials [30, 66]. However, the fact that we have four particles in the final state, and the difficulties in obtaining a good parameterization of the wave function for different asymptotic momenta, makes this task quite complicated and imposes the need of strong approximations [4]. For this reason, we will follow here an alternative approach and take a wave function obtained from a separable potential. With such wave function, one can reproduce the basic properties of the NN interaction like the scattering length, effective radius and phase shifts, with the significant advantage that it is possible to obtain an analytic expression for it. In fact, let us consider a generalized form of the Schrödinger equation for the two-nucleon system with a non-local potential [67]

$$-\frac{1}{2\mu} \nabla^2 \varphi(\mathbf{r}) + \int d\mathbf{r}' V(\mathbf{r}, \mathbf{r}') \varphi(\mathbf{r}') = E \varphi(\mathbf{r}) \quad (2.13)$$

with $\mu = M/2$ being the two-nucleon reduced mass. For $V(\mathbf{r}, \mathbf{r}') = V(\mathbf{r})\delta(\mathbf{r} - \mathbf{r}')$ this reduces to the usual Schrödinger equation with a local potential. In momentum space one has

$$\frac{1}{M} (\mathbf{p}^2 - \mathbf{k}^2) \tilde{\varphi}(\mathbf{p}) = - \int \frac{d\mathbf{p}'}{(2\pi)^3} V(\mathbf{p}, \mathbf{p}') \tilde{\varphi}(\mathbf{p}') \quad (2.14)$$

where

$$V(\mathbf{p}, \mathbf{p}') = \langle \mathbf{p} | V | \mathbf{p}' \rangle = \int d\mathbf{r} d\mathbf{r}' e^{-i\mathbf{p}\mathbf{r}} e^{i\mathbf{p}'\mathbf{r}'} V(\mathbf{r}, \mathbf{r}'). \quad (2.15)$$

Following Refs. [68, 69], where a fit to p-n and p-p phase shifts was performed for various partial waves, we take $V(\mathbf{p}, \mathbf{p}')$ to be

$$V(\mathbf{p}, \mathbf{p}') = \lambda_1 g_1(p) g_1(p') + \lambda_2 g_2(p) g_2(p') \quad (2.16)$$

with $p = |\mathbf{p}|, p' = |\mathbf{p}'|$ and

$$\begin{aligned} g_1(p) &= \frac{1}{p^2 + \beta_{11}^2} + \gamma_1 \frac{p^2}{(p^2 + \beta_{12}^2)^2} \\ g_2(p) &= \frac{p^2}{(p^2 + \beta_{21}^2)^2} + \gamma_2 \frac{p^4}{(p^2 + \beta_{22}^2)^3}. \end{aligned} \quad (2.17)$$

With this potential, and for the scattering problem, the solution of Eq. (2.14) is

$$\tilde{\varphi}_{\mathbf{k}}(\mathbf{p}) = (2\pi)^3 \delta(\mathbf{p} - \mathbf{k}) + \frac{M}{k^2 - p^2 + i\epsilon} [\lambda_1 g_1(p) \alpha_1(k) + \lambda_2 g_2(p) \alpha_2(k)], \quad (2.18)$$

with

$$\alpha_i(k) = \int \frac{d\mathbf{q}}{(2\pi)^3} g_i(q) \tilde{\varphi}_{\mathbf{k}}(\mathbf{q}) \quad i = 1, 2. \quad (2.19)$$

Multiplying Eq. (2.18) by $g_{1(2)}(p)/(2\pi)^3$ and integrating over \mathbf{p} , one gets a system of two linear equations for $\alpha_{1(2)}(k)$ whose solutions are

$$\begin{aligned} \alpha_1(k) &= r [g_1 - \lambda_2 (g_1 \mathcal{I}_{22} - g_2 \mathcal{I}_{12})] \\ \alpha_2(k) &= r [g_2 - \lambda_1 (g_2 \mathcal{I}_{11} - g_1 \mathcal{I}_{12})] \end{aligned} \quad (2.20)$$

with

$$r = [1 - \lambda_1 \mathcal{I}_{11} - \lambda_2 \mathcal{I}_{22} + \lambda_1 \lambda_2 (\mathcal{I}_{11} \mathcal{I}_{22} - \mathcal{I}_{12}^2)]^{-1} \quad (2.21)$$

and

$$\mathcal{I}_{ij}(k) = M \int \frac{d\mathbf{q}}{(2\pi)^3} \frac{g_i(q) g_j(q)}{k^2 - q^2 + i\epsilon} \quad i, j = 1, 2. \quad (2.22)$$

These integrals can be calculated analytically for the given choice of $g_{1(2)}$; their explicit expressions are given in Appendix D. Once we have the solution of the Schrödinger equation, it is straightforward to obtain the 1S_0 phase shifts $\delta_S(k)$

$$\cot \delta_S(k) = i - \frac{4\pi}{Mk} [\lambda_1 g_1(k) \alpha_1(k) + \lambda_2 g_2(k) \alpha_2(k)]^{-1} \quad (2.23)$$

as well as the scattering length (a_0) and effective radius (r_0), defined from the expansion of $k \cot \delta_S(k)$ in powers of k^2

$$kcot\delta_S(k) = -\frac{1}{a_0} + \frac{1}{2}r_0k^2 + \dots \quad (2.24)$$

With these ingredients, we can make use of the set of parameters obtained in Refs. [68, 69] for the strong part of the NN potential, from a fit to the experimental values of a_0 , r_0 and $k \cot \delta_S(k)$. The resulting phase shifts for the pp channel as a function of the incoming

	n-p	p-p
β_{11} (fm $^{-1}$)	1.04556	0.8131678
β_{12} (fm $^{-1}$)	1.30148	1.288463
β_{21} (fm $^{-1}$)	3.66099	7.496476
β_{22} (fm $^{-1}$)	2.05321	1.661386
γ_1	0.563456	2.698168
γ_2	0.991115	0.3270664
λ_1 (MeV fm $^{-1}$)	$-52.7856/(2\pi^2)$	$-17.87098/(2\pi^2)$
λ_2 (MeV fm $^{-1}$)	$48492.3/(2\pi^2)$	$82710.93/(2\pi^2)$

Table 2.1: Numerical values of the separable potential parameters [68, 69].

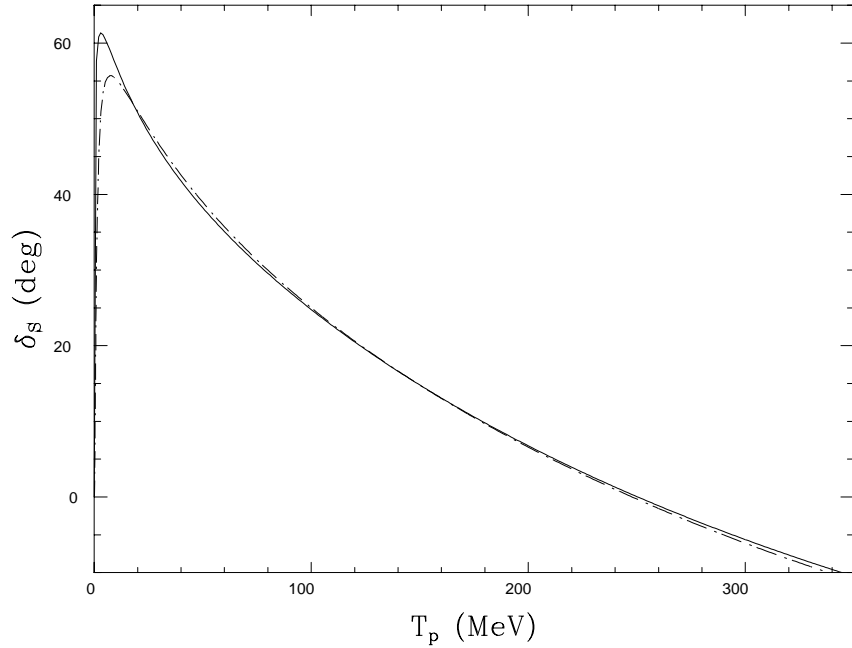


Figure 2.2: 1S_0 p-p phase shifts as a function of LA kinetic energy. The solid line is obtained from Eq. (2.23) with the parameters of Table 2.1, and the dash-dotted one is from Nijmegen PWA93 [70].

proton kinetic energy in LA is shown in Fig. 2.2, compared to the corresponding ones from

the Nijmegen multienergy partial wave analysis (PWA93) [70]. The overall agreement is excellent, except at very low energies where the Coulomb repulsion, not considered in our calculation, although taken into account for the fit [69], plays an important role. Notice that the anzatz of Eq. (2.16) for the separable potential is suited to take into account the repulsion at short distances (if λ_1 and λ_2 have opposite signs) as becomes clear from the fact that the phase shifts become negative at $T_p \approx 250$ MeV. The pioneering work of Yamaguchi [71] assumed only one term in the potential (the first of g_1) and produced, therefore, positive phase shifts. Apart from that, in the construction of the potential [68], care was taken that its off-shell behavior was reasonable i.e. similar to that of the realistic Paris potential.

2.4 Results and discussion

With the expression of Eq. (2.18) for the wave function, evaluated using the set of parameters of Table 2.1 for the p-p channel, one can substitute Eq. (2.7) in Eq. (1.24) in order

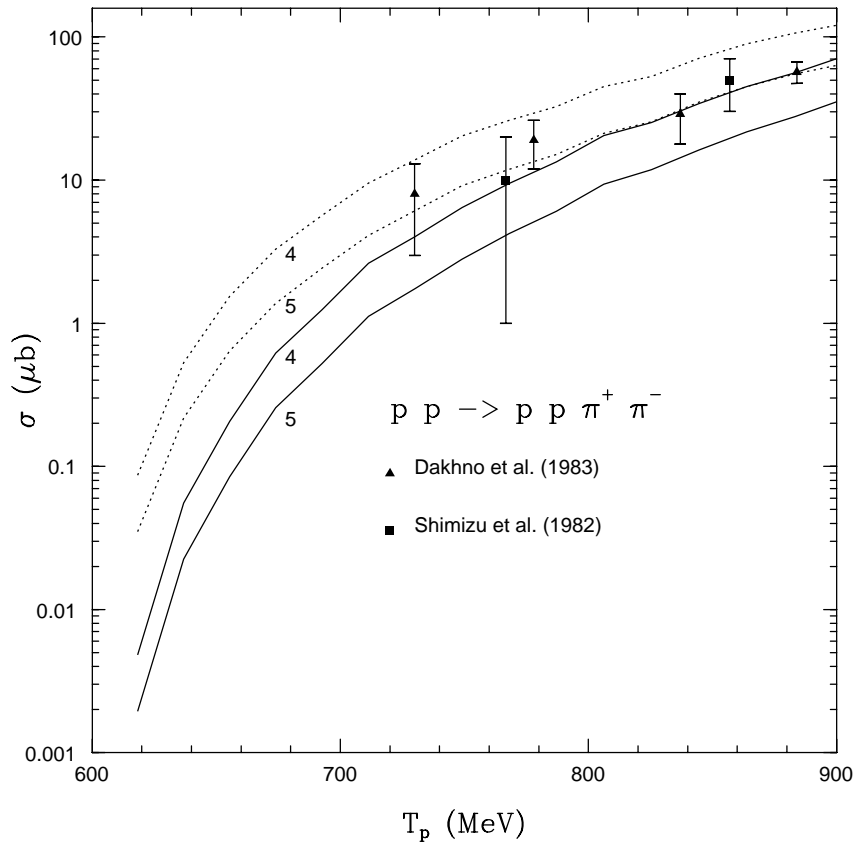


Figure 2.3: Total cross section for $pp \rightarrow pp\pi^+\pi^-$ with (dotted lines) and without (solid lines) FSI. Labels 4 and 5 stand for the choice of c_1^* and c_2^* parameters (see Fig. 1.3).

to see how the total cross section is modified by the strong part of the FSI. We restrict ourselves to $T_p < 900$ MeV, since it is the region where the mechanism of Fig. 2.1 is clearly dominant, as can be viewed in Figs. 1.6, 1.7(b). FSI causes an enhancement of more than a factor 10 close to threshold and about a factor 2 at $T_p \sim 900$ MeV. Such increase brings the calculation with point 5 much closer to the data. Next, we study how FSI affects differential cross sections. In particular we choose the proton-proton invariant mass distribution, since it is particularly sensitive to the effect of FSI. The plot of Fig. 2.4 is made for $T_p = 750$ MeV, corresponding to the energy of the first measurements at CELSIUS [13]. The figure displays a large enhancement at low p-p masses, as one would naively

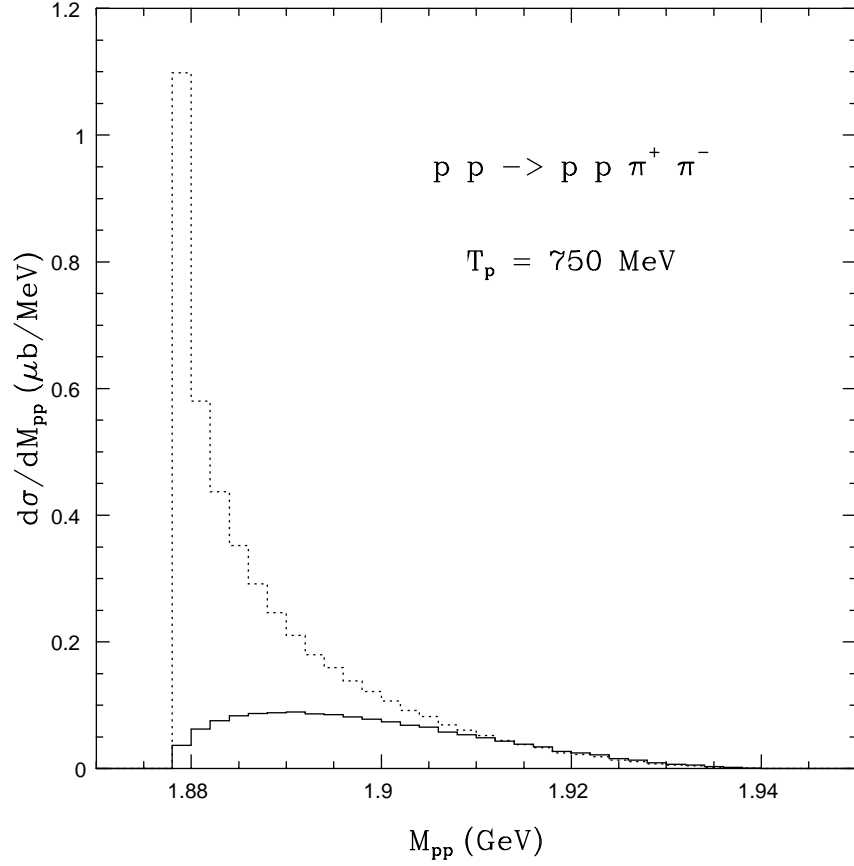


Figure 2.4: Proton-proton invariant mass distribution with (dotted line) and without (solid line) FSI. The choice of $c_{1(2)}^*$ corresponds to point 5.

expect since FSI should be stronger for those protons that travel together. However, one should bear in mind that precisely at low masses, the Coulomb repulsion not considered here could be important, inducing some decrease of the differential cross section.

At this stage, we would like to compare the previous results with the Watson-Migdal approximation discussed at the end of Sec. 2.2, where the FSI was accounted by factor (given by the inverse of the Jost function) that multiplies the free amplitude. For the sake

of consistency, we take $a_0 = -19.1$ fm and $r_0 = 2.85$ fm; these values are obtained from Eqs. (2.23),(2.24) with the choice of parameters considered above. The total cross section is found to be very similar to the one we got with the full wave function, specially at lower energies. Meanwhile, the invariant mass distribution shows small but appreciable differences, namely, a larger yield at higher pp masses, and a decrease at lower ones. This approach

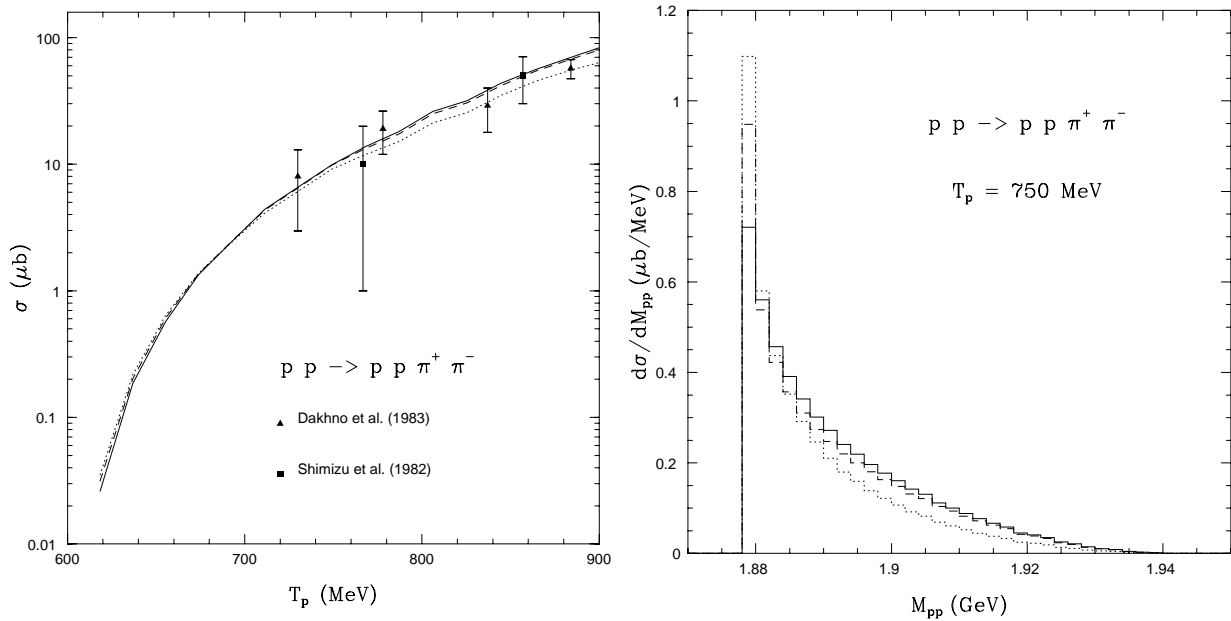


Figure 2.5: Different approaches to FSI. The dotted lines are the same as in Figs. 2.3,2.4. The dashed lines correspond to the Watson-Migdal approximation using the effective range expansion of Eq. 2.11 with $a_0 = -19.1$ fm and $r_0 = 2.85$ fm obtained from the strong p-p separable potential potential. In the solid lines, Coulomb repulsion is included by taking the experimental values $a_0 = -7.83$ fm and $r_0 = 2.80$ fm.

has the advantage that the effect of Coulomb repulsion, can be easily incorporated, just substituting a_0 and r_0 by their experimental values $a_0 = -7.83$ fm and $r_0 = 2.80$ fm [72]. Once more, the effect of this correction in the total cross section appears to be negligible. In the differential cross section, the enhancement at low masses is reduced (from 0.95 to 0.72 $\mu\text{b}/\text{MeV}$ at $M_{pp} \approx 1.88$ GeV) as expected. However, this result should be taken only as a qualitative indication of the relevance of Coulomb repulsion in the absence of a more accurate calculation, since, as pointed out in the literature in the case of single pion production [63, 64], this procedure might not be well justified.

2.5 Summary

In this chapter, we have studied the effect of NN final state interaction in double pion production at low energies and for the $pp \rightarrow pp\pi^+\pi^-$ channel, where the reaction mechanism is simple. The pp 1S_0 wave function, which appears in the derivation of the amplitude has been obtained as the solution of the Schrödinger equation with a separable potential, whose parameters fit the pp phase shifts. An important enhancement (up to a factor 10 close to threshold) has been found for the total cross section. This increase is concentrated at low pp invariant masses, since the FSI is stronger when the protons move in the same direction. We have also tested an approximation of the FSI based on the multiplication of the free amplitude by a factor that reflects how the wave function is modified at very short distances with respect to the undistorted one. We have obtained that, for the mechanism considered here, the results are compatible with those given by a more accurate expression. Then, we have shown that corrections due to the electromagnetic repulsion can be appreciable for differential cross sections, and, therefore, a more accurate evaluation of its effects should be undertaken.

Our main conclusion is that, in order to be able to extract physically meaningful information about the relevant dynamics involved in double pion production from the new generation of experiments close to threshold, the final state interaction must be carefully studied and properly taken into account in the analyses.

Chapter 3

The $np \rightarrow d(\pi\pi)^0$ reaction

3.1 Introduction

Most of the work, both experimental and theoretical, on two-pion production in nucleon-nucleon collisions was performed in the seventies, and in connection with the so called ABC effect. The ABC anomaly is an enhancement in the missing mass spectra close to the $\pi\pi$ production threshold ($M_X \approx 300 - 350$ MeV). It was first observed in an experiment on $pd \rightarrow {}^3HeX$ by A. Abashian, N. E. Booth and K. M. Crowe [73] carried on at the Berkeley 184 inc synchrocyclotron. The anomaly was detected as a sharp peak in the 3He momentum spectrum at a fixed LA angle of 11.7° and for incident proton energies ranging from 624 to 743 MeV. It was initially believed to be the sign of a new particle or $\pi\pi$ resonance. No straightforward evidence for the ABC particle was found in the reaction $pd \rightarrow {}^3HX$, so it was concluded that the isospin of the ABC particle $T_{ABC} = 0$. Later, similar structures were discovered in $np \rightarrow dX$ [74, 12, 75] and were again absent in the case of $T=1$ pion pairs: $pp \rightarrow d\pi\pi$ [76]. The reaction $dd \rightarrow {}^4HeX$ leads to a pure $T_x = 0$, which is probably the reason for the more pronounced peaks in this case [77]. The full set of experiments reveals that the mass and the width of the effect vary according to the kinematic conditions, excluding any interpretation of it as a resonance or a new particle. Moreover, in all three reactions: $np \rightarrow dX$, $pd \rightarrow {}^3HeX$ and $dd \rightarrow {}^4HeX$, there are evidences that the ABC effect disappears at low beam energies [78, 3, 79] suggesting that any explanation should involve strongly energy and angular dependent amplitudes in order to reproduce the quite different dynamics observed in the different energy regions.

Theoretical investigations have focused on the $np \rightarrow dX$ reaction since it is the simplest one where the effect has been observed. Two different theoretical models have been developed attempting to describe the data without assuming the existence of a new hadron or a strong pion-pion interaction. The first one [80] proposes a double-nucleon exchange model consisting of three separated diagrams summed incoherently in order to produce the three peaks observed by Plouin et al. in the forward direction [75]. The approach followed in this work in the evaluation of the npd vertex and the nucleon exchange amplitude does not allow to predict the absolute normalization. In the relativistic model of Bar-Nir,

Risser and Shuster [81], after a pion exchange an intermediate state of two Δ 's is formed with a subsequent decay into the $d\pi\pi$ state. In spite of the fact that both these models show the characteristic triple-peak structure at a kinetic energy $T_n = 1160$ MeV of the incoming neutron beam (where the ABC bumps are observed), they fail in describing the isotropic angular behavior [75]. A recent paper [82] attempts to improve the $\Delta\Delta$ model on the basis of a coupled channel formalism, which allows to include the residual interaction within the intermediate $\Delta\Delta$ systems; this calculation also falls short at higher angles. A better angular dependence were achieved in Ref. [83], where effective chiral Lagrangians at tree level were considered in the evaluation of the amplitudes coming from more than 80 diagrams. Chiral bag model form factors were used for the vertices and the bag radius was taken as a free parameter and fitted to the absolute value of the differential cross section. The deuteron wave function included the d-wave part, which had been neglected in the previous works. The agreement obtained with the data of Plouin et al. [75] at two deuteron angles ($\theta_{lab} = 0^\circ, 10.5^\circ$) is quite good. The major shortcoming of this approach is the lack of intermediate nucleon excited states at an energy where they are important, specially the Δ . The authors chose a value of the bag radius to fit the data and claimed that this choice effectively accounts for the contribution of resonances.

An important step towards the understanding of the ABC effect has been taken in Ref. [84], where the 4He spectra from the $dd \rightarrow {}^4HeX$ reaction at a deuteron beam energy of 1250 MeV [77] has been explained assuming that pions are independently produced in reactions involving two different pairs of nucleons from the projectile and target deuterons. This model explains the ABC effect through the production of p-wave pions that emerge with parallel momenta. It does not, however, describe the data close to threshold, where the data are structureless and consistent with phase space [79]; moreover, the predicted total cross sections are a factor of about 20 too low. Such fact calls for some other mechanism, which will be responsible for the behavior at threshold.

Here, I focus the attention on the deuteron spectrum in $np \rightarrow d(\pi\pi)^0$ measured by Hollas and collaborators [78] using a nearly monokinetic neutron beam with central momentum $p_n = 1.463$ GeV/c. This experiment is somewhat similar to the one of Plouin et al. [75], but at lower energies ($T_n = 795$ MeV in [78] vs 1160 MeV in [75]). Therefore, the analysis is simpler since, once the π^0 peaks are subtracted, only the double pion production mechanism is present (at higher energies, other mechanisms like three pion production and subthreshold η production could contribute [85]). Apart from that, one expects that, being closer to threshold, the reaction mechanism might be simpler. The ABC peaks are not present in the data; they rather show a well defined bump at high $\pi\pi$ missing masses, in disagreement with the models available in the literature [80, 81]. From this comparison, the authors concluded [78] that neither double- Δ formation nor double-nucleon exchange provides the appropriate description of the reaction at $p_n = 1.46$ GeV/c. A similar enhancement has also been observed for the reaction $pd \rightarrow {}^3He\pi^+\pi^-$, which is being studied using a beam of protons from COSY (MOMO experiment) [3], at a Q value close to the one of the experiment by Hollas et al. [78].

Our aim is to show that the deuteron spectra for $np \rightarrow d(\pi\pi)^0$ at $p_n = 1.46$ GeV/c can be understood as a consequence of the interference of two mechanisms involving the

excitation of the Roper resonance $N^*(1440)$ and its subsequent decay into $N(\pi\pi)_{S-wave}^{T=0}$ and $\Delta\pi$ respectively [86]. The model will be also compared to the data at higher energies; there, it is unable to describe the details of the spectra and angular distributions, but shows the appearance of the so called ABC peaks. In spite of this, there is a clear indication that the $\Delta\Delta$ mechanism alone is not sufficient to solve this long standing problem.

3.2 The model

The model is schematically presented in Fig. 3.1. It is a reduced version of the model presented in Chapter 1 and Ref. [4], modified for the case where one has a deuteron instead of two free nucleons in the final state. The choice of the mechanisms was based on their contribution to the total cross section for the $pn \rightarrow pn\pi^+\pi^-$ reaction; the situation for the $pn \rightarrow pn\pi^0\pi^0$ channel is similar. At $T_p = 800$ MeV, the mechanism with $N^* \rightarrow N(\pi\pi)_{S-wave}^{T=0}$ gives $\sigma \sim 11 \mu b$, being by far the most important. The second largest contribution comes from $N^* \rightarrow \Delta\pi$ with $\sigma \sim 0.5 \mu b$; as we will see, in the case of a deuteron in the final state, its contribution is larger with respect to the dominant $N^* \rightarrow N(\pi\pi)_{S-wave}^{T=0}$ and crucial to obtain the right shape. All other mechanisms give $\sigma \lesssim 0.3 \mu b$; I do not include them all, but just the double- Δ ($\sigma \sim 0.1 \mu b$) one since it becomes the largest contribution at $T_p > 1140$ MeV. In fact, at $T_p = 1160$ MeV, which correspond to the neutron beam energy of the experiment of Plouin et al. [75], where the ABC peaks were directly observed in the $np \rightarrow dX$ reaction, the $pn \rightarrow pn\pi^+\pi^-$ total cross sections are $\sigma \sim 160 \mu b$ for both $N^* \rightarrow N(\pi\pi)_{S-wave}^{T=0}$ and $N^* \rightarrow \Delta\pi$ mechanisms, while $\sigma \sim 200 \mu b$ for the double- Δ one. The inclusion of the later mechanisms will also allow us to make contact with the model of Ref. [81].

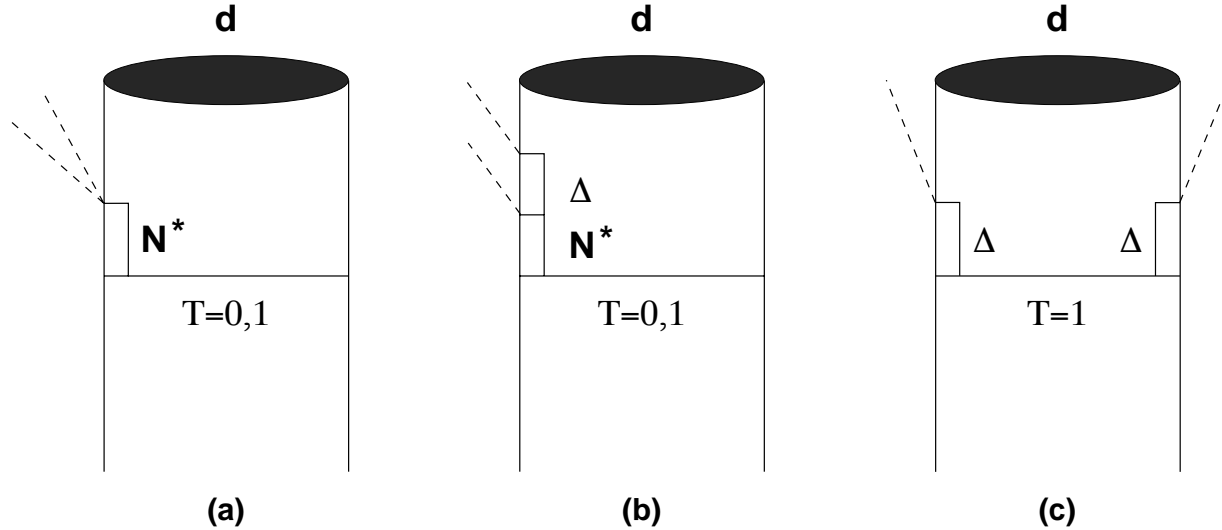


Figure 3.1: Set of diagrams of the model.

The deuteron momentum spectrum is the sum of the $\pi^+\pi^-$ and the $\pi^0\pi^0$ contributions.

In the Laboratory frame, the charged pions piece is given by

$$\frac{d^2\sigma}{dp'_d d\Omega'_d} = \frac{1}{4} \frac{1}{(2\pi)^5} \frac{MM_d(p'_d)^2}{E'_d p'_n p_d} \left[\int dE_\pi d\varphi_\pi \frac{1}{4} \sum_{Rr_1r_2} |\mathcal{M}_{Rr_1r_2}|^2 (\hat{\mathcal{R}}^{-1} \mathbf{p}_\pi^R) \right]_{CM}. \quad (3.1)$$

Here, E'_d and p'_d are the deuteron energy and the modulus of its momentum, both in LA frame; p_d is the modulus of the deuteron momentum in CM; M and M_d stand for the nucleon and deuteron masses respectively. The integral in brackets must be calculated with all the kinematical variables defined in CM; it runs over the polar angle and the energy of one of the outgoing pions. The amplitude squared is summed over the deuteron spin (R) and averaged over the spins of the incoming nucleons (r_1, r_2). The rotation matrix $\hat{\mathcal{R}}^{-1}$ has the same structure as the one defined in Eq. (1.26); by choosing the coordinate axes in such a way that the third axis coincides with the direction of the incoming particle, and the deuteron 3-momentum belong to the P_{23} plane, one gets

$$\hat{\mathcal{R}}^{-1} = \begin{pmatrix} 0 & -1 & 0 \\ \cos\theta & 0 & \sin\theta \\ -\sin\theta & 0 & \cos\theta \end{pmatrix} \quad (3.2)$$

with

$$\cos\theta = \frac{(\mathbf{p}_d)_3}{p_d} \quad \sin\theta = \sqrt{1 - \cos^2\theta} \quad (3.3)$$

For the neutral pions channel, the expression is the same but with an extra $1/2$ factor, which is a consequence of having two identical pions in the final state. The difference of masses between charged and neutral pions is taken into account for the phase space, but isospin symmetry is assumed in the calculation of the amplitude.

The amplitude can be expressed as

$$\begin{aligned} \mathcal{M}_{Rr_1r_2} = & \sum_{r'_1 r'_2} \left(\frac{1}{2} r'_1 \frac{1}{2} r'_2 \right| 1R \int \frac{d\mathbf{q}}{(2\pi)^3} D_{T=0,1}(q) \times \\ & \left\{ \left(\langle pr'_1 | \hat{V}_1 | pr_1 \rangle \langle nr'_2 | \hat{V}_2 | nr_2 \rangle - \langle nr'_1 | \hat{V}_1 | pr_1 \rangle \langle pr'_2 | \hat{V}_2 | nr_2 \rangle \right) \tilde{\varphi}_d(\mathbf{P}_2) \right. \\ & \left. + \left(\langle pr'_1 | \hat{V}_2 | pr_1 \rangle \langle nr'_2 | \hat{V}_1 | nr_2 \rangle - \langle nr'_1 | \hat{V}_2 | pr_1 \rangle \langle pr'_2 | \hat{V}_1 | nr_2 \rangle \right) \tilde{\varphi}_d(\mathbf{P}_1) \right\} \end{aligned} \quad (3.4)$$

where $\tilde{\varphi}_d(\mathbf{P})$ is the s-wave deuteron wave function in momentum space, normalized as

$$\int \frac{d\mathbf{k}}{(2\pi)^3} \tilde{\varphi}_d^2(\mathbf{k}) = 1. \quad (3.5)$$

The d-wave part has been neglected; I will come back to this question later. For the wave function, different expressions and parameterizations can be used [66, 30, 87]. Their explicit expressions are given in Appendix E. The value of $\mathbf{P}_{1(2)}$ depends on the mechanism;

for those of Figs. 3.1 a and 3.1 b, $\mathbf{P}_{1(2)} = \mathbf{q} + \mathbf{p}_{1(2)} - \mathbf{p}_d/2$ and for the $\Delta - \Delta$ mechanism (Fig. 3.1 c) $\mathbf{P}_{1(2)} = \mathbf{q} + \mathbf{p}_{1(2)} - \mathbf{p}_d/2 - \mathbf{p}_\pi$, $\mathbf{p}_{1(2)}$ and \mathbf{p}_d being the momenta of the proton (neutron) and deuteron respectively; \mathbf{p}_π is the momentum of the pion, over whose energy the integral in Eq. (3.1) is performed.

The matrix elements in Eq. 3.4 are evaluated for the different mechanisms using the phenomenological Lagrangians (Eqs. 1.50, 1.56, 1.61, 1.72, 1.77, 1.104, 1.105) and N^* , Δ propagators of Eqs. (1.67, 1.83), all defined in Chapter 1. In the case of $\mathcal{L}_{N^*N\pi\pi}$, point 5 in the ellipse of parameters c_1^* , c_2^* of Fig. 1.3 will be used except where a different choice is explicitly indicated. The function $D_{T=0,1}(q)$ stands for the meson propagators and form factors of the exchanged particles. For $T=0$:

$$D_{T=0}(q) = \frac{1}{q^2 - m_\sigma^2} \left(\frac{\Lambda_\sigma^2 - m_\sigma^2}{\Lambda_\sigma^2 - q^2} \right)^2. \quad (3.6)$$

In the case of $T=1$, if one considers only π exchange

$$D_{T=1}^{(\pi)}(q) = \frac{1}{q^2 - m_\pi^2} \left(\frac{\Lambda_\pi^2 - m_\pi^2}{\Lambda_\pi^2 - q^2} \right)^2. \quad (3.7)$$

Then, in order to take into account the transversal rho exchange, and the short range correlations that take into account the repulsive force at short distances one makes the substitution

$$D_{T=1}^{(\pi)}(q)q_i q_j \rightarrow V'_L(q)\hat{q}_i \hat{q}_j + V'_T(q)(\delta_{ij} - \hat{q}_i \hat{q}_j) \quad (3.8)$$

with $V'_L(q)$, $V'_T(q)$ defined in Eq. (1.103); $q = (q_0, \mathbf{q})$ is the 4-momentum transfer from one nucleon to the other; q_0 is given by energy conservation in the vertices and, therefore, depends on the energy of one of the outgoing nucleons, taken to be one half of the deuteron energy. Explicit expressions for the amplitudes are given in Appendix F

3.3 Results and discussion

At $\mathbf{p}_n = 1.46 \text{ GeV}/c$

With the ingredients described in the previous section, one can calculate the deuteron spectra at $p_n = 1.46 \text{ GeV}/c$ for different angles. The results are shown in Fig. 3.2. They compare quite well with the data of Hollas et al. [78], and certainly much better than the previous models [80, 81]. The curves, in general, underestimate the data, maybe because there are many other mechanisms, not considered for the sake of simplicity, that, even being individually small, could in sum enhance the cross section. Some of the approximations made, like the neglect of the deuteron d-wave and non-relativistic approximation in the vertices, as well as the intrinsic uncertainties of the mechanisms included can also be a source of discrepancies; they are discussed below. The large data point at the edges of the spectra show the contamination of the π^0 peaks [78]. I have also estimated the influence of the width of the neutron beam by averaging the double differential cross sections over

a Breit-Wigner profile of 40 MeV width and centered at $p_n = 1.46$ GeV/c, corresponding to the momentum resolution achieved, and the momentum of the primary proton beam used to produce the neutron beam via the $pd \rightarrow npp$ reaction [78]; the contribution of this effect is very small and irrelevant for our study. The plotted curves are obtained using the deuteron wave function derived from the Paris potential [66]; with the Bonn wave functions [30] the results are very similar, while for the Hulthen one [87] the distributions are overall larger, up to a factor two at the position of the central bump.

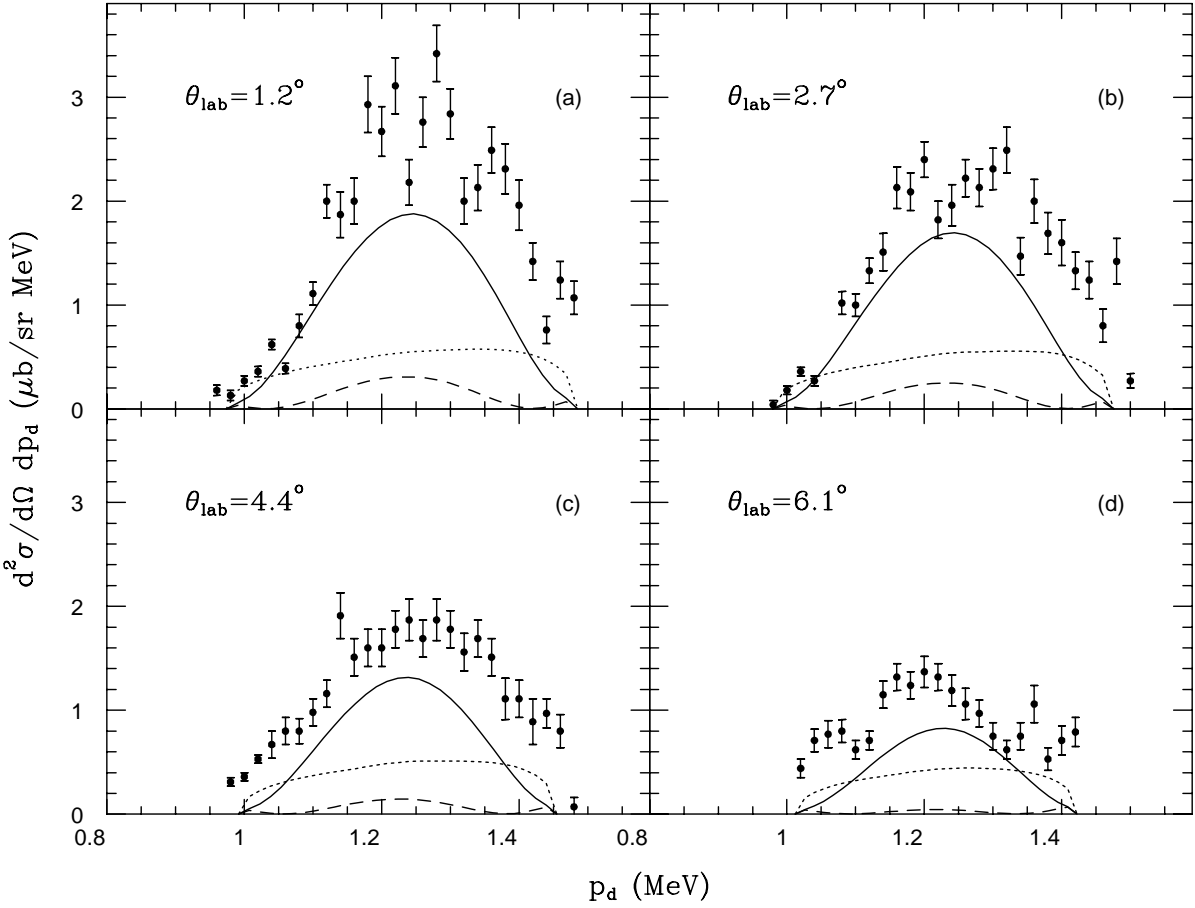


Figure 3.2: Deuteron momentum spectra for $np \rightarrow d(\pi\pi)^0$ at $p_n = 1.46$ GeV/c and different laboratory angles (solid lines) compared to the measured data [78]. The dotted line corresponds to the $N^* \rightarrow N(\pi\pi)^{T=0}_{S-wave}$ mechanism (Fig. 3.1 a); the short-dashed line stands for the $N^* \rightarrow \Delta\pi$ (Fig. 3.1 b).

The mechanism $N^* \rightarrow N(\pi\pi)^{T=0}_{S-wave}$ (Fig. 3.1 a) produces spectra very similar to phase space; its contribution is certainly the largest, but its relative size with respect to the $N^* \rightarrow \Delta\pi$ mechanism is not as large as one would naively expect from estimations based on the total cross sections obtained for both mechanisms in the free $NN \rightarrow NN\pi\pi$ reaction. Nevertheless, it is not surprising since here we are sensitive only to a reduced

phase space region and choosing a particular combination of the quantum numbers of the outgoing nucleons (those of the deuteron). For this mechanism, I have calculated the contribution of the d-wave part of the deuteron wave function and found it negligible. The situation could, however, be different at higher energies and for other mechanisms as stated in Ref. [83], where the d-wave was found to account for 10-30 % of the cross section.

The $N^* \rightarrow \Delta\pi$ mechanism (Fig. 3.1 b) exhibits a wide bump at the center of the spectra (high $\pi\pi$ masses), whose maximum falls fast with the increase of the deuteron angle, and small peaks at the edges of the spectra (low $\pi\pi$ masses); the size of these peaks does not vary appreciably with the angle. This mechanism plays a crucial role in providing the right shape to the distributions through its interference with the larger $N^* \rightarrow N(\pi\pi)_{S\text{-wave}}^{T=0}$ contribution. This interference is constructive at high $\pi\pi$ masses and destructive at low ones. Such pattern can be understood by realizing that the $N^* \rightarrow \Delta\pi$ amplitude is dominated by terms proportional to the scalar product of the outgoing pions three momenta; this scalar product has different signs in the center of the spectra, where the pions go back to back, and at the edges, where they travel together. In order to further illustrate the effect of the interference, Fig. 3.3 shows the effect of changing the relative sign of the two amplitudes. The data clearly favor a choice of the sign of $g_{N^*\Delta\pi}$ in agreement with earlier works [6, 46, 37, 47].

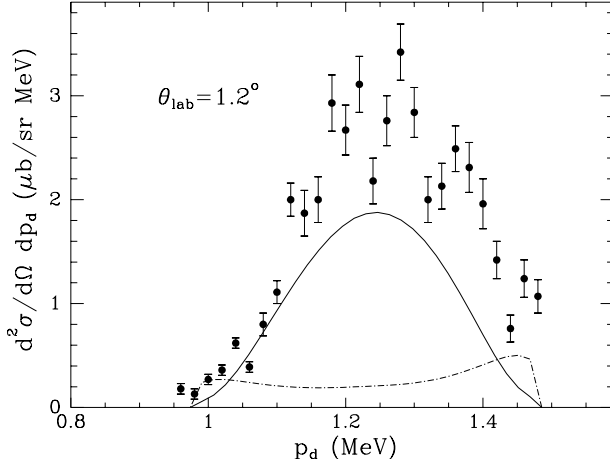


Figure 3.3: Calculated spectra for two different choices of the $g_{N^*\Delta\pi}$ sign. The data clearly favor the positive sign (solid line) with respect to the negative (dash-dotted line).

The double- Δ mechanism (Fig. 3.1) is too small to be represented in Fig. 3.2. In Fig. 3.4, the contribution of this mechanism alone is shown for $p_n = 1.5$ GeV/c, $\theta_{lab} = 4.5^\circ$ and using the Hulthen wave function, in order to compare with the result of Bar-Nir, Risser and Shuster (Fig. 4 b of Ref. [81]). The differential cross section obtained in the case of only pion exchange is very similar to the one given by the relativistic model of Ref. [81]; the inclusion of the rho exchange modifies the result, and the short range correlations between the initial nucleons cause a strong reduction of the strength of this mechanism (see the solid line of Fig. 3.4).

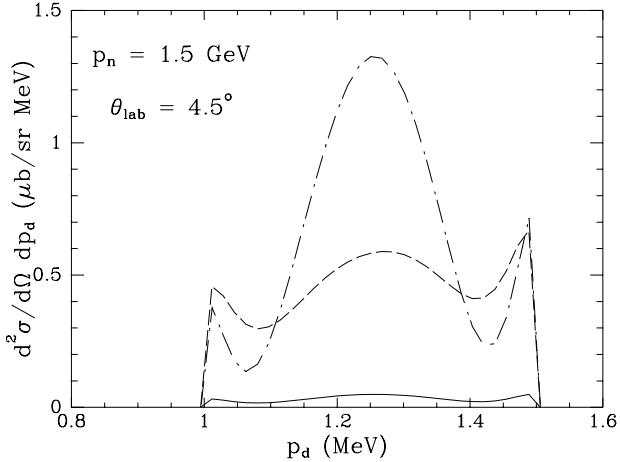


Figure 3.4: Contribution of the double- Δ mechanism in the case of π exchange alone (dashed line), $\pi + \rho$ exchange (dash-dotted line) and $\pi + \rho +$ short range correlations (solid line). In this case the calculation uses a Hulthen wave function for the deuteron.

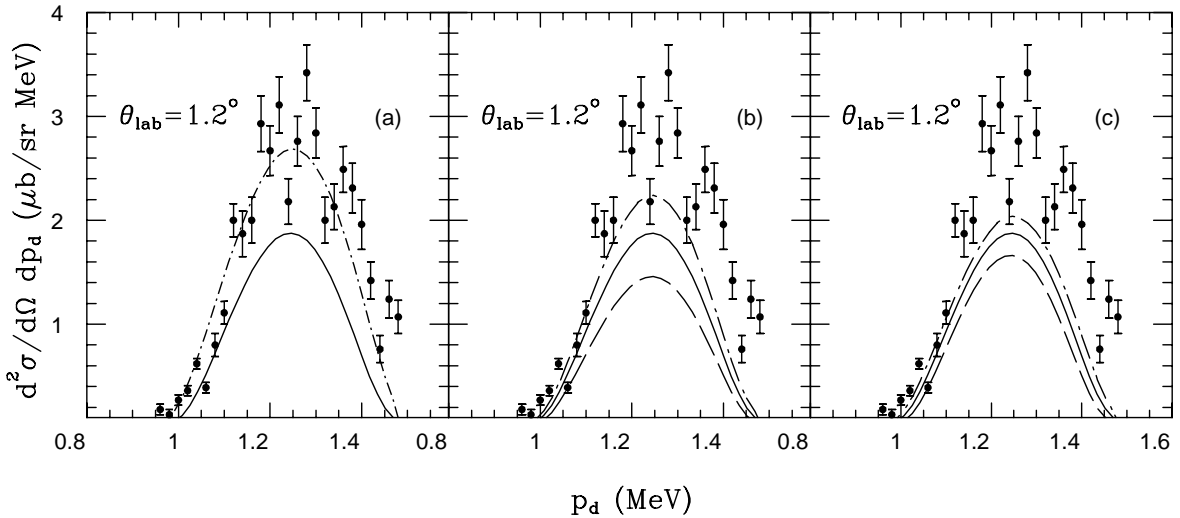


Figure 3.5: Dependence of the spectrum on certain decay properties of the $N^*(1440)$. The solid line in (a) shows the result for the point 5 of parameters c_1^* , c_2^* used everywhere else ($c_1^* = 0$), and the dash-dotted one is obtained with point 4. In Fig. (b), different values of the N^* total width are considered: dashed line, 250 MeV; solid line, 350 MeV; dash-dotted line, 450 MeV. The branching ratios of the different decay channels of the N^* are modified in (c), with the total width fixed to 350 MeV; dashed line: $Br(N(\pi\pi)_{S-wave}^{T=0}) = 5\%$ and $Br(\Delta\pi) = 30\%$; solid line: 7.5% and 25%; dash-dotted line: 10% and 20%.

Wherever dealing with the Roper resonance, the lack of a precise determination of its properties is a problem that should be faced. In Fig. 3.5, I investigate how the results

vary with some of the uncertainties. As can be noticed, the shape is not affected by these changes, but some set of values are preferred. Fig. 3.5 a, shows how the spectrum changes with the modification of c_1^* , c_2^* within the previously accepted values, while keeping the total width and the partial branching ratios fixed; the set of values corresponding to the point 4 in the ellipse of Fig. 1.3 gives a better agreement with the data. In Fig. 3.5 b, we show the range of uncertainties that come from the variation of the total width of the N^* in the limits given by the Particle Data Book [18], that is from 250 MeV (lower line) to 450 MeV (upper line). Finally, the dependence on the partial branchings of the N^* to $N(\pi\pi)_{S-wave}^{T=0}$ and $\Delta\pi$, with the total width fixed to 350 MeV, is studied in Fig. 3.5 c. The dashed line corresponds to a 5% branching of N^* to $N(\pi\pi)_{S-wave}^{T=0}$ and a 30% to $\Delta\pi$, while for the dash-dotted one, a larger 10% of $N(\pi\pi)_{S-wave}^{T=0}$ and a smaller 20% of $\Delta\pi$; the data prefer the latter choice. These data alone do not allow to disentangle the different effects, but, in combination with other data that will be available in the future (like the data on $pp \rightarrow d\pi\pi$ at $T_p = 600 - 775$ MeV from CELSIUS), would be an important source of information about the Roper resonance.

At $p_n = 1.70$ GeV/c

Deuteron spectra ($d^2\sigma/d\Omega dp_d$) for the inclusive reaction $np \rightarrow dX$ have been recently measured at KEK, Japan, using a quasi-monochromatic neutron beam and a liquid hydrogen target [88]. The measurements were performed at two different energies $T_n = 1, 2$ GeV. The second of these energies is too high to be considered here; notice that at this energy both ρ and η production are clearly identified in the spectra. Hence, the present analysis is restricted to $T_n = 1$ GeV ($p_n = 1.70$ GeV/c). At this energy, the three mechanisms of the model appear to be the dominant ones in the case of the free $pn \rightarrow pn\pi^+\pi^-$ reaction.

Our results compared to the data are shown in Fig 3.6. At forward angles, the model produces the right strength in the center of the spectrum (high $(\pi\pi)$ invariant masses) as a result of a constructive interference of the mechanisms. The contribution $N^* \rightarrow \Delta\pi$ is the largest one and conditions the obtained shape. At low $(\pi\pi)$ masses we see the appearance of the ABC peaks, formed by the $N^* \rightarrow \Delta\pi$ and double- Δ mechanisms. These peaks are not seen at lower energies because the relative strength of these mechanisms is too small. From the figures it seems that we miss strength at the edges of the spectra and in the region of the deups, but it is difficult to draw definitive conclusions since the data do not allow to separate double-pion production from other mechanisms. In particular, the π^0 peaks from the reaction $np \rightarrow d\pi^0$, which are responsible for the measured deuteron yield below and above the kinematic limits of two-pion production, cannot be disentangled. On the other side, one should bare in mind that the error bars reflect only statistical uncertainties, and the overall systematic uncertainty is about 30 % [88]. In spite of the experimental errors, it seems that the model follows short at larger angles. It is interesting to notice that at $\theta_{lab} = 12^\circ$, the central bump has already disappeared from the calculated spectrum.

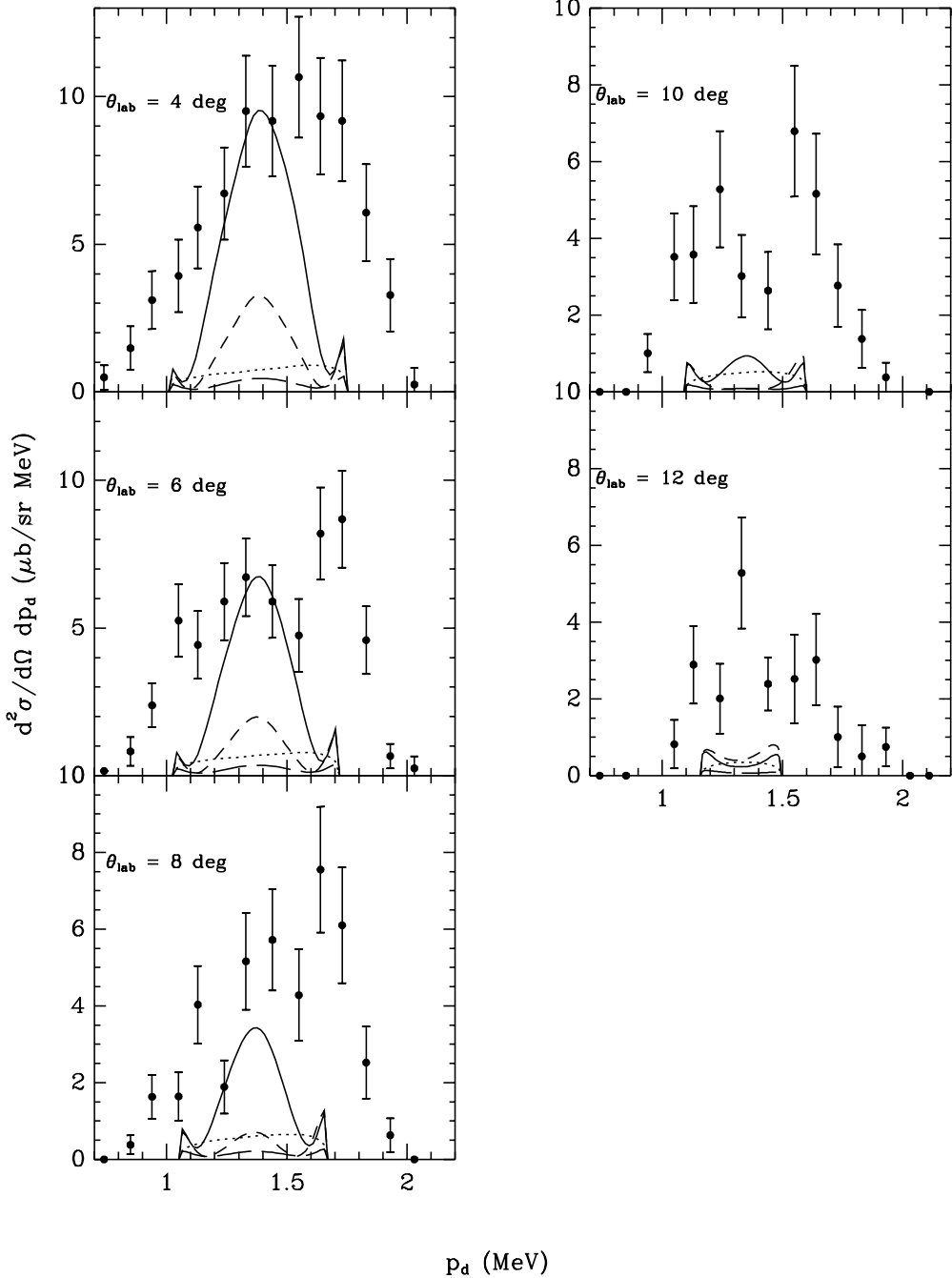


Figure 3.6: Deuteron momentum spectra for $np \rightarrow d(\pi\pi)^0$ at $p_n = 1.7$ GeV/c and different laboratory angles (solid lines) compared to the measured data [88]. The dotted line corresponds to the $N^* \rightarrow N(\pi\pi)^0_{S-wave}$ mechanism (Fig. 3.1 a); the short-dashed line stands for the $N^* \rightarrow \Delta\pi$ (Fig. 3.1 b) and the long-dashed one, for the double- Δ (Fig. 3.1 c).

At $p_n = 1.88$ GeV/c

The experimental work of F. Plouin and collaborators [75] performed at Saclay synchrotron (Saturne) was the first where the ABC effect was directly observed in the elementary reaction $pn \rightarrow dX$ (earlier work extracted information about this reaction from $pd \rightarrow dX + p_{spect}$) and was an important incentive for the theoretical work in this field. The experiment measured inclusive deuteron momentum spectra using a neutron beam with $p_n = 1.88$ GeV/c. At this energy, the ABC anomaly is in clear evidence at both ends of the spectra. At this energy, the analysis of the reaction presents an additional complication since η and 3π production could contribute to the spectra [85].

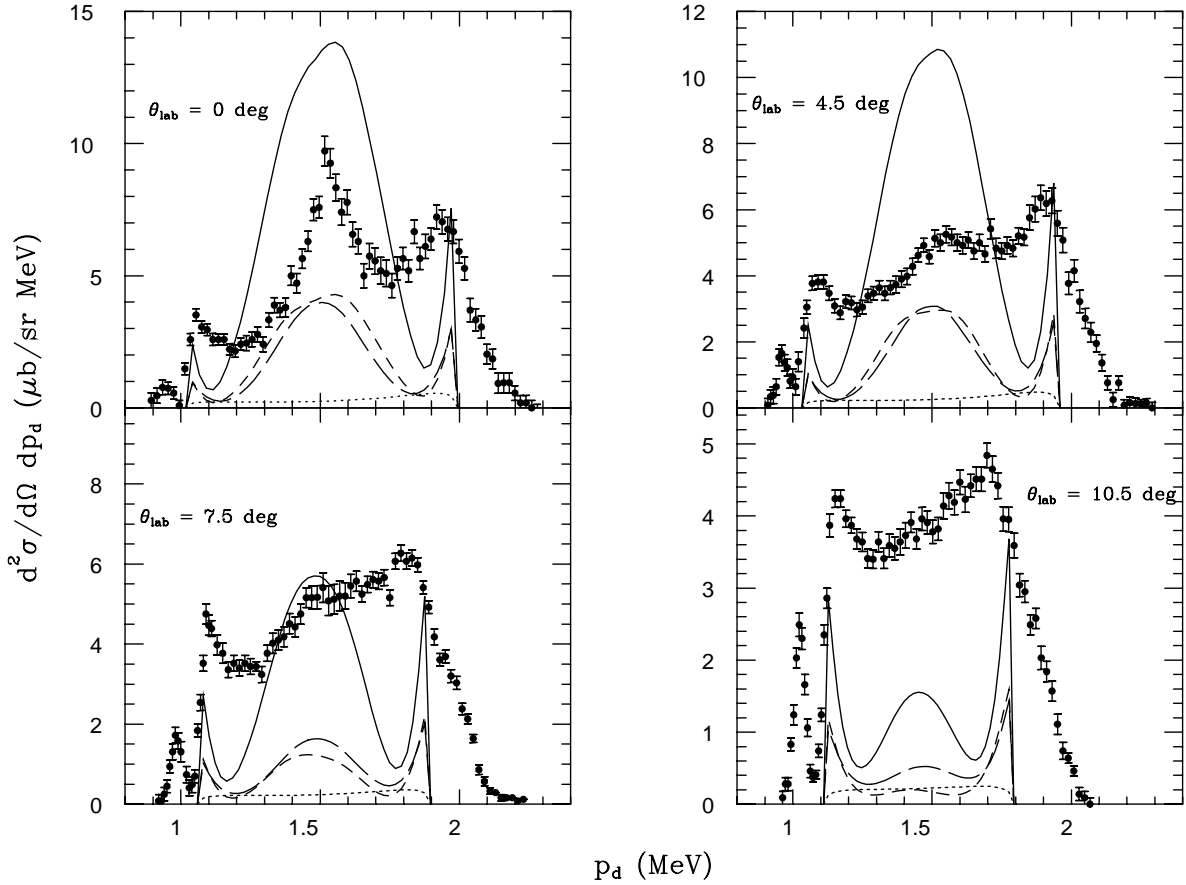


Figure 3.7: Deuteron momentum spectra for $np \rightarrow d(\pi\pi)^0$ at $p_n = 1.88$ GeV/c and different laboratory angles (solid lines) compared to the measured data [75]. Line styles have the same meanings as in Fig. 3.6.

In Fig. 3.7 our results are compared to the data of Plouin et al. [75]. Even if a three peak structure is clearly present, the model fails in explaining the details of the spectra. In particular, the size of the central bump is clearly overestimated, and our ABC peaks are

appreciably sharper than the measured ones. This is, in part, due to the fact that neither the width of the neutron beam, nor the detector acceptance have been taken into account. Calculated spectra also decrease too fast with the increase of the deuteron angle; this is a common feature to most models of the $np \rightarrow d(\pi\pi)^0$ reaction [80, 81, 82] (except the one of Ref. [83]). Again, the strength of the $N^* \rightarrow N(\pi\pi)_{S-wave}^{T=0}$ is smaller than expected from estimations based on the equivalent free reaction (all three mechanisms produce similar total cross sections at this energy in the case of $pn \rightarrow pn\pi^+\pi^-$). Therefore, our hope that this mechanism could be responsible for the isotropic angular behavior [4] is not confirmed. In spite of this, we show that the $N^* \rightarrow \Delta\pi$, which has been systematically neglected in all ABC models, is as large as the double- Δ one, and could play a significant role in any further understanding of the ABC effect. For this reason, if the effects of $\Delta\Delta$ and ΔN rescatterings were important, as claimed in a recent paper [82], then the Roper resonance should not be ignored in this type of calculations.

Total cross section

The relative importance of each mechanism of the model as a function of energy is clearly shown in Fig. 3.8. In general, this calculation underestimates the total cross section as one would expect from the results above, but the agreement is good, at least, not worse than for the analogous free reaction $pn \rightarrow pn\pi^+\pi^-$. Such agreement, specially at low energies,

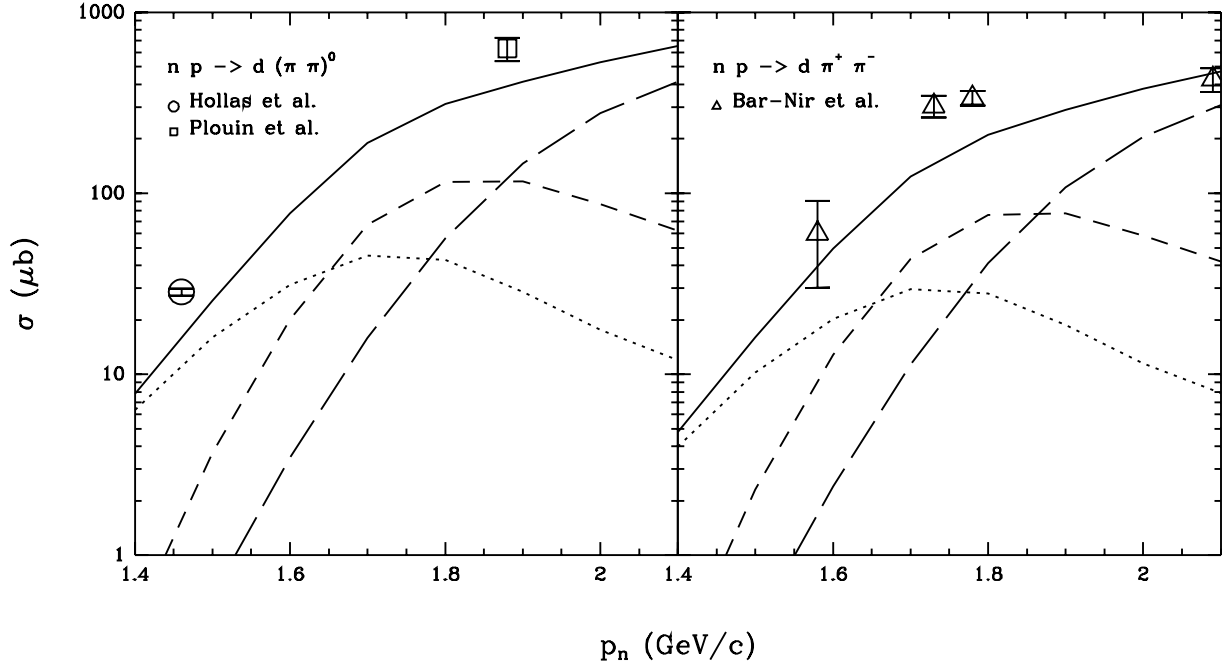


Figure 3.8: Total cross section for $np \rightarrow d(\pi\pi)$ as a function of the incoming nucleon LA momentum. Experimental data are from Refs. [78, 75, 74].

can be hardly understood without taking into account the Roper contribution. Notice that the difference between the two graphics is due to the fact that in the experiments of Hollas et al. [78], and Plouin et al. [75] only the deuteron is detected, and, therefore, both $\pi^+\pi^-$, $\pi^0\pi^0$ channels must be included, whereas in the case of Bar-Nir et al. [74], charged pions are detected by their trace in the bubble chamber.

3.4 Summary

In summary, a simple model for the $np \rightarrow d(\pi\pi)^0$ reaction has been developed, based on a previous model for the free $NN \rightarrow NN\pi\pi$ and including the most important resonance contributions. The total cross section has been calculated and the results found to be in good agreement with the limited experimental information. At the level of double differential cross section, it has been shown that the bump in the center of the deuteron momentum spectra (high $\pi\pi$ masses) observed at a neutron beam momentum of $p_n = 1.463$ GeV/c ($T_n = 795$ MeV) can be explained as a result of the interference of two mechanisms involving the excitation of the Roper resonance: the dominant and phase-space like $N^* \rightarrow N(\pi\pi)_{S-wave}^{T=0}$ (Fig. 3.1 a) and the smaller in size $N^* \rightarrow \Delta\pi$ (Fig. 3.1 b), but determinant to obtain the right profile. The mechanism of double- Δ (Fig. 3.1 c) excitation, considered in an earlier model for the same reaction, but only including pion exchange, is significantly reduced by the short range correlations. At high energy the model fails to reproduce the details of the deuteron spectra, in particular, the almost isotropic angular behavior observed at $p_n = 1.88$ GeV/c ($T_n = 1160$ MeV). In spite of this we have qualitatively understood how the ABC peaks disappear at low energies and remarked the importance of the Roper resonance in this process. A further understanding of the ABC effect would require a better knowledge of the deuteron wave function at high momentum transfer and the $NN \rightarrow NN^*$, $NN \rightarrow \Delta\Delta$ transition potentials, as well as a renewed relativistic treatment of the reaction. The present experimental program on double pion production in NN collisions at CELSIUS can be the basis for such research.

Part II

Charge changing weak production of the Δ resonance

The study of the nucleon and its excitation spectrum has been pursued for a long time both experimentally and theoretically, seeking a better understanding of the structure and interactions of hadrons. These investigations provide insight into the non-perturbative regime of QCD. In this context, the extraction of electromagnetic and weak form factors in the $N - \Delta(1232)$ transition can appear as valuable source of information. There are clear advantages in considering the $\Delta(1232)$ since it is nicely isolated from the densely populated region of excited states that appear at higher energies, and has a largely dominant πN decay channel, which allows for an easier identification.

At low and intermediate energies, the study of various electromagnetic excitation processes, induced by electrons and photons, has been made at many research facilities around the world, and there exists extensive literature on electromagnetic transition form factors [89, 90]. Similar studies on the corresponding weak form factors have been performed in a series of experiments carried out with wide band neutrino beams at ANL, BNL and CERN laboratories, where attempts have been made to isolate the transition form factors for the charge changing weak current, and there exists a fair amount of data to determine these form factors [91, 92, 93, 94, 95]. This is not the case with the neutral current processes, where there are very few experiments [96] in the intermediate energy range, and no serious analysis has been made of the transition form factors. Although, the main interest in the neutral current sector has been to study the parity violating asymmetry in polarized electron scattering with nucleons and nuclei in order to explore the nonzero strangeness content of the nucleon [97], it was also suggested to measure the parity violating asymmetry for the $N - \Delta$ transition in order to extract the isovector part of the hadronic neutral current [98], but it was a difficult experiment at the time.

The availability of continuous wave electron accelerators with 100 % duty cycle in the energy range of few GeV, and the possibility of achieving very high luminosities at these accelerators has led to the feasibility of performing electron scattering experiments in the resonance region with very good statistics [99]. These experimental studies can be extended to explore weak interaction physics in the Δ resonance region. In particular, the asymmetry studies mentioned above have been reconsidered [100, 101, 102]. In Chapter 4, we explore the possibility of doing similar experiments in the charge changing sector as an alternative way to extract the transition form factors.

Since the vector $N - \Delta$ form factors are related to the isovector electromagnetic ones and can be obtained from the electromagnetic production data, these experiments would provide information about the axial form factors. Among them, the dominant one is $C_5^A(q^2)$. The determination of its value at $q^2 = 0$ is important because the value of $C_5^A(0)$ obtained using the approximation of Partially Conserved Axial Current (PCAC) is found to be 30 % larger than the theoretical estimates obtained in most of the quark models [103]. The situation is similar in the electromagnetic sector, where the magnetic dipole (M_{1+}) and electric quadrupole (E_{1+}) transition amplitudes, determined from the experiments on photoproduction and electroproduction of the Δ resonance are found to be about 30 % larger than those computed in many theoretical models of hadron structure [104]. This underestimation of the electromagnetic and weak couplings in the $N - \Delta$ transitions may be a manifestation of large violations of the $SU(6)$ symmetry, while maintaining the chiral

symmetry of the Lagrangian, and needs further investigation.

In Chapter 5 we study the reaction $\nu d \rightarrow \mu^- \Delta^{++} n$ in order to extract $C_5^A(0)$ from the available low q^2 data, paying special attention to the effects of deuteron structure and width of the Δ resonance. We also discuss the possibility of extracting the value of this coupling from electron scattering experiments.

Chapter 4

Charged current weak electroproduction of Δ resonance

4.1 Introduction

Our aim is to make a general analysis of the weak production of Δ through the processes

$$e^- p \rightarrow \Delta^0 \nu_e \quad (4.1)$$

and

$$e^+ p \rightarrow \Delta^{++} \bar{\nu}_e , \quad (4.2)$$

and to examine critically the feasibility of doing such an experiment at the Mainz Microtron and/or at TJNAF [105]. These reactions were earlier studied by Hwang et al. [106], where a bag model was used to calculate the $N - \Delta$ form factors and the effect of the Δ width was not taken into account. In this work we retain all the weak vector and axial vector form factors in the matrix elements of $N - \Delta$ transitions. The present available information on these form factors from the experimental data on electromagnetic and neutrino production of Δ has been fully utilized through the application of Conserved Vector Current (CVC) and Partially Conserved Axial Current (PCAC) hypotheses in the $N - \Delta$ sector [107, 103, 108, 109, 110, 111]. In addition, the width of the Δ resonance is properly taken into account and is found to give important effects on the differential cross section. The effect of various parametrizations of the $N - \Delta$ form factors, discussed recently in the literature [107, 103], has been studied to explore the possibility of distinguishing between them experimentally. Finally, we have also estimated the production cross section for the Roper, $N^*(1440)$, the next higher resonance, in order to understand its effect in the kinematic region of Δ production; we find it to be sufficiently small and well separated from the kinematic region of present interest to allow for a clean identification of Δ through observation of the pions and nucleons produced as decay products.

Next, we describe the transition currents for the production of Δ and $N^*(1440)$, and derive expressions for the cross sections. In Sec. 4.3, we present the numerical results for

the differential cross sections for the considered reactions and discuss the possibility of experimentally observing them, in Sec. 4.4.

4.2 Transition currents and cross sections

4.2.1 $e^- p \rightarrow \Delta^0 \nu_e$ and $e^+ p \rightarrow \Delta^{++} \bar{\nu}_e$

Since the characteristic momentum transfers in these reactions are far below the W boson mass $|q^2| \ll M_W^2$, we can restrict ourselves to the effective contact weak interaction. Following the standard notation, the matrix element for the process $e^-(k) + p(p) \rightarrow \Delta^0(p') + \nu_e(k')$ is then written in terms of a product of the leptonic and hadronic currents [108, 110, 111]

$$\mathcal{M} = \frac{G}{\sqrt{2}} \cos \theta_c l_\alpha J^\alpha, \quad (4.3)$$

with

$$l_\alpha = \bar{u}(k') B_\alpha u(k), \quad B_\alpha = \gamma_\alpha (1 - \gamma_5), \quad (4.4)$$

and

$$\begin{aligned} J^\alpha &= \bar{u}_\mu(p') A^{\mu\alpha} u(p), \\ A^{\mu\alpha} &= \left[\frac{C_3^V}{M} (g^{\mu\alpha} \not{q} - q^\mu \gamma^\alpha) + \frac{C_4^V}{M^2} (g^{\mu\alpha} q \cdot p' - q^\mu p'^\alpha) + \frac{C_5^V}{M^2} (g^{\mu\alpha} q \cdot p - q^\mu p^\alpha) \right] \gamma_5 \\ &+ \frac{C_3^A}{M} (g^{\mu\alpha} \not{q} - q^\mu \gamma^\alpha) + \frac{C_4^A}{M^2} (g^{\mu\alpha} q \cdot p' - q^\mu p'^\alpha) + C_5^A g^{\mu\alpha} + \frac{C_6^A}{M^2} q^\mu q^\alpha, \end{aligned} \quad (4.5)$$

where G is the well known Fermi constant

$$\frac{G}{\sqrt{2}} = \frac{e^2}{8 \sin^2 \theta_W M_W^2} = 1.16639 \times 10^{-5} \text{ GeV}^{-2}, \quad (4.6)$$

$\cos \theta_c = 0.975$, the cosine of the Cabibbo angle and M , the nucleon mass; $u_\mu(p')$ and $u(p)$ are the Rarita-Schwinger and Dirac spinors for Δ and nucleon of momentum p' and p ; $q = p' - p = k - k'$ is the momentum transfer. The hadronic current is conveniently expressed in terms of vector and axial vector transition form factors C_i^V and C_i^A ($i = 3, 4, 5, 6$) as defined by Llewellyn Smith [111]; they are discussed in detail in Sec. 4.2.2. With the matrix element given in Eqs. (4.3)-(4.5), the differential cross section $d\sigma/d\Omega_\Delta$ is calculated to be

$$\frac{d\sigma}{d\Omega_\Delta} = \frac{1}{128\pi^3} G^2 \cos^2 \theta_c \int d|\mathbf{p}'| \frac{|\mathbf{p}'|^2}{E_\nu E_\nu} \frac{\Gamma_\Delta(W)/2}{(W - M_\Delta)^2 + \Gamma_\Delta^2(W)/4} L_{\alpha\beta} J^{\alpha\beta}, \quad (4.7)$$

with the leptonic tensor $L_{\alpha\beta}$ defined as

$$\begin{aligned} L_{\alpha\beta} &\equiv \text{Tr} \left[(\not{k} + m_e) \tilde{B}_\alpha (\not{k}' + m_{\nu_e}) B_\beta \right] \\ &= 8 \left(k_\alpha k'_\beta + k'_\alpha k_\beta - g_{\alpha\beta} k \cdot k' + i\epsilon_{\alpha\beta\gamma\delta} k^\delta k'^\gamma \right), \end{aligned} \quad (4.8)$$

and the hadronic tensor is

$$J^{\alpha\beta} \equiv \text{Tr} \left[(\not{p} + M) \tilde{A}^{\mu\alpha} P_{\mu\nu} A^{\nu\beta} \right] \quad (4.9)$$

where

$$\tilde{R} \equiv \gamma_0 R^\dagger \gamma_0, \quad R = A_{\mu\alpha}, B_\alpha. \quad (4.10)$$

Here, $P_{\mu\nu}$ is the spin 3/2 projection operator which, for the usual choice $A = -1$ (see Appendix B and Ref. [36]), is given by

$$P_{\mu\nu} = -\frac{\not{p} + M_\Delta}{2M_\Delta} \left(g_{\mu\nu} - \frac{2}{3} \frac{p'_\mu p'_\nu}{M_\Delta^2} + \frac{1}{3} \frac{p'_\mu \gamma_\nu - p'_\nu \gamma_\mu}{M_\Delta} - \frac{1}{3} \gamma_\mu \gamma_\nu \right). \quad (4.11)$$

In Eq. (4.7), W is the invariant mass of the Δ given by $W^2 = p'^2$, M_Δ is the Δ mass and Γ_Δ is its decay width given by Eq. (1.59). The Δ width has been accounted for in the cross section calculation by means of the standard substitution

$$\delta(p'^2 - M_\Delta^2) \rightarrow -\frac{1}{\pi} \frac{1}{2M_\Delta} \text{Im} [D_\Delta(p')], \quad (4.12)$$

with $D_\Delta(p')$ being the non-relativistic Δ propagator, as defined in Eq. (1.67).

We now turn to the process $e^+ p \rightarrow \Delta^{++} \bar{\nu}_e$. The matrix element is written in the same way as in Eqs. (4.3)-(4.5) with the following replacements:

- (i) The leptonic current l_α in Eq. (4.4), now involves antiparticles and is written in terms of v spinors instead of u spinors,
- (ii) The matrix element of the hadronic current J_α in Eq. (4.5) is now evaluated between initial proton and final Δ^{++} states, with the relation

$$\langle \Delta^{++} | J_\alpha | p \rangle = \sqrt{3} \langle \Delta^0 | J_\alpha | p \rangle, \quad (4.13)$$

which is a direct consequence of the Wigner-Eckart theorem.

With these two changes the differential cross section is effectively given by Eq. (4.7), with $L_{\alpha\beta}(k, k') \rightarrow L_{\alpha\beta}(k', k)$ and $J_{\alpha\beta}(p, p') \rightarrow 3J_{\alpha\beta}(p, p')$.

4.2.2 $N - \Delta$ transition form factors

The $N - \Delta$ transition form factors relevant to the weak transition current have been discussed in the literature in connection with the analysis of neutrino scattering experiments [108, 109, 110, 111, 112] and in the context of quark model calculations [107, 103]. We summarize in this section some details of these form factors, needed for present calculations.

Vector form factors

As stated in Sec. 4.2.1, there are four weak vector form factors C_3^V , C_4^V , C_5^V and C_6^V occurring in this transition. The imposition of the CVC hypothesis, which in momentum space reads $q_\mu J_V^\mu = 0$, implies $C_6^V = 0$. The other three form factors are then given in terms of the isovector electromagnetic form factors of the $p\text{-}\Delta^+$ electromagnetic transition because, as a consequence of the global $SU(2)$ invariance, the vector hadronic weak current, its Hermitian conjugate and the isovector part of the electromagnetic current form an isospin triplet of conserved currents [113]. Specifically, the hadronic matrix element for the reactions (4.1) and (4.2) are given as

$$\langle \Delta^0 | J_V^\alpha | p \rangle = \langle \Delta^+ | J_{em}^\alpha(T=1) | p \rangle \quad (4.14)$$

and

$$\langle \Delta^{++} | J_V^\alpha | p \rangle = \sqrt{3} \langle \Delta^+ | J_{em}^\alpha(T=1) | p \rangle, \quad (4.15)$$

where $J_{em}^\alpha(T=1)$ is the isovector electromagnetic current.

The information on the isovector electromagnetic form factors $C_i^V(q^2)$ ($i = 3, 4, 5$) is obtained from the analysis of photo and electroproduction data of Δ , which is done in terms of the multipole amplitudes E_{1+} (electric quadrupole), M_{1+} (magnetic dipole) and S_{1+} (scalar quadrupole) [114]. The present data on E_{1+} and S_{1+} amplitudes are very meager and these amplitudes are expected to be small. Assuming M_{1+} dominance of the electroproduction amplitude, which is predicted by the non-relativistic quark model, the form factors $C_i^V(q^2)$ satisfy the relations:

$$C_5^V = 0, \quad C_4^V = -\frac{M}{M_\Delta} C_3^V; \quad (4.16)$$

they have been used in the analysis of the electroproduction experiments and $C_3^V(q^2)$ has been determined. The following parametrizations of $C_3^V(q^2)$, available in the literature [107, 103], are used in our present calculations:

$$C_3^V(q^2) = \frac{2.05}{(1 - q^2/0.54 \text{ GeV}^2)^2}, \quad (4.17)$$

$$C_3^V(q^2) = \frac{1.39}{\sqrt{1 - q^2/1.43 \text{ GeV}^2}(1 - q^2/0.71 \text{ GeV}^2)^2}. \quad (4.18)$$

For the purpose of comparison with a simple form factor obtained in the $SU(6)$ quark model, we also use [107]

$$C_3^V(q^2) = \frac{M}{\sqrt{3}m} e^{-\bar{q}^2/6} \quad (4.19)$$

where $m = 330$ MeV is the quark mass and $\bar{q} = |\mathbf{q}|/\alpha_{HO}$, with $\alpha_{HO} = 320$ MeV, being the harmonic oscillator parameter.

Axial vector form factors

There are four axial vector form factors C_3^A , C_4^A , C_5^A and C_6^A , as defined in Eq. (4.5). If we consider the one-pion exchange amplitude (Fig. 4.1), we find from the first term of the

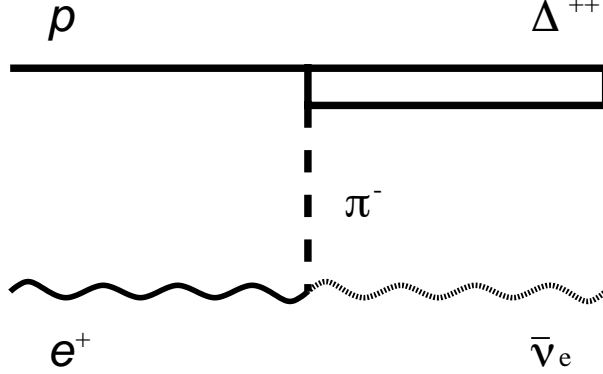


Figure 4.1: One-pion exchange diagram.

relativistic effective $\Delta N\pi$ Lagrangian of Eq. (1.55) a contribution to C_6^A

$$C_6^A(q^2) = \frac{g_{\Delta N\pi} f_\pi}{\sqrt{6}M} \frac{M^2}{m_\pi^2 - q^2} F_\pi(q^2), \quad (4.20)$$

where $F_\pi(q^2)$ is the form factor of the $\Delta N\pi$ vertex, $g_{\Delta N\pi} = 2f^*M/m_\pi$, the $\Delta^{++} \rightarrow p\pi^+$ coupling constant and $f_\pi = 92.4$ MeV, the pion decay constant. We neglect other contributions to $C_6^A(q^2)$. Substituting Eq. (4.20) in the expression of the axial part of the hadronic current, and making use of PCAC ($q_\mu J_A^\mu = 0$ in the limit of $m_\pi \rightarrow 0$) one gets

$$C_5^A(q^2) = \frac{g_{\Delta N\pi} f_\pi}{\sqrt{6}M} F_\pi(q^2). \quad (4.21)$$

The assumption that this result remains valid when m_π takes its actual value leads to the relation

$$C_6^A(q^2) = C_5^A(q^2) \frac{M^2}{m_\pi^2 - q^2}. \quad (4.22)$$

If, in addition, we assume that $F_\pi(q^2)$ is a slowly varying function, and extrapolate from $q^2 = m_\pi^2$, where $F_\pi = 1$, to $q^2 = 0$, we obtain the following formula for the axial vector coupling $C_5^A(0)$ [110]

$$C_5^A(0) = \frac{g_{\Delta N\pi} f_\pi}{\sqrt{6}M} \quad (4.23)$$

known as the off-diagonal Goldberger-Treiman relation. When the experimental values are used, Eq. (4.23) gives $C_5^A(0) = 1.15$. We shall return to this coupling in the next chapter.

In absence of any other theoretical input, $C_3^A(q^2)$, $C_4^A(q^2)$ and $C_5^A(q^2)/C_5^A(0)$ remain undetermined. The data on neutrino scattering are analyzed using these form factors as

free parameters (C_6^A is not determined from these experiments as its contribution is proportional to the lepton mass, which is neglected in the analyses), and using Eqs. (4.16)-(4.18) for the vector form factors. The parametrizations used for the various axial form factors are given below, where dipole form factors have been modified for a better fit to the data [91, 92, 93, 94, 95]

$$C_{i=3,4,5}^A(q^2) = C_i(0) \left[1 - \frac{a_i q^2}{b_i - q^2} \right] \left(1 - \frac{q^2}{M_A^2} \right)^{-2} \quad (4.24)$$

with $C_3^A(0) = 0$, $C_4^A(0) = -0.3$, $a_4 = a_5 = -1.21$, $b_4 = b_5 = 2$ GeV 2 and $M_A = 1.28$ GeV. The value of M_A comes from a best fit to the $\mu^- \Delta^{++}$ events at BNL [91] with the other parameters fixed. For a comparison, with the phenomenological form factors, we also use a recent non-relativistic quark model calculation [107]

$$C_5^A(q^2) = \left(\frac{2}{\sqrt{3}} + \frac{1}{3\sqrt{3}} \frac{q^0}{m} \right) e^{-\bar{q}^2/6}, \quad C_4^A(q^2) = -\frac{1}{3\sqrt{3}} \frac{M^2}{M_\Delta m} e^{-\bar{q}^2/6}, \quad C_3^A(q^2) = 0. \quad (4.25)$$

4.2.3 $e^- p \rightarrow N^* \nu_e$

The Roper resonance N^* , with mass 1440 MeV and decay width of about 350 MeV [18], is the next higher resonance which has appreciable strength into the $N\pi$ decay channel. The $N\pi$ events coming from the N^* decay can lie in the invariant mass region of the Δ resonance. Therefore, we also calculate the production cross section of the N^* resonance and evaluate the possibility to separate it from the Δ resonance signal. It is to be noted that there is no corresponding reaction with an e^+ beam thus, the Δ^{++} production signal is cleaner than the Δ^0 production signal.

The matrix element for the process $e^-(k) + p(p) \rightarrow N^*(p') + \nu_e(k')$ is written assuming standard properties of the charged weak current J^α in the $\Delta S = 0$ sector, neglecting second class currents [115]. Using constraints free form factors and manifestly gauge invariant operators for the vector current matrix element [116], J^α is written as

$$J^\alpha = \bar{u}_{N^*}(p') \left[F_1^V(q^2) (\not{q}^\alpha - q^2 \gamma^\alpha) + i F_2^V(q^2) \sigma^{\alpha\beta} q_\beta + F_A^V(q^2) \gamma^\alpha \gamma_5 + F_P^V(q^2) q^\alpha \gamma_5 \right] u(p), \quad (4.26)$$

where $F_{1,2}^V(q^2)$ and $F_{A,P}^V(q^2)$ are the isovector vector and axial vector form factors. Note that there are, in principle three vector form factors, but only two of them are independent once the requirement of CVC is fulfilled.

The expression for the differential cross section $d\sigma/d\Omega_{N^*}$ is given by Eq. (4.7) with M_Δ and Γ_Δ replaced by the N^* mass and its width respectively. The N^* width is taken to be $\Gamma^* = \Gamma_{N\pi} + \Gamma_{\Delta\pi}$, given by Eqs. (1.70),(1.73).

4.2.4 $N - N^*$ transition form factors

As in the Δ case, vector form factors $F_1^V(q^2)$ and $F_2^V(q^2)$ are related to the isovector electromagnetic ones

$$F_i^V = F_i^p - F_i^n, \quad i = (1, 2) \quad (4.27)$$

and can, in principle, be determined from the available experimental data on photoproduction and electroproduction of the Roper resonance from protons and neutrons. The data on photoproduction on protons and neutrons fix only $F_2^V(0)$. The electroproduction of Roper resonance has been measured only for the proton, and data are not of very good quality [117]. In absence of any data on the neutron target, we have to rely on a model to determine the isovector form factors $F_1^V(q^2)$ and $F_2^V(q^2)/F_2^V(0)$. There are many models in the literature for the electroproduction of Roper resonance with very different results [118, 119]. For the purpose of present estimates, we use the following relations

$$A_{1/2}^n = -\frac{2}{3}A_{1/2}^p, \quad S_{1/2}^n = 0, \quad (4.28)$$

which are valid in the non-relativistic constituent quark model without configuration mixing [120]. Therefore, for the isovector transverse and longitudinal helicity amplitudes $A_{1/2}^V(q^2)$ and $S_{1/2}^V(q^2)$ one gets

$$A_{1/2}^V(q^2) = \frac{5}{3}A_{1/2}^p(q^2), \quad S_{1/2}^V(q^2) = S_{1/2}^p(q^2). \quad (4.29)$$

The helicity amplitudes $A_{1/2}^p$ and $S_{1/2}^p$ (the superscript p referring to the proton) are defined in the standard way [121],

$$\begin{aligned} A_{1/2}^p &= \sqrt{\frac{2\pi\alpha}{k_R}} \langle N^* \downarrow | \sum_{pol.} \epsilon^{(+)} \cdot J_{em}^p | N \uparrow \rangle, \\ S_{1/2}^p &= \sqrt{\frac{2\pi\alpha}{k_R}} \frac{|\mathbf{q}|}{\sqrt{-q^2}} \langle N^* \uparrow | \sum_{pol.} \epsilon^{(+)} \cdot J_{em}^p | N \uparrow \rangle, \end{aligned} \quad (4.30)$$

where $\alpha^2 = 1/137$; the electromagnetic current J_α^p is given by [116]

$$J_\alpha^p = \bar{u}_{N^*}(p') [F_1^p(q^2) (\not{q}_\alpha - q^2 \gamma_\alpha) + F_2^p i\sigma_{\alpha\beta} q^\beta] u(p) \quad (4.31)$$

where $F_{1,2}^p(q^2)$ are the electromagnetic $p - p^*$ transition form factors; $q^\mu = (q^0, \mathbf{q})$ is the momentum of the virtual photon and k_R is the energy of an equivalent real photon (i.e. q^0 in the particular case of $q^2 = 0$). In the resonance rest frame, $|\mathbf{q}|$ and k_R are expressed as

$$k_R = \frac{W^2 - M^2}{2W}, \quad \mathbf{q}^2 = \frac{(W^2 - M^2 + q^2)^2}{4W^2} - q^2, \quad W^2 = (k + p)^2. \quad (4.32)$$

The transverse polarization vectors are

$$\epsilon^{(\pm)} = \frac{1}{\sqrt{2}}(0, \mp 1, -i, 0) \quad (4.33)$$

and $\epsilon^{(0)}$ satisfies

$$\epsilon_\mu^{(0)} \epsilon^{(0)\mu} = 1, \quad \epsilon_\mu^{(0)} q^\mu = \epsilon_\mu^{(0)} \epsilon^{(\pm)\mu} = 0. \quad (4.34)$$

If one now goes to the resonance rest frame and takes the z axis along the direction of the photon 3-momentum i.e. $\mathbf{q} = (0, 0, |\mathbf{q}|)$, then

$$\epsilon^{(0)} = \frac{1}{\sqrt{-q^2}}(|\mathbf{q}|, 0, 0, q^0); \quad (4.35)$$

Using Eqs. (4.29)-(4.35), the isovector helicity amplitudes are derived to be

$$A_{1/2}^V(q^2) = |\mathbf{q}| g(q^2) \left[F_2^V(q^2) - \frac{q^2}{W+M} F_1^V(q^2) \right], \quad (4.36)$$

$$S_{1/2}^V(q^2) = \frac{1}{\sqrt{2}} \mathbf{q}^2 g(q^2) \left[F_1^V(q^2) - \frac{F_2^V(q^2)}{W+M} \right], \quad (4.37)$$

with

$$g(q^2) = \sqrt{\frac{8\pi\alpha(W+M)W^2}{M(W-M)((W+M)^2-q^2)}}. \quad (4.38)$$

Inverting Eqs. (4.36),(4.37) we calculate the isovector form factors $F_1^V(q^2)$ and $F_2^V(q^2)$ in terms of the helicity amplitudes and use Eq. (4.29) to obtain them from the presently available data on $A_{1/2}^p(q^2)$ and $S_{1/2}^p(q^2)$, quoted by Li et al. [118].

In the case of axial vector form factors $F_A^V(q^2)$ and $F_P^V(q^2)$, there is no experimental information available. We use the pion pole dominance of the divergence of axial current hypothesis, as done for the Δ in section 4.2.2, to relate $F_A^V(q^2)$ and $F_P^V(q^2)$ to each other and also to obtain a corresponding off-diagonal Goldberger-Treiman relation relating $F_A^V(0)$ to the $N^* \rightarrow N\pi$ coupling \tilde{f} and f_π . A straightforward calculation gives

$$F_A^V(0) = 2 f_\pi \frac{\tilde{f}}{m_\pi}, \quad F_P^V = \frac{M+M^*}{m_\pi^2 - q^2} F_A^V, \quad (4.39)$$

where \tilde{f} is the $N^* \rightarrow N\pi$ coupling (see Sec. 1.5.3). A dipole form for the q^2 dependence of $F_A^V(q^2)$ is used

$$F_A^V(q^2) = \frac{F_A^V(0)}{(1 - q^2/M_A^2)^2}, \quad (4.40)$$

where $M_A = 1.0$ GeV, as taken in the case of $N - \Delta$ form factors.

4.3 Numerical results

In this section we present numerical results for the differential cross section for the processes $e^- p \rightarrow \Delta^0 \nu_e$, $e^+ p \rightarrow \Delta^{++} \bar{\nu}_e$, $e^- p \rightarrow N^* \nu_e$ and study them using various form factors. We stress here the importance of the decay width in the angular dependence of the cross sections and the effect of changing various form factors in the vector and axial vector sectors.

4.3.1 $e^- p \rightarrow \Delta^0 \nu_e$

We show in Fig. 4.2 the Δ angular distribution for energies $E_e = 0.5, 0.855$ and 4.0 GeV using the expressions for the form factors of $N - \Delta$ transition, given in Sec. 4.2.2. The electron energies are chosen to correspond to those reachable at Mainz and TJNAF accelerators. The invariant mass has been restricted to $W < 1.4$ GeV to include the Δ dominated events only. The differential cross section is found to be forward peaked at lower electron energies, for example at $E_e = 500$ MeV, but the peak shifts to higher angles as we increase the energy. There is a gain of 50 % in the total cross section as we go from the maximum Mainz energy (0.855 GeV) to 4 GeV. We also study the cross section sensitivity to the transition form factors by employing three different sets of vector and axial vector form factors. In the first set, we use Eqs. (4.16),(4.17) for the vector form factors and Eq. (4.24) for the axial vector form factors, and the results are shown in Fig. 4.2 (solid line). In the second set, we take the form factors recently discussed in Ref. [103], which use Eqs. (4.16),(4.18) for the vector form factors and Eq. (4.24) with $C_5^A(0) = 0.87$, $C_4^A(0) = -0.29$ MeV for the axial vector form factors. The results are shown by the short-dashed line. In the third set, we use the non-relativistic quark model form factors given by Eqs. (4.19),(4.25) and taken from Ref. [107]; the results are shown by the long dashed line.

In Fig. 4.3, using the first set of form factors, we show the effect of the decay width Γ on the differential cross sections $d\sigma/d\Omega_\Delta$ for $E_e = 500$ and 4000 MeV. It is clear from Fig. 4.3 that the Δ width plays an important role in the angular cross section. In the limit of $\Gamma \rightarrow 0$, our results qualitatively agree with those of Hwang et al. [106]. The narrow angular range in which the cross sections were earlier predicted to dominate is not there when the effect of decay width is taken into account. On the other hand there is a considerable cross section over a wide angular region, which increases as energy raises and corresponds to $0 < \theta < 45^\circ$ for $E_e = 4.0$ GeV. Therefore, a high angular resolution is not really needed in the experiments and large acceptance detectors can be used to study this reaction. This feature of angular dependence of the cross section is maintained with all the form factors used in this study.

4.3.2 $e^+ p \rightarrow \Delta^{++} \bar{\nu}_e$

The results for $e^+ p \rightarrow \Delta^{++} \bar{\nu}_e$ are given in Fig. 4.4. For this process, the cross section is overall enhanced by an isospin factor of 3 and reduced due to the different sign of the

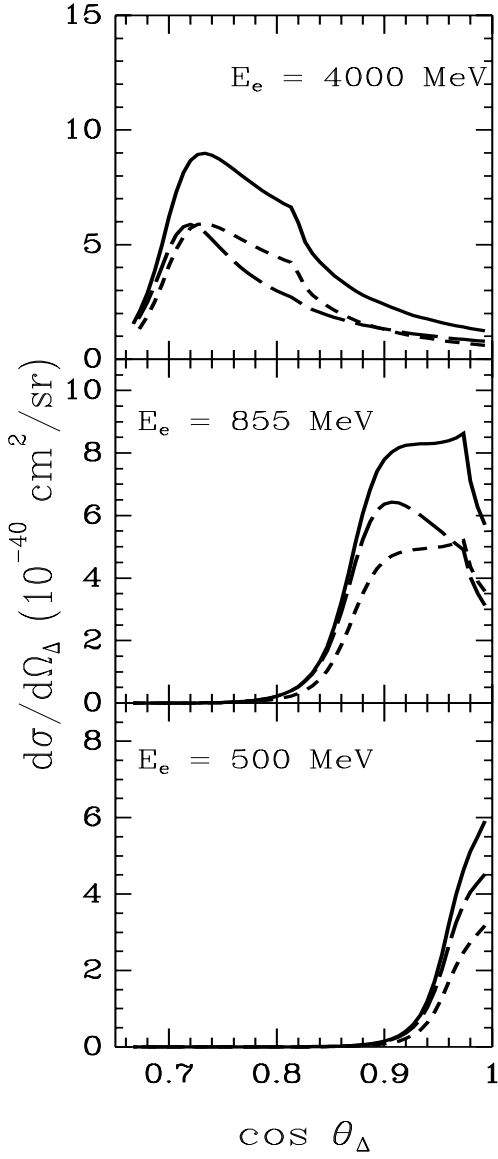


Figure 4.2: Δ^0 angular distribution for the reaction $e^- p \rightarrow \Delta^0 \nu_e$ with three different sets of form factors.

interference term, which depends on energy and momentum transfer. The angular dependence of the cross section and its increase with the energy are, otherwise, quite similar to the $e^- p \rightarrow \Delta^0 \nu_e$.

The role of interference terms is very interesting in the case of the $N - \Delta$ transition. As a comparison of Figs. 4.2 and 4.4 shows, the suppression due to the opposite sign of interference terms is quite large at lower energies to overtake the overall increase by a factor of

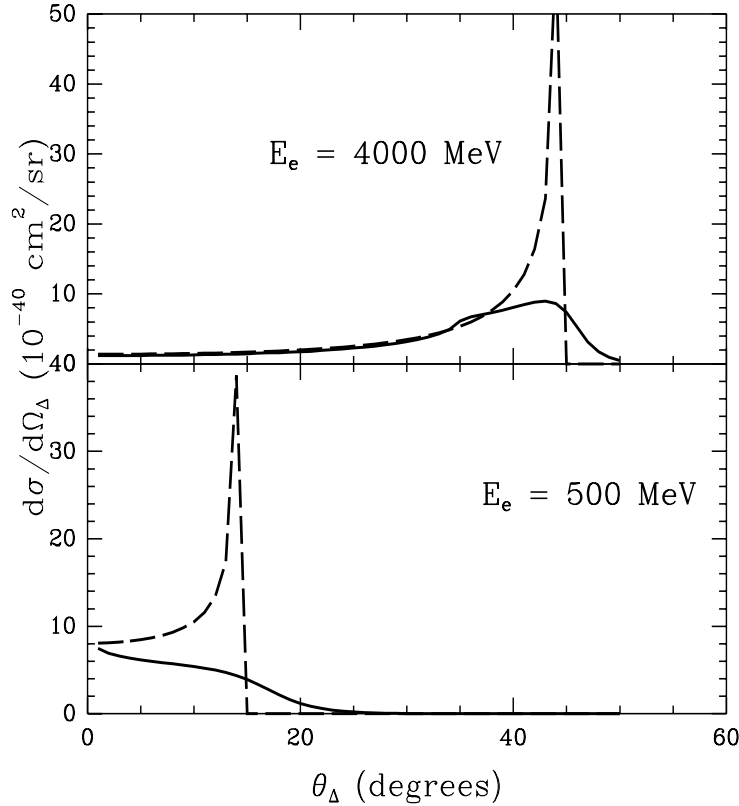


Figure 4.3: Δ^0 angular distribution for the reaction $e^- p \rightarrow \Delta^0 \nu_e$ with finite (solid line) and zero (dashed line) widths. The form factors are taken to be the same as for the solid line of Fig. 4.2.

3 due to isospin. As the energy increases, the relative importance of the interference terms becomes small and the cross section $e^+ p \rightarrow \Delta^{++} \bar{\nu}_e$ dominates. At around $E_\nu \sim 1.5$ GeV, the cross sections for $e^- p \rightarrow \Delta^0 \nu_e$ and $e^+ p \rightarrow \Delta^{++} \bar{\nu}_e$ are comparable. The effect of the decay width of the Δ is the same as discussed in Sec. 4.3.1, and our results with $\Gamma = 0$ are in qualitative agreement with the results of Hwang et al. [106], except that we obtain a larger cross section compared to the cross sections obtained by them in the region away from the peak.

4.3.3 $e^- p \rightarrow N^* \nu_e$

The vector form factors required in this calculation are obtained from Eqs. (4.36)-(4.38) by taking two different parametrizations of $A_{1/2}^p$ and $S_{1/2}^p$ from an analysis performed by Gerhardt, as quoted by Li et al [118]. They are shown in Fig. 4.5. There is some confusion in the literature concerning the sign of $S_{1/2}^p$, as can be judged from Ref. [118, 119], but our results are not sensitive to the change of this sign. In Fig. 4.6, we present the results for the $d\sigma/d\Omega_{N^*}$ at $E_e = 4$ GeV with the same invariant mass cut for N^* production as

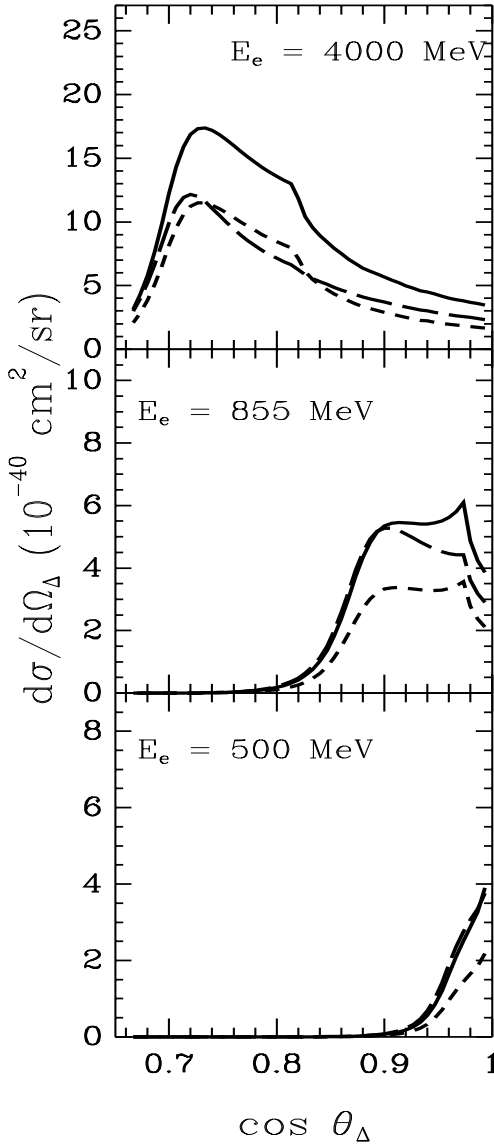


Figure 4.4: Same as Fig. 4.2 for the reaction $e^+ p \rightarrow \Delta^{++} \bar{\nu}_e$.

for Δ production ($W < 1.4$ GeV). We find that the cross sections for N^* production are smaller than the Δ production cross sections by an order of magnitude. Furthermore, the N^* angular cross section peaks around $\cos \theta = 0.82$ as compared to the Δ production that peaks around $\cos \theta = 0.73$. The present uncertainty in the determination of the form factors $F_1^V(q^2)$ and $F_2^V(q^2)$ leads to an uncertainty of 20 % in the cross section in the peak region, as shown in Fig. 4.2. This uncertainty does not affect the main conclusion of this study as the contribution of N^* production in the kinematic region of pions coming from Δ

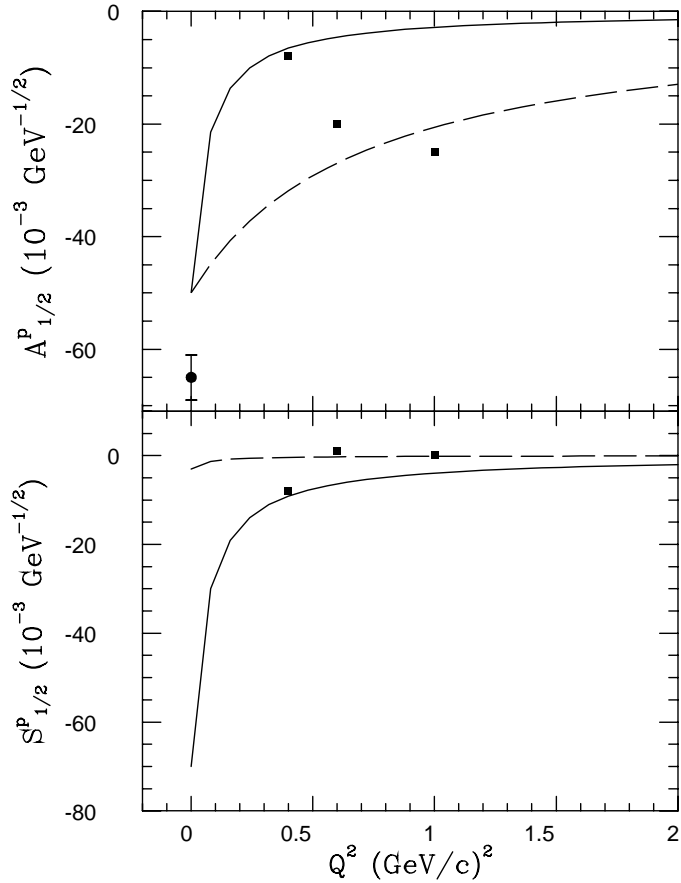


Figure 4.5: $N - N^*(1440)$ helicity amplitudes as a function of Q^2 for two different parametrizations of Gerhardt's analysis [117]. The full dot is the PDG value [18] of $A_{1/2}^p$ at the photon point and the full squares are the results of Gerhardt's analysis of the electroproduction data.

decay is still too small and peaks at a different angle than the Δ 's. Increasing the invariant mass cut from 1.4 GeV to $(M^* + m_\pi)$, shifts the peak of N^* to still lower angles. Therefore, the larger width of the N^* affects pion production rates in an angular region well separated from the Δ produced pions.

4.3.4 Experimental considerations

We now address ourselves to the present experimental situation and the possibility of observing these reactions at Mainz and/or TJNAF accelerators. At these accelerators luminosities of the order of $10^{38} \text{ cm}^{-2} \text{ sec}^{-1}$ or more are expected. The estimated count rate is given by

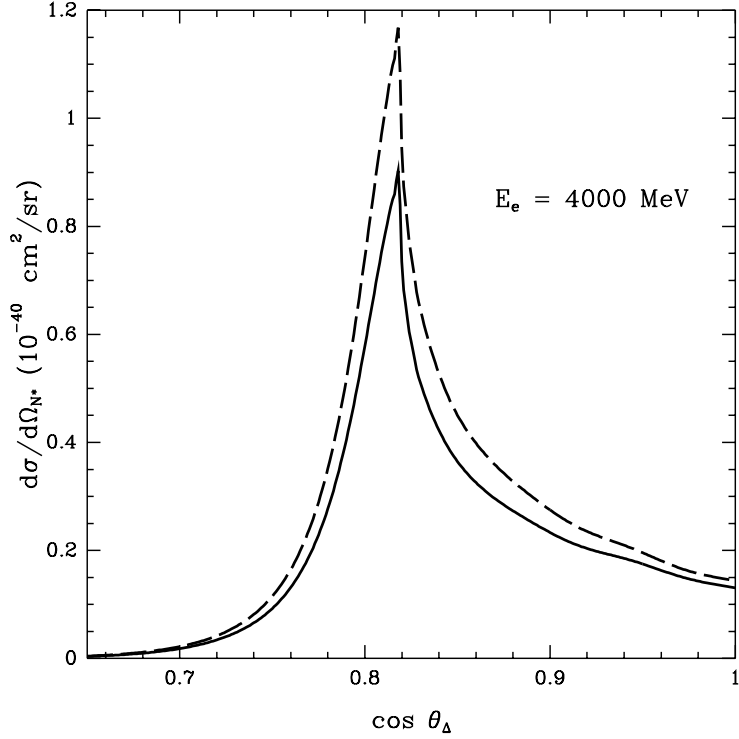


Figure 4.6: N^* angular distribution for the reaction $e^- p \rightarrow N^* \nu_e$ for the two parametrizations of the vector form factors extracted from Gerhardt's analysis [117] and shown in Fig. 4.5.

$$\text{counts/hour} = \Delta\Omega \times \frac{d\sigma}{d\Omega} \times \text{luminosity} \times 3600 \text{ sec/hour} \times \text{detector efficiency.} \quad (4.41)$$

Using this formula, for example at 4.0 GeV, in the peak region of around 40° where the cross sections are of the order of 10^{-39} cm^2 , we find the count rate to be

$$\text{counts/hour} \sim 360 \times \Delta\Omega(\text{sr}) \times \text{detector efficiency/hour.} \quad (4.42)$$

A similar count rate is expected at $E_e = 855 \text{ MeV}$ in the vicinity of 20° , where the cross sections are of the same order. Keeping in mind the finite angular range over which the cross sections are appreciably larger than 10^{-40} cm^2 , the estimates made above suggest that the number of counts could be high enough for considering the feasibility of doing such experiment.

4.4 Summary

We have made a theoretical study of the weak production of Δ and $N^*(1440)$ through the charge changing reactions induced by electron beams of energies corresponding to Mainz and TJNAF accelerators. We find that :

1. The differential cross section for the weak production of Δ resonance with electron beams is of the order of 10^{-39} cm^2/sr , which is quite sizeable. At $E_e = 855$ MeV, the cross section for $e^- p \rightarrow \Delta^0 \nu_e$ is larger than the cross section for $e^+ p \rightarrow \Delta^{++} \bar{\nu}_e$ while at $E_e = 4.0$ GeV, the cross section for $e^+ p \rightarrow \Delta^{++} \bar{\nu}_e$ process is about a factor two larger than the $e^- p \rightarrow \Delta^0 \nu_e$. As we increase the energy from 855 to 4000 MeV the peak in the cross section shifts to a higher angle from 20° to 40° .
2. There is a large angular region in which the differential cross sections are appreciable. This feature of the differential cross sections facilitates the observation of this reaction at current electron accelerators, where large angle acceptance detectors are planned to be used in electron scattering experiments. There is no need for a sharp angular resolution in the vicinity of 0.1° as found earlier, based on a calculation neglecting the decay width of the Δ resonance.
3. The production cross section for $N^*(1440)$ is an order of magnitude smaller than the production cross section of the Δ and peaks at an angle well separated from the Δ production peak region. This makes the identification of Δ^0 through the measurement of pions and protons quite clean for the invariant mass cut of $W < 1.4$ GeV. There is no such contamination from N^* resonances in the identification of Δ^{++} .
4. The production cross section is dominated by the three form factors C_5^A , C_3^V and C_4^V and an experimental measurement could discriminate between the various models used for these form factors. If the electromagnetic production cross sections for the Δ resonance are precise enough to fix the C_3^V and C_4^V form factors, this will make the determination of C_5^A quite model independent.
5. There is a very strong energy dependence of the V-A interference terms in Δ production process which can be used for determining the other form factors like $C_3^A(q^2)$ and $C_4^A(q^2)$. An experimental information on these form factors is extremely important for the theoretical models currently used for nucleon structure as well as for some earlier analyses which use quite different values of C_3^A and C_4^A for explaining the experimental data on neutrino scattering in the intermediate energy region.

Chapter 5

$\nu d \rightarrow \mu^- \Delta^{++} n$ reaction and axial vector $N - \Delta$ coupling

5.1 Introduction

In this chapter, we focus our attention on the axial vector coupling $C_5^A(0)$, whose extraction from experiment might be useful to discriminate among different models and to understand better the nature of the $SU(6)$ symmetry breaking [107, 103]. We undertake the determination of $C_5^A(0)$ [122] using the data from the BNL experiment of Kitagaki et al. [91] on the ratio of the differential cross sections for the inelastic $\nu d \rightarrow \mu^- \Delta^{++} n$ and the quasielastic $\nu d \rightarrow \mu^- pp$ reactions. We also analyze the experimental results from the ANL experiment of Radecky et al. [93], which has about three times more events than the experiment of Barish et al. [95]. In the case of the inelastic reaction, all the experimental analyses [95, 91, 93] exclude the region of very low $|q^2|$ i.e. $|q^2| \leq 0.1 \text{ GeV}^2$. In this region, the nuclear corrections due to the deuteron target have not been calculated. We take into account the effect of deuteron structure in the present work. We also study the effect of the width of the Δ resonance on the differential cross section, and its influence in the determination of $C_5^A(0)$. We use an energy dependent P-wave width for the Δ while in earlier analyses of this reaction [95, 91, 93], an energy dependent S-wave width was considered. These effects were not taken into account in a similar analysis [103], where the low q^2 data was used to obtain $C_5^A(0)$ from the ratio of the differential cross section of the inelastic reaction $\nu d \rightarrow \mu^- \Delta^{++} n$ and the quasielastic reaction $\nu d \rightarrow \mu^- pp$. The analysis presented here brings out in detail the various uncertainties involved in the extraction of $C_5^A(0)$ from the data when extrapolated to $q^2 = 0$.

In Sec. 5.2, we calculate the effects of deuteron structure and width of the Δ resonance on the differential cross sections. We determine the value of $C_5^A(0)$ in Sec. 5.3, where the possibility of extracting it from electron scattering experiments is also discussed. Section 5.4 provides a summary of the results.

5.2 Differential cross section

5.2.1 Differential cross section for $\nu d \rightarrow \mu^- \Delta^{++} n$

Let us first consider the case of the free reaction $\nu_\mu(k) + p(p) \rightarrow \mu^-(p') + \Delta^{++}(k')$, i.e. in absence of nuclear effects. The differential cross section is written as

$$\frac{d^2\sigma}{dq^2} = \frac{1}{128\pi^2} \frac{M}{M_\Delta} \frac{1}{(s - M^2)^2} G^2 \cos^2 \theta_c \int dk'^0 L_{\alpha\beta} J^{\alpha\beta} \frac{\Gamma_\Delta(W)}{(W - M_\Delta)^2 + \Gamma_\Delta^2(W)/4}. \quad (5.1)$$

where $s = (p+k)^2$; the other ingredients have been described in detail in the previous chapter (Sec. 4.2). The expressions given there can be directly translated here, keeping in mind that in Eq. (4.8) for the leptonic tensor $L_{\alpha\beta}$, k now refers to the initial neutrino and k' to the final muon. As for the $N - \Delta$ transition vector and axial vector form factors $C_i^{V,A}$ ($i = 3-6$) is concerned, we take the phenomenological set consisting of Eqs. (4.16), (4.17), (4.22)-(4.24)

Effect of Deuteron Structure

When the reaction takes place in the deuteron, i.e. $\nu(k) + d(p) \rightarrow \mu^-(k') + \Delta^{++}(p'_1) + n(p'_2)$, the differential cross section in the impulse approximation is calculated to be

$$\begin{aligned} \frac{d^2\sigma}{dq^2} &= \frac{1}{128\pi^2} \frac{M_d^2}{M_\Delta(s - M_d^2)^2} G^2 \cos^2 \theta_c \int dk'^0 L_{\alpha\beta} J^{\alpha\beta} \\ &\times \int \frac{d\mathbf{p}'_2}{(2\pi)^3 p'_2} \frac{\Gamma_\Delta(W)}{(W - M_\Delta)^2 + \Gamma_\Delta^2(W)/4} \tilde{\varphi}^2(|\mathbf{p}'_2|), \end{aligned} \quad (5.2)$$

where M_d is the deuteron mass and $\tilde{\varphi}(|\mathbf{p}'_2|)$ is the Fourier transform of the deuteron radial wave function, normalized as in Eq. (3.5). This expression is derived assuming the neutron to be spectator, and neglecting meson exchange currents and final state interactions. The contribution of these effects to the differential cross section $d\sigma/dq^2$ has been studied earlier for the case of the quasielastic reaction [123] and found to be small in the kinematical region considered here. Using Eq. (5.2), we calculate the differential cross section for various deuteron wave functions corresponding to Hulthen [87], Paris [66] and Bonn [30] potentials, and compare them with the differential cross section obtained in the free case, calculated from Eq. (5.1).

The results for $d\sigma/dq^2$ as a function of $Q^2 \equiv -q^2$ for the incident neutrino energy $E_\nu = 1.6$ GeV, which is the mean energy of the BNL ν_μ beam [92], are shown in Fig. 5.1. We see that deuteron effects are small, not exceeding 8 % even at low Q^2 i.e. $Q^2 < 0.1$ GeV 2 . This is the region where they give a large reduction in the quasielastic reaction $\nu d \rightarrow \mu^- pp$ [123]. The different behavior of deuteron effects in these two reactions is due to the nature of the vector current contribution. In the inelastic reaction, the vector part vanishes for proton as well as for deuteron targets in the limit of $Q^2 \rightarrow 0$, and the only contribution

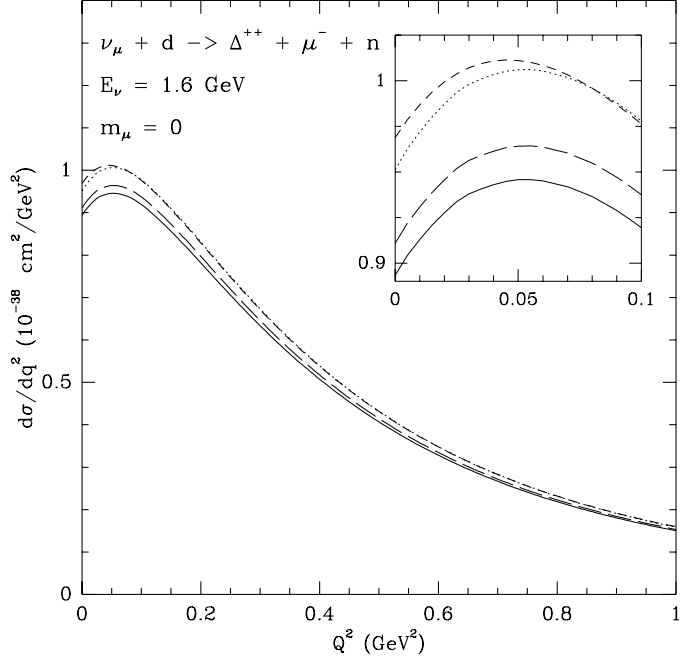


Figure 5.1: Differential cross section for weak charged current neutrino production of the Δ resonance on the deuteron. In the short-dashed line, deuteron effects are neglected while dotted, long-dashed and solid lines include these effect using Hulthen, Bonn and Paris deuteron wave functions respectively.

comes from the axial vector piece, which is only slightly affected by the deuteron structure. On the other hand, in the quasielastic reaction, while both vector and axial vector currents contribute for the nucleon case, the vector piece is completely suppressed in the deuteron. Therefore, the only contribution left in the case of the deuteron is from the axial vector current with an effective strength, which is strongly reduced due to symmetry considerations of the two nucleons in the final state [123]. In the range of $Q^2 > 0.1$ GeV² the deuteron effects are found to be quite small on the differential cross section $d\sigma/dq^2$ for both inelastic and quasielastic reactions.

We compare the deuteron structure effects in both reactions by computing the ratio $R(Q^2)$ defined as

$$R(Q^2) = \frac{(d\sigma/dq^2)(\nu d \rightarrow \mu^- \Delta^{++} n)}{(d\sigma/dq^2)(\nu d \rightarrow \mu^- pp)}, \quad (5.3)$$

and plotting it as a function of Q^2 . In calculating $R(Q^2)$, we use the deuteron wave function obtained from the Paris potential. The differential cross sections for the quasielastic reaction is taken from Singh and Arenhoevel [123] for the case where meson exchange currents and final state interaction effects are neglected, in order to be consistent with our present calculation for the inelastic reaction. In Fig. 5.2, we show $R(Q^2)$ for the range of low Q^2 ,

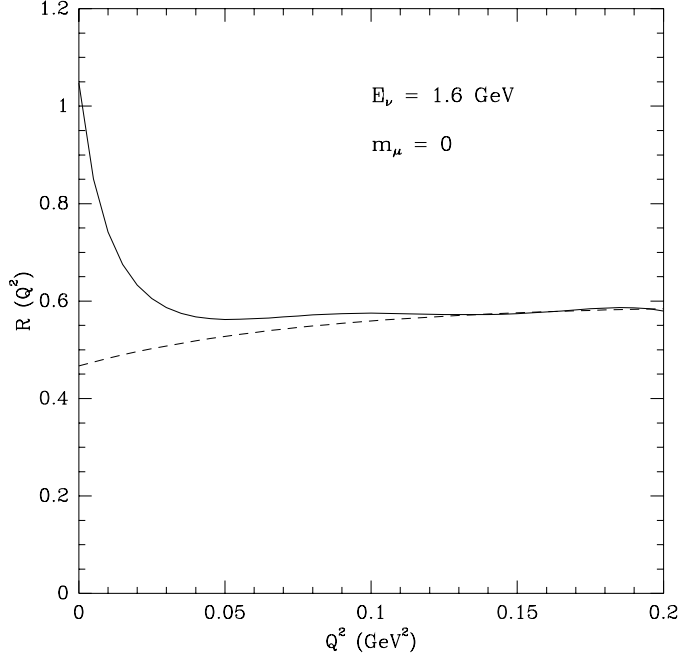


Figure 5.2: Ratio of Δ production and quasielastic reactions differential cross sections with (solid line) and without (dashed line) deuteron effects.

where deuteron effects are known to be important in the case of quasielastic reaction. We also show in this figure the ratio for the equivalent reactions on the free nucleon, given by

$$R_0(Q^2) = \frac{(d\sigma/dq^2)(\nu p \rightarrow \mu^- \Delta^{++})}{(d\sigma/dq^2)(\nu n \rightarrow \mu^- p)}; \quad (5.4)$$

such a ratio is not directly measurable because of the absence of neutron targets. We see that $R_0(Q^2)$ remains approximately constant for the range of Q^2 considered here. For values of $Q^2 < 0.05 \text{ GeV}^2$, the ratio increases; this is mainly due to the decrease in the cross sections of the quasielastic reaction. In the region of $0.05 < Q^2 < 0.10 \text{ GeV}^2$, the comparison between R and R_0 shows that deuteron effects are always less than 7% according to our calculation. At $Q^2 \geq 0.1 \text{ GeV}^2$, the region measured experimentally, $R(Q^2) \approx R_0(Q^2)$; this implies that one can treat the data on $R(Q^2)$ at $Q^2 \geq 0.1 \text{ GeV}^2$ obtained in Ref. [91], as if they were data on $R_0(Q^2)$. This fact will be used in Sec. 5.3 to extract the coupling $C_5^A(0)$.

In the region of very low Q^2 , the nonzero muon mass may play a role. In order to see its effect, we have evaluated the differential cross section $d\sigma/dq^2$ from Eq. (5.2), keeping the muon mass term and the induced pseudoscalar form factor $C_6^A(Q^2)$. We show our results in Fig. 5.3 for the case of the Paris wave function. The effect of the nonzero muon mass is important in the region of very low Q^2 and is noticed in a fast decrease of the differential cross section as Q^2 decreases and reaches a value Q_{min}^2 , below which the reaction is kine-

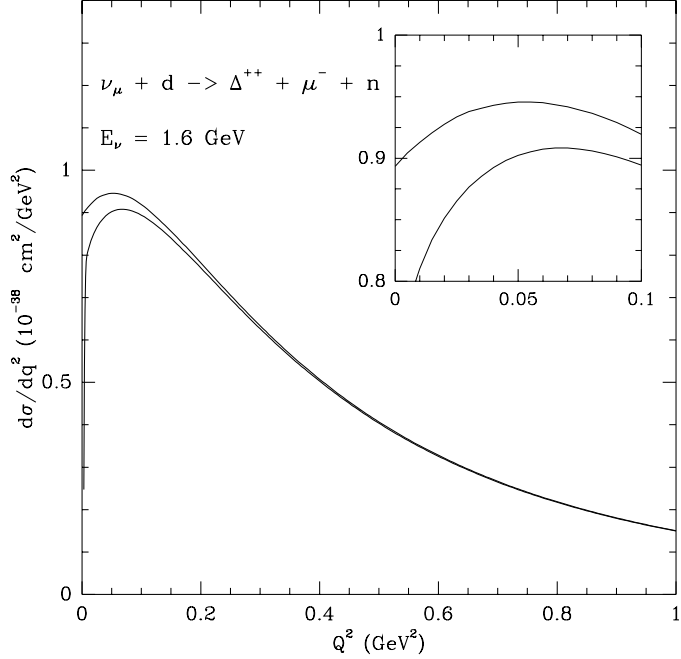


Figure 5.3: Effect of the muon mass on the differential cross section for the $\nu d \rightarrow \mu^- \Delta^{++} n$ reaction. In the upper line, the muon mass is neglected while it is considered in the lower one. Both curves include deuteron effects using the Paris parametrization of the deuteron wave function.

matically not allowed. In fact, in an earlier analysis of the Brookhaven experiment [92], this trend is clearly visible (see Fig. 11 of Ref. [92]) but, as no cross sections are quoted in this experiment, a direct comparison with our present theoretical results can not be made.

Finally, to conclude this section on the effect of deuteron structure in the reaction $\nu d \rightarrow \mu^- \Delta^{++} n$, we would like to elaborate and extend the comments made by Kitagaki et al. [91] about these effects and state that, at $E_\nu = 1.6 \text{ GeV}$:

- The effects of deuteron structure are small for all Q^2 , even for $Q^2 < 0.1 \text{ GeV}^2$, not exceeding 10 %.
- There is an additional reduction in the cross sections in the region of $Q^2 \sim 0.05 \text{ GeV}^2$ due to the nonzero muon mass, which is about 5 %, and could be larger as Q^2 decreases further.

5.2.2 Effect of the width of Δ resonance

The analysis of Schreiner and von Hippel [110] uses an S-wave width for the Δ resonance, which has also been used in the ANL and BNL experiments [95, 91, 93]. The recent paper of Ref. [103], dealing with the $N - \Delta$ couplings and the extraction of $C_5^A(0)$, uses an

expression for the differential cross section at $Q^2 = 0$, which neglects the width of the Δ resonance. In this situation, it seems worthwhile to examine the effect of the width of the Δ resonance. Therefore, we study the sensitivity of the differential cross section for the process $\nu p \rightarrow \mu^- \Delta^{++}$ to the width of the Δ resonance and its energy dependence. In order to do this, we evaluate the differential cross section given in Eq. (5.1) with

- P-wave Δ resonance width given in Eq. (1.59)
- S-wave Δ resonance width given by [110]

$$\Gamma = \Gamma_0 \frac{q_{cm}(W)}{q_{cm}(M_\Delta)}, \quad (5.5)$$

with $\Gamma_0 = 120$ MeV [18].

- narrow resonance limit i.e. $\Gamma \rightarrow 0$, in which the differential cross section is given by

$$\frac{d\sigma}{dq^2} = \frac{1}{64\pi} \frac{1}{(s - M^2)^2} G^2 \cos^2 \theta_c L_{\alpha\beta} J^{\alpha\beta}, \quad (5.6)$$

obtained from Eq. (5.1) by integrating over k'^0 after taking the limit $\Gamma_0 \rightarrow 0$.

In Fig. 5.4, we present the results of $R(Q^2)$ for free nucleon targets in the three cases discussed above. We see here that the inclusion of the width gives a considerable reduction of the cross section, but the detailed form of its energy dependence is not very important when an invariant mass of $W \leq W_{cut} = 1.4$ GeV is used. We have also found that the uncertainties in the width of about 10 – 15 MeV [18] at the resonance energy do not lead to any substantial change in the cross section.

5.3 Axial vector $N - \Delta$ coupling

5.3.1 Neutrino scattering experiments

In this section, we evaluate the value of $C_5^A(0)$ using the data of Kitagaki et al. [91] on $R(Q^2)$, and use it later to describe the data of Radecky et al. [93] for the differential cross section $d\sigma/dq^2$.

In the limit $Q^2 \rightarrow 0$, the cross sections required to evaluate $R_0(0)$ are

$$\frac{d\sigma}{dq^2}(q^2 = 0) = (F_A^2 + F_{1V}^2) \frac{1}{2\pi} G^2 \cos^2 \theta_c \quad (5.7)$$

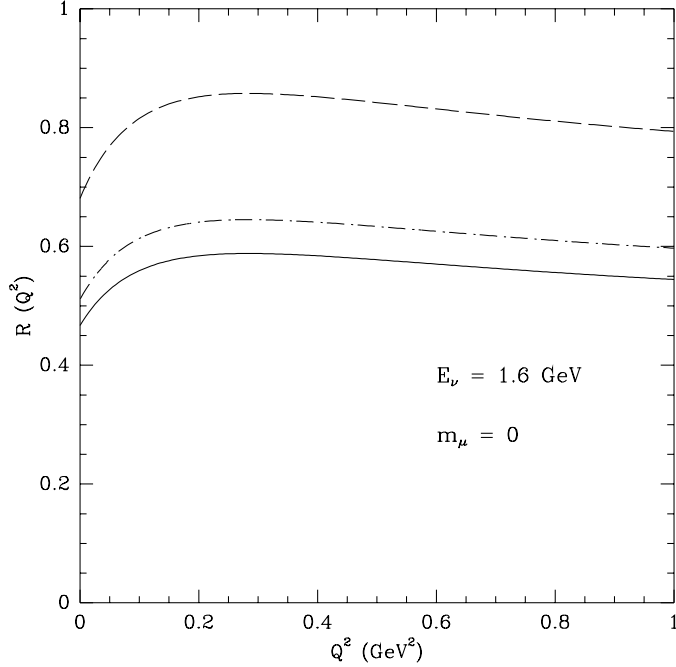


Figure 5.4: Effect of the Δ width in $R(Q^2)$: the solid line corresponds to a P-wave width, the dash-dotted line, to an S-wave width and the dashed line, to the case of zero width resonance. Deuteron effects have been neglected in all curves.

for the quasielastic reaction (details of the derivation of this formula and the values of F_A , F_{1V} are given in Appendix G), and

$$\begin{aligned} \frac{d\sigma}{dq^2}(q^2 = 0) &= [C_5^A(0)]^2 \frac{1}{24\pi^2} G^2 \cos^2 \theta_c \frac{\sqrt{s}(M + M_\Delta)^2(s - M_\Delta^2)^2}{(s - M^2)M_\Delta^3} \\ &\times \int_{k'^0_{min}}^{k'^0_{max}} dk'^0 \frac{\Gamma_\Delta(W)}{(W - M_\Delta)^2 + \Gamma_\Delta^2(W)/4} \end{aligned} \quad (5.8)$$

for the inelastic one; k'^0_{min} and k'^0_{max} are given by

$$k'^0_{min} = \max \left(\frac{s - W_{cut}^2}{2\sqrt{s}}, 0 \right), \quad k'^0_{max} = \frac{s - (M + m_\pi)^2}{2\sqrt{s}}. \quad (5.9)$$

This result depends only on the coupling constant $C_5^A(0)$, at variance with the result of Ref. [103], but in agreement with the result of Ref. [95]; it also agrees with Albright and Liu [124] (Eq. (3.15)) when their Eq. (2.12) is used along with the conversion table of the various definitions for the transition form factors given by Llewellyn Smith [111]. In an expansion of R_0 in powers of Q^2 , the first term that depends on the axial mass and other couplings is the one proportional to Q^2 . Thus, data at low enough Q^2 would allow a model

independent extraction of $C_5^A(0)$. The experimental data of Ref. [92] begin at quite low Q^2 ($Q^2 \sim 0.1$ GeV 2). In the region where the first points lie, we obtain an approximately constant value for $R_0(Q^2)$ with the choice of parameters given in Eqs. (4.16), (4.17), (4.22)-(4.24), as can be seen in Fig. 5.2; this behavior remains the same for moderate changes of the form factors. For this reason, we can use a constant value to extrapolate the R_0 data to $Q^2 = 0$.

Equating the ratio of these two cross sections given in Eqs. (5.7) and (5.8) i.e. $R_0(Q^2 = 0)$ to the extrapolated experimental value of 0.55 ± 0.05 , obtained as an average of the data on $R(Q^2)$ for $R(Q^2) \geq 0.1$ GeV 2 [91] (that is, in the region where we know that $R \approx R_0$). We obtain

$$C_5^A = 1.22 \pm 0.06. \quad (5.10)$$

Eq. (5.8) could also be directly used to extract $C_5^A(0)$ from data on the $\nu p \rightarrow \mu^- \Delta^{++}$ reaction. However, the uncertainties, both statistical and related to the neutrino flux, in the existing data do not allow for a better determination of the coupling constants. The quoted error comes exclusively from experiment. It does not include an estimation of the theoretical uncertainties implicit in our approximations, such as the neglect of meson exchange currents and final state interactions, that were discussed in Sec. 5.2.1.

In Table 5.1, we compare the values of this coupling constant with the theoretical values obtained in various models. With the exception of the quark model treatment of Liu et al. [107], all the quark models underestimate the value of $C_5^A(0)$ when compared to the central values quoted from experimental analyses. On the other hand, it is in good agreement with the prediction of PCAC. It is expected that the various extensions of the quark models currently proposed to explain the quadrupole moment of Δ , and the E_{+1}/M_{+1} ratio measured in Δ photoproduction and electroproduction will be applied to the problem of explaining $C_5^A(0)$ and other $N - \Delta$ couplings in these models.

Using our value of $C_5^A(0)$, at $Q^2 = 0$ and its Q^2 behavior, together with other form factors as given in Eqs. (4.16), (4.17), (4.22)-(4.24), we calculate the flux averaged differential cross section for the neutrino energy spectrum of the Argonne experiment of Radecky et al. [93]. The ν_μ spectrum at Argonne was calculated in Ref. [130]; it peaks around

Table 5.1: The numerical values of axial $N - \Delta$ coupling C_5^A in various quark model and empirical approaches. The earlier, prior to 1973, evaluations of these couplings in these approaches have been summarized by Schreiner and von Hippel [110] and Llewellyn Smith [111].

	$C_5^A(0)$
Quark Model approaches	0.97 [125, 126], 0.83 [127], 1.17 [107], 1.06 [128], 0.87 [103]
Empirical approaches	1.15 ± 0.23 [95], 1.39 ± 0.14 [103], 1.1 ± 0.2 [129], 1.22 ± 0.06^a

^aPresent result.

$E_\nu = 0.5$ GeV and has a tail extending to 6 GeV. The results are presented in Fig. 5.5. We

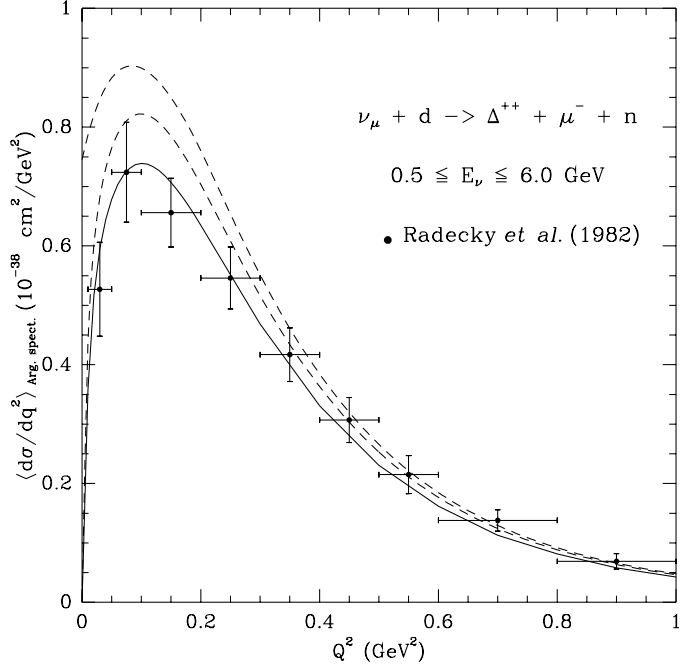


Figure 5.5: Differential cross section for weak charged current neutrino production of Δ on deuteron, averaged over the spectrum of the ANL experiment, compared to the experimental results given in Ref. [93]. The solid curve includes both nonzero muon mass and deuteron effects. The upper dashed curve neglects muon mass and deuteron effects. The lower dashed curve neglects only deuteron effects.

see that the inclusion of deuteron and mass effects lead to a better description of the data. It is to be emphasized that a small reduction in the differential cross section due to these effects is quite important in bringing out a good agreement with the experimental data, specially in the low q^2 region. The proper inclusion of the neutrino spectrum appears also to be important, in contrast to the case where a ratio is considered.

5.3.2 Electron scattering experiments

It is possible to get information about the axial vector coupling $C_5^A(0)$ from the observation of the parity violating asymmetry in the polarized electron scattering experiments performed in the Δ region. The feasibility of doing such experiments was discussed in the past by many authors [98], but it seems now possible to perform them at high intensity electron accelerators [97, 99, 100]. In the case of the neutral current reaction $e^- p \rightarrow e^- \Delta^+$ with polarized electrons the asymmetry $A(Q^2)$ is defined as

$$A(Q^2) = \frac{(d\sigma/dq^2)(+1) - (d\sigma/dq^2)(-1)}{d\sigma/dq^2(+1) + d\sigma/dq^2(-1)}, \quad (5.11)$$

where $d\sigma/dq^2(\lambda)$ is the differential cross section for an electron with helicity λ . It has been calculated to be [100]

$$\begin{aligned} A(Q^2) = & -\frac{G}{2\sqrt{2}\pi\alpha} |Q^2| \left[(1 - 2\sin^2\theta_W) \right. \\ & + (1 - 4\sin^2\theta_W) \frac{C_5^A}{C_3^V} \left(1 + \frac{M_\Delta^2 + Q^2 - M^2}{2M^2} \frac{C_4^A}{C_5^A} \right) P(Q^2, s) \Big] \\ & + \text{non-resonant contribution,} \end{aligned} \quad (5.12)$$

where $P(Q^2, s)$ is a purely kinematical factor.

In principle, one can determine the value of C_5^A/C_3^V from asymmetry measurements by selecting the kinematics where non-resonant contributions are negligible. However, as we see from Eq. (5.12), the hadronic axial vector current contribution containing C_5^A is multiplied by a factor $(1 - 4\sin^2\theta_W)$, which reduces the sensitivity of the asymmetry $A(Q^2)$ to this term. This makes the extraction of C_5^A from a measurement of the asymmetry very difficult. Even in the favorable kinematical region of $0.5 < E_e < 1$ GeV and $Q^2 < 1.0$ GeV 2 , this term contributes only (10-20) %, as emphasized by Mukhopadhyay et al. [100].

There is also a possibility of observing the charged current reaction $e^- p \rightarrow \Delta^0 \nu$ with unpolarized electrons through the detection of the protons and pions from the decay of the Δ resonance [105], as discussed in the previous chapter. At an incident electron energy of 4 GeV, the differential cross section $d\sigma/dq^2$ in the forward direction near $Q^2 = 0$ is estimated to be $2 \cdot 10^{-39}$ cm 2 /GeV 2 . For an incident intensity of about $2 \cdot 10^{38}$ cm 2 /sec [103] and Q^2 bin of 0.05 GeV 2 , one would expect 72 events per hour for the production of Δ^0 , assuming 100% efficiency of the detector. One third of these Δ 's will produce negatively charged pions and protons, which can be easily observed. Since in the region of $Q^2 \sim 0$, C_5^A gives the dominant contribution, its determination from the weak charged current experiment of Δ production seems feasible. Note, however, that in the analysis of this process, a theoretical study of the non-resonant background is required to extract the resonant contribution from the data, which would lead to further uncertainties. In the case discussed in Sec. 5.3 (Δ^{++} production in deuterium), the non-resonant background was found to be around 1 %, whereas for other isospin channels, it was found to be considerably larger [91].

5.3.3 Pion photoproduction and electroproduction experiments

It is well known that, in the threshold region of pion photoproduction and electro production on the nucleon, the matrix element of these processes in the soft pion limit is related with the nucleonic matrix element of the axial vector current using the methods of current

algebra and PCAC. This relation has been exploited to obtain information about the axial vector form factor of the nucleon [131]. In a similar way, threshold pion production in the processes $e^- p \rightarrow e^- \Delta^+ \pi^0$ and $\gamma p \rightarrow \Delta^{++} \pi^-$ is related, in the soft pion limit, with the $N - \Delta$ transition matrix element of the axial vector current. The axial vector transition form factors can, in principle, be determined from these processes in the limit of soft pions. Such attempts have been made in the past and they yield $C_5^A(0) = 1.1 \pm 0.2$ [129].

However, in this case, the treatment of higher resonances and their effective couplings used for evaluating the matrix elements of the time ordered product of the vector and axial vector current operators involve many approximations, which need further justification. Recently, there has been some progress in calculating the contribution of higher resonances to the production of two pions in the photo and electroproduction processes using effective Lagrangians [45, 132]. It should be possible to isolate the dominant contributions from higher order resonances, which are relevant for the $\Delta\pi$ production in the soft pion limit. This will help to reduce the theoretical uncertainties in the application of the methods of PCAC and current algebra to the processes where a Δ resonance is produced. In addition, when dealing with the Δ resonance, its width has to be properly taken into account as remarked by Bartl et al. [129], and also shown by us in the weak charged current production of the Δ resonance. The analysis of Ref. [129] uses the older data which suffers from poor statistics. When the results of a recent experiment proposed at TJNAF [133] become available in near future, it will be possible to get precise information about the axial vector form factor and, in particular, its value at $q^2 = 0$.

5.4 Summary

We have calculated the effect of deuteron structure and width of the Δ resonance in the differential cross section for the reaction $\nu d \rightarrow \mu^- \Delta^{++} n$ and found that these effects are small, but important in order to explain the experimental results at low q^2 , where they were initially expected to be important. Furthermore, in the region of very low q^2 , the muon mass, which is usually neglected in the calculations, also reduces the cross section.

The effect of the width of the Δ resonance on the cross section is important and plays a crucial role in bringing out good agreement with the experimental data. The detailed shape and 10-15 % uncertainty in the width of the resonance do not affect the cross sections very much.

The axial vector $N - \Delta$ coupling C_5^A is extracted from the BNL data on $\nu d \rightarrow \mu^- \Delta^{++} n$, incorporating the effect of the deuteron structure and the width of the Δ resonance. This value of $C_5^A(0)$ is found to be larger than the values predicted in most of the quark models and is consistent with the prediction of PCAC and Adler's model.

Finally, we have discussed the possibility of determining this coupling from electron scattering experiments, and find that the weak charged current electroproduction of the Δ resonance is an interesting alternative to the asymmetry measurements.

Chapter 6

Conclusions and outlook

Part I

We have developed the first microscopic model for the reaction $NN \rightarrow NN\pi\pi$, meant to work in a wide range of energies, from threshold ($T_p = 600$ MeV) up to $T_p = 1400$ MeV. It includes the leading order terms of the effective pion-pion and pion -nucleon Lagrangians, as well as the explicit inclusion of the low lying resonances $\Delta(1232)$ and $N^*(1440)$. The phenomenological information presently available, specially the analyses of nucleon-nucleon and pion nucleon elastic and inelastic reactions, has been used in order to obtain the required coupling constants and off-shell form factors. Contrary to naive expectations, the Roper resonance plays a prominent role in this reaction through its two-pion decay channels $N^* \rightarrow \Delta\pi$ and $N^* \rightarrow N(\pi\pi)_{S-wave}^{T=0}$. The $N^* \rightarrow N(\pi\pi)_{S-wave}^{T=0}$ decay, in spite of its small relative strength (5-10 % branching ratio), is very important because its contribution to the amplitude does not vanish at threshold. A similar feature has been already observed in the $(\pi, \pi\pi)$ reactions in nucleons and nuclei. The $NN \rightarrow NN^*$ transition has been found to be dominated by an isoscalar potential, parametrized in terms of an effective σ exchange, whose strength was extracted in a recent analysis of the (α, α') reaction on a proton target. The isovector part is diminished because of the short range correlations. Therefore, in those channels where the outgoing pions can be in isospin zero ($\pi^+\pi^-$ and $\pi^0\pi^0$), the isoscalar excitation of the $N^*(1440)$ and its subsequent decay into $N(\pi\pi)_{S-wave}^{T=0}$ gives the dominant contribution to double-pion production below $T_p = 1$ GeV. The mechanism with $N^* \rightarrow \Delta\pi$ and the one with two Δ 's grow faster with the energy and become important at higher energies. Finally, the double- Δ amplitude becomes dominant above 1.3 GeV; the presence of the Δ at $T_p \approx 1.4$ GeV is clearly seen in the πN invariant mass distributions. In those channels where the pions cannot be in a T=0 state, the strength is appreciably smaller and distributed between different mechanisms. Further experimental information about this reaction at low energies and for most of the isospin channels will become available from CELSIUS in the near future.

In order to be able to extract relevant information about the dynamics of double-pion production in NN collisions at low energies, the role of the final state interaction should be properly understood. We have studied the NN FSI in a simplified version of the model

for the reaction channel $pp \rightarrow pp\pi^+\pi^-$ consisting only of the Roper isoscalar excitation and its decay $N^* \rightarrow N(\pi\pi)_{S-wave}^{T=0}$; this approximation is accurate below 900 MeV, which is the region where FSI should be important. FSI is implemented by introducing the strong part of the 1S_0 proton-proton wave function in the amplitude. The wave function has been obtained using a separable potential, whose parameters were obtained from a fit to the phase shifts. This approach has the advantage that one can obtain an analytic expression for the wave function, which simplifies appreciably the numerical calculations. FSI is found to cause a strong enhancement of the cross section, concentrated mainly in the region of low pp invariant masses. This is in agreement with the result obtained with a simplified approach based on the multiplication of the free production amplitude by the inverse of the Jost function for the pp scattering, calculated using the effective range approximation. We have also estimated the effect of Coulomb repulsion between the protons and found that it can be appreciable at low pp invariant masses; therefore, a more accurate calculation including this effect is required.

Next, the reaction $np \rightarrow d(\pi\pi)^0$ has been considered. This process received special attention in the past since it was the simplest reaction where the ABC was observed. In spite of the interest, many features of energy and angular behaviors observed remain unexplained. Our model is a simplified version of the one for the free reaction including the relevant resonance contributions: N^* and double- Δ excitation. The inclusion of the N^* contribution improves considerably the agreement in the total cross sections with respect to other models that do not include it, specially in the low energy region, where we are also able to describe the bumps observed at high $(\pi\pi)$ masses in the deuteron momentum spectra. This structure appears as a consequence of the interference of the dominant $N^* \rightarrow N(\pi\pi)_{S-wave}^{T=0}$ and the smaller in size $N^* \rightarrow \Delta\pi$ one. The contribution of the $\Delta\Delta$ mechanism is considerably reduced due to the short range correlations. At higher energies, we see the appearance of the ABC peaks, but the model is not accurate in the description of the deuteron spectra and clearly underestimates them at high angles. Further understanding of this reaction would require a better knowledge of the $NN \rightarrow NN^*$, $NN \rightarrow \Delta\Delta$ transition potentials, mainly its short range part, the deuteron wave function at high momentum transfer and also a relativistic treatment.

The present findings will be useful to understand the low energy behavior of other double pion production reactions. In the case of $dd \rightarrow \alpha X$, recent measurements close to threshold obtain structureless data and cross sections 20 times larger than those obtained with a model in which every pion is independently produced, and which is successful in the ABC region. The Roper excitation mechanisms could be responsible for the strength at low energies. On the other side, the reaction $pd \rightarrow {}^3He\pi\pi$ is being currently investigated experimentally at COSY and CELSIUS. The preliminary results show an enhancement at high (π, π) masses at $T_p \sim 500$ MeV, which is not yet understood.

Part II

We have studied the excitation of the Δ resonance via charge changing weak reactions induced by electrons ($e^- p \rightarrow \Delta^0 \nu_e$ and $e^+ p \rightarrow \Delta^{++} \bar{\nu}_e$), making use of the present available

information on the $N - \Delta$ vector and axial vector transition form factors in a relativistic calculation and including a proper treatment of the Δ width. At the typical energies of TJNAF or MAMI, the differential cross section are of the order of 10^{-39} cm 2 /sr, which are high enough to consider the possibility of measuring then. In addition, the differential cross sections span over a large angular region; therefore, the angular resolution in the vicinity of 0.1° predicted by a calculation that neglected the Δ width in the kinematics is not required. Among the axial form factors, the large contributions to the cross section comes from C_5^A . For this reason, relying on a precise enough determination of C_3^V and C_4^V from electromagnetic experiments, $C_5^A(q^2)$ and, in particular, the axial vector coupling $C_5^A(0)$ could be obtained in a quite model independent way. Such a determination would be valuable in order to reach a better understanding of the $SU(6)$ symmetry breaking pattern. We have also studied the excitation of the next resonance $N^*(1440)$ and found that its differential cross section is small and peaks in a region well off the peak of Δ^0 production; this implies that the contamination of the Roper resonance in the suggested experiment is negligible.

Finally, we have tried to achieve the best possible determination of $C_5^A(0)$ using the available data; we have extracted it from the BNL data on the ratio of Δ production events upon quasielastic events measured with a wide band neutrino beam with a mean energy of $\langle E_\nu \rangle = 1.6$ GeV and a deuterium target. The effects of the deuteron structure in the q^2 dependence of the ratio are found to be important at low q^2 but negligible in the region where the data were taken and, for this reason, are not taken into account in our determination. On the contrary, the proper inclusion of the Δ width causes a 30 % reduction of the cross section and cannot be neglected in the extraction of $C_5^A(0)$. The value of $C_5^A(0)$ is in agreement with the prediction of PCAC, which is higher than the values given by most quark model calculations. In addition, we have calculated the q^2 distribution for the reaction $\nu_\mu d \rightarrow \Delta^{++} \mu^- n$ averaged over the Argonne ν_μ spectrum, and found that the inclusion of deuteron effects and the muon mass leads to an appreciable improvement in the agreement with the data, specially at low q^2 .

Part III

Appendices

Appendix A

Monte Carlo Quadrature

There are many numerical methods for the computation of integrals but, when the integration domain is complicated and/or there are many variables involved, Monte Carlo method is one of the most efficient. A simple and straightforward algorithm for Monte Carlo integration is the so called Crude Monte Carlo [134]. It is a direct application of the central limit theorem. In fact, let \mathcal{H} be a hypercube of volume $V_{\mathcal{H}}$ and $f(x)$ with $x \in \mathcal{D} \subseteq \mathcal{H}$, the function to be integrated (f is obviously set to zero in $\mathcal{H} - \mathcal{D}$). Then

$$\sigma = \int_{\mathcal{H}} f(x) dx = V_{\mathcal{H}} \int_{\mathcal{H}} f(x) U_{\mathcal{H}}(x) dx \quad (\text{A.1})$$

which may be interpreted as the expectation value $\langle f \rangle$ with respect to the uniform distribution

$$U_{\mathcal{H}}(x) = \begin{cases} 1/V_{\mathcal{H}} & : x \in \mathcal{H} \\ 0 & : x \notin \mathcal{H} \end{cases} \quad (\text{A.2})$$

multiplied by the volume. According to the central limit theorem

$$\sigma = V_{\mathcal{H}} \langle f \rangle = \lim_{N \rightarrow \infty} \frac{V_{\mathcal{H}}}{N} \sum_{i=1}^N f(x_i) \quad (\text{A.3})$$

and the variance is given by

$$s^2 = \frac{(V_{\mathcal{H}})^2}{N} \left[\frac{1}{N} \sum_i f^2(x_i) - \left(\frac{1}{N} \sum_i f(x_i) \right)^2 \right] \quad (\text{A.4})$$

This procedure can be directly used to evaluate the phase space integrals leading to total cross section. It can also be easily adapted to the calculation of differential cross sections. In order to illustrate this, let us assume that we want to obtain the observable $d\sigma/dx$. We know that

$$\sigma = \int_{\mathcal{D}} dx \frac{d\sigma}{dx} \approx \sum_b \Delta x_b \frac{\Delta\sigma}{\Delta x_b} \quad (\text{A.5})$$

where $\{b\}$ is a partition of the interval \mathcal{D} . For a large enough value of N , using Eq. (A.3) one obtains

$$\sigma \approx \frac{V_{\mathcal{H}}}{N} \sum_b \sum_{i \in b} f(x_i) \approx \sum_b \Delta x_b \frac{\Delta\sigma}{\Delta x_b} \quad (\text{A.6})$$

and hence

$$\frac{\Delta\sigma}{\Delta x_b} \approx \frac{1}{\Delta x_b} \frac{V}{N} \sum_{i \in b} f(x_i) \quad (\text{A.7})$$

This formula is more exact for larger values of N and smaller Δx_b . In practice, both N and Δx_b are chosen to correspond to the binning and the statistics of the experiment for the observable under analysis.

Appendix B

Non-relativistic baryon propagators

The nucleon

The nucleon propagator is not required for our calculations, but, in order to introduce some details of the formalism, and also for the sake of completeness, we shall consider it here. The nucleon propagator in momentum space can be written as a sum of positive and negative states

$$\frac{1}{\not{p} - M} = \frac{1}{p^0 - E + i\epsilon} \frac{M}{E} \Lambda_+(E, \mathbf{p}) - \frac{1}{p^0 + E - i\epsilon} \frac{M}{E} \Lambda_-(E, -\mathbf{p}) \quad (\text{B.1})$$

with $E = \sqrt{\mathbf{p}^2 + M^2}$ and

$$\begin{aligned} \Lambda_+(p) &= \sum_s u(p, s) \bar{u}(p, s) = \frac{\not{p} + M}{2M} \\ \Lambda_-(p) &= -\sum_s v(p, s) \bar{v}(p, s) = -\frac{\not{p} - M}{2M} \end{aligned} \quad (\text{B.2})$$

The second term in the sum can be neglected with respect to the first. For instance, in the vicinity of the pole ($p^0 = M$, \mathbf{p} small), $p^0 - E \sim \mathbf{p}^2/(2M)$, while $p^0 + E$ gives a much larger value of about $2M$. If we now write Λ_+ in our usual non-relativistic approximation (neglecting terms of order $|\mathbf{p}|/M$), the result is

$$\Lambda_+(E, \mathbf{p}) = \text{diag}(1, 1, 0, 0) \quad (\text{B.3})$$

i.e., the unity matrix for two component spinors. Hence, the non-relativistic nucleon propagator can be written as

$$D_N(p) = \frac{1}{p^0 - E + i\epsilon} \frac{M}{E} \quad (\text{B.4})$$

Needless to say that the separation of Eq. (B.1) is frame-dependent. In the vicinity of the pole the result of Eq. (B.4) can strongly differ from one reference frame to another, at least for large relative velocities of the frames. When $p^0 > |\mathbf{p}|$, there is an alternative way of writing the propagator, namely [135]

$$\frac{1}{\not{p} - M} = \frac{1}{2W} \frac{\not{p} + W}{W - M + i\epsilon} + \frac{1}{2W} \frac{\not{p} - W}{W + M - i\epsilon}, \quad (\text{B.5})$$

with $W = \sqrt{\not{p}^2}$. This separation coincides with the one of Eq. (B.1) in the nucleon rest frame. As in the previous case, the second term can be neglected. If one also neglects $|\mathbf{p}|/W$, the propagator reads

$$D_N(p) = \frac{1}{W - M + i\epsilon}. \quad (\text{B.6})$$

This formula is accurate in the vicinity of the pole independently of the reference frame.

The Roper resonance

The discussion above applies to the case of the Roper resonance propagator with no modification but the mass. The major difference arises from the fact that the $N^*(1440)$ has a width around 350 MeV, which cannot be ignored in the calculations. We then modify the propagator following the usual procedure to account for the width

$$D_{N^*}(p) = \frac{1}{W - M^* + i\frac{1}{2}\Gamma^*(p)}. \quad (\text{B.7})$$

Delta resonance

Let us recall the free Lagrangian for the massive spin 3/2 field.

$$\mathcal{L} = \bar{\psi}^\mu \Lambda_{\mu\nu} \psi^\nu \quad (\text{B.8})$$

with

$$\begin{aligned} \Lambda_{\mu\nu} = & (-i\not{\partial} + M_\Delta)g_{\mu\nu} - iA(\gamma_\mu \partial_\nu + \gamma_\nu \partial_\mu) \\ & - \frac{i}{2}(3A^2 + 2A + 1)\gamma_\mu \not{\partial} \gamma_\nu - M_\Delta(3A^2 + 3A + 1)\gamma_\mu \gamma_\nu, \end{aligned} \quad (\text{B.9})$$

where A is an arbitrary parameter subject to the restriction $A \neq -1/2$. Since the physical properties of the free field are independent of the parameter A , one can make a particular choice and take $A = -1$. This yields to the expression most often found in literature for the spin 3/2 propagator [36]

$$D_{\mu\nu}(p) = -\frac{1}{\not{p} - M_\Delta} \left(g_{\mu\nu} - \frac{1}{3}\gamma_\mu \gamma_\nu - \frac{2p_\mu p_\nu}{3M_\Delta^2} + \frac{p_\mu \gamma_\nu - p_\nu \gamma_\mu}{3M_\Delta} \right). \quad (\text{B.10})$$

The factor $\frac{1}{\not{p} - M_\Delta}$ can be decomposed as done in Eq. (B.5). Neglecting the second term one obtains

$$D_{\mu\nu}(p) = \frac{1}{W - M_\Delta + i\epsilon} \hat{\Lambda}_{\mu\nu} \quad (B.11)$$

with

$$\hat{\Lambda}_{\mu\nu} = - \left(\frac{\gamma_0 + 1}{2} \right) \left(g_{\mu\nu} - \frac{1}{3} \gamma_\mu \gamma_\nu - \frac{2p_\mu p_\nu}{3M_\Delta^2} + \frac{p_\mu \gamma_\nu - p_\nu \gamma_\mu}{3M_\Delta} \right). \quad (B.12)$$

In the non-relativistic limit, $\hat{\Lambda}_{\mu\nu}$ is reduced to

$$\begin{aligned} \hat{\Lambda}_{ij} &= \delta_{ij} - \frac{1}{3} \sigma_i \sigma_j \\ &= \frac{2}{3} \delta_{ij} - \frac{i}{3} \epsilon_{ijk} \sigma_k \end{aligned} \quad (B.13)$$

which gives precisely the closure sum for the $1/2 \rightarrow 3/2$ transition operator [Eq. (1.58)]. That is to say

$$D_{ij}(p) = \frac{\sum_s S_i \left| \frac{3}{2} s \right\rangle \langle \left| \frac{3}{2} s \right| S_j^\dagger}{W - M_\Delta + i\epsilon}. \quad (B.14)$$

Provided that the operators $\mathbf{S}, \mathbf{S}^\dagger$ are already included in the phenomenological Lagrangians of Eqs. (1.56), (1.63) we drop them from our expression of the propagator. One shall also include the width of the resonance as in the case of the N^* . Therefore, the non-relativistic Δ propagator takes the following final form

$$D_\Delta(p) = \frac{\sum_s \left| \frac{3}{2} s \right\rangle \langle \left| \frac{3}{2} s \right|}{W - M_\Delta + i\frac{1}{2}\Gamma(p)}. \quad (B.15)$$

Appendix C

Amplitudes for the $pp \rightarrow pp\pi^+\pi^-$ channel

In this channel, the total double-pion production amplitude can be expressed as

$$\mathcal{M}^{(T)} = \mathcal{M}_{r_3 r_4 r_1 r_2}(p_3, p_4, p_1, p_2) - \mathcal{M}(1 \leftrightarrow 2) + \mathcal{M}(3 \leftrightarrow 4, 1 \leftrightarrow 2) - \mathcal{M}(3 \leftrightarrow 4) \quad (C.1)$$

where the first term in the sum is given below for all mechanisms included in the calculation. The subindex stands for the number of the diagrams in Fig. 1.2

$$\begin{aligned} \mathcal{M}_{1+2} = & i \frac{1}{6f_\pi^2} \left(\frac{f_{NN\pi}}{m_\pi} \right)^2 \left\{ \frac{(\boldsymbol{\sigma} \mathbf{q}_1)_{r_3 r_1} (\boldsymbol{\sigma} (3\mathbf{q}_1 + \mathbf{q}_2))_{r_4 r_2}}{q_1^2 - m_\pi^2} \right. \\ & \left. - \frac{(\boldsymbol{\sigma} \mathbf{q}_1)_{r_3 r_1}}{q_1^2 - m_\pi^2} \frac{(\boldsymbol{\sigma} \mathbf{q}_2)_{r_4 r_2}}{q_2^2 - m_\pi^2} [2(q_1 q_2) + 4(p_5 p_6) + 3m_\pi^2] \right\} F_\pi(q_1) F_\pi(q_2) \end{aligned} \quad (C.2)$$

$$\mathcal{M}_3 = i \frac{1}{16f_\pi^4} \frac{(q_1^0 + 2p_5^0)\delta_{r_3 r_1}(q_1^0 + 2p_5^0)\delta_{r_4 r_2}}{(q_1 + p_5)^2 - m_\pi^2} \quad (C.3)$$

$$\begin{aligned} \mathcal{M}_{4+5} = & -i2 \frac{m_\pi^2}{f_\pi^2} \left(c_1^* + \frac{p_5^0 p_6^0}{m_\pi^2} c_2^* \right) \left\{ \frac{f_{NN\pi}}{m_\pi} \frac{\tilde{f}}{m_\pi} \left[\frac{(\boldsymbol{\sigma} \mathbf{q}_2)_{r_3 r_1} (\boldsymbol{\sigma} \mathbf{q}_2)_{r_4 r_2}}{\mathbf{q}_2^2} \right. \right. \\ & \times (V'_L(q_2) - V'_T(q_2)) + V'_T(q_2) (\boldsymbol{\sigma})_{r_3 r_1} (\boldsymbol{\sigma})_{r_4 r_2}] \\ & \left. + g_{NN\sigma} g_{N^* N \sigma} \frac{\delta_{r_3 r_1} \delta_{r_4 r_2}}{q_2^2 - m_\sigma^2} F_\sigma^2(q_2) \right\} \\ & \times [D_{N^*}(p_5 + p_6 + p_3) + D_{N^*}(p_5 + p_6 - p_1)] \end{aligned} \quad (C.4)$$

$$\mathcal{M}_{6+7} = 0 \quad (\text{not allowed by isospin symmetry}) \quad (\text{C.5})$$

$$\begin{aligned} \mathcal{M}_8 = & i \frac{1}{9} \frac{f^*}{m_\pi} \frac{g_{N^*\Delta\pi}}{m_\pi} \left\{ \frac{f_{NN\pi}}{m_\pi} \frac{\tilde{f}}{m_\pi} \left[\frac{(\boldsymbol{\sigma}\mathbf{q}_2)_{mr_1}(\boldsymbol{\sigma}\mathbf{q}_2)_{r_4r_2}}{\mathbf{q}_2^2} (V'_L(q_2) - V'_T(q_2)) \right. \right. \\ & \left. \left. + V'_T(q_2)(\boldsymbol{\sigma})_{mr_1}(\boldsymbol{\sigma})_{r_4r_2} \right] + g_{NN\sigma} g_{N^*N\sigma} \frac{\delta_{mr_1}\delta_{r_4r_2}}{q_2^2 - m_\sigma^2} F_\sigma^2(q_2) \right\} \\ & \times \{2(\mathbf{p}_5\mathbf{p}_6)\delta_{r_3m} [D_\Delta(p_5 + p_3) + 3D_\Delta(p_6 + p_3)] - i(\boldsymbol{\sigma}[\mathbf{p}_5 \times \mathbf{p}_6])_{r_3m} \\ & \times [D_\Delta(p_5 + p_3) - 3D_\Delta(p_6 + p_3)]\} D_{N^*}(p_5 + p_6 + p_3) \end{aligned} \quad (\text{C.6})$$

$$\begin{aligned} \mathcal{M}_9 = & i \left(\frac{f^*}{m_\pi} \right)^2 \frac{f_{NN\pi}}{m_\pi} \frac{f_\Delta}{m_\pi} D_\Delta(p_5 + p_6 + p_3) \\ & \times \left[\frac{1}{9} \left\{ \frac{(\boldsymbol{\sigma}\mathbf{q}_2)_{r_4r_2}}{\mathbf{q}_2^2} [5i(\mathbf{q}_2[\mathbf{p}_5\mathbf{p}_6])\delta_{r_3r_1} - (\mathbf{p}_5\mathbf{p}_6)(\boldsymbol{\sigma}\mathbf{q}_2)_{r_3r_1} \right. \right. \\ & + 4(\mathbf{p}_5\mathbf{q}_2)(\boldsymbol{\sigma}\mathbf{p}_6)_{r_3r_1} - (\mathbf{p}_6\mathbf{q}_2)(\boldsymbol{\sigma}\mathbf{p}_5)_{r_3r_1}] (V'_L(q_2) - V'_T(q_2)) \\ & + [5i\delta_{r_3r_1}(\boldsymbol{\sigma}[\mathbf{p}_5 \times \mathbf{p}_6])_{r_4r_2} - (\mathbf{p}_5\mathbf{p}_6)(\boldsymbol{\sigma})_{r_3r_1}(\boldsymbol{\sigma})_{r_4r_2} \\ & \left. \left. + 4(\boldsymbol{\sigma}\mathbf{p}_6)_{r_3r_1}(\boldsymbol{\sigma}\mathbf{p}_5)_{r_4r_2} - (\boldsymbol{\sigma}\mathbf{p}_5)_{r_3r_1}(\boldsymbol{\sigma}\mathbf{p}_6)_{r_4r_2}] V'_T(q_2) \right\} D_\Delta(p_5 + p_3) \right. \\ & \left. - \frac{1}{6} \left\{ \mathbf{p}_5 \leftrightarrow \mathbf{p}_6 \right\} D_\Delta(p_6 + p_3) \right] \end{aligned} \quad (\text{C.7})$$

$$\begin{aligned} \mathcal{M}_{10} = & i \frac{1}{12f_\pi^2} \left(\frac{f^*}{m_\pi} \right)^2 \left[\frac{1}{3} \frac{(q_2^0 + 2p_6^0)\delta_{r_4r_2}}{(q_2 + p_6)^2 - m_\pi^2} \{2(\mathbf{p}_5(\mathbf{q}_2 + \mathbf{p}_6))\delta_{r_3r_1} \right. \\ & - i(\boldsymbol{\sigma}[\mathbf{p}_5 \times (\mathbf{q}_2 + \mathbf{p}_6)])_{r_3r_1}\} D_\Delta(p_5 + p_3) \\ & - \frac{(q_2^0 + 2p_5^0)\delta_{r_4r_2}}{(q_2 + p_5)^2 - m_\pi^2} \{2(\mathbf{p}_6(\mathbf{q}_2 + \mathbf{p}_5))\delta_{r_3r_1} \\ & \left. - i(\boldsymbol{\sigma}[\mathbf{p}_6 \times (\mathbf{q}_2 + \mathbf{p}_5)])_{r_3r_1}\} D_\Delta(p_6 + p_3) \right] \end{aligned} \quad (\text{C.8})$$

$$\begin{aligned}
\mathcal{M}_{11} = & i \frac{1}{12 f_\pi^2} \left(\frac{f^*}{m_\pi} \right)^2 \left[\frac{(q_2^0 + 2p_6^0)\delta_{r_4 r_2}}{(q_2 + p_6)^2 - m_\pi^2} \{ 2(\mathbf{p}_5(\mathbf{q}_2 + \mathbf{p}_6))\delta_{r_3 r_1} \right. \\
& + i(\boldsymbol{\sigma}[\mathbf{p}_5 \times (\mathbf{q}_2 + \mathbf{p}_6)])_{r_3 r_1} \} D_\Delta(p_1 - p_5) \\
& - \frac{1}{3} \frac{(q_2^0 + 2p_5^0)\delta_{r_4 r_2}}{(q_2 + p_5)^2 - m_\pi^2} \{ 2(\mathbf{p}_6(\mathbf{q}_2 + \mathbf{p}_5))\delta_{r_3 r_1} \\
& \left. + i(\boldsymbol{\sigma}[\mathbf{p}_6 \times (\mathbf{q}_2 + \mathbf{p}_5)])_{r_3 r_1} \} D_\Delta(p_1 - p_6) \right] \quad (C.9)
\end{aligned}$$

$$\begin{aligned}
\mathcal{M}_{12} = & i \frac{1}{3} \frac{1}{9} \left(\frac{f^*}{m_\pi} \right)^4 \left(\frac{1}{(\mathbf{q}_2 + \mathbf{p}_6)^2} \{ 2(\mathbf{p}_6(\mathbf{p}_6 + \mathbf{q}_2))\delta_{r_4 r_2} - i(\boldsymbol{\sigma}[\mathbf{p}_6 \times (\mathbf{q}_2 + \mathbf{p}_6)])_{r_4 r_2} \} \right. \\
& \times \{ 2(\mathbf{p}_5(\mathbf{p}_6 + \mathbf{q}_2))\delta_{r_3 r_1} - i(\boldsymbol{\sigma}[\mathbf{p}_5 \times (\mathbf{q}_2 + \mathbf{p}_6)])_{r_3 r_1} \} (V'_L(q_2 + p_6) - V'_T(q_2 + p_6)) \\
& + \{ (\mathbf{p}_5 \mathbf{p}_6)(-2\delta_{r_4 r_1}\delta_{r_3 r_2} + 5\delta_{r_3 r_1}\delta_{r_4 r_2}) + (\boldsymbol{\sigma} \mathbf{p}_5)_{r_4 r_2} (\boldsymbol{\sigma} \mathbf{p}_6)_{r_3 r_1} \\
& \left. + 2i(\boldsymbol{\sigma}[\mathbf{p}_5 \times \mathbf{p}_6])_{r_4 r_2}\delta_{r_3 r_1} - 2i(\boldsymbol{\sigma}[\mathbf{p}_5 \times \mathbf{p}_6])_{r_3 r_1}\delta_{r_4 r_2} \} V'_T(q_2 + p_6) \right) \\
& \times D_\Delta(p_4 + p_6) D_\Delta(p_3 + p_5) \quad (C.10)
\end{aligned}$$

$$\begin{aligned}
\mathcal{M}_{13} = & i \frac{1}{3} \frac{1}{9} \left(\frac{f^*}{m_\pi} \right)^4 \left(\frac{1}{(\mathbf{q}_2 + \mathbf{p}_6)^2} \{ 2(\mathbf{p}_6(\mathbf{p}_6 + \mathbf{q}_2))\delta_{r_4 r_2} + i(\boldsymbol{\sigma}[\mathbf{p}_6 \times (\mathbf{q}_2 + \mathbf{p}_6)])_{r_4 r_2} \} \right. \\
& \times \{ 2(\mathbf{p}_5(\mathbf{p}_6 + \mathbf{q}_2))\delta_{r_3 r_1} + i(\boldsymbol{\sigma}[\mathbf{p}_5 \times (\mathbf{q}_2 + \mathbf{p}_6)])_{r_3 r_1} \} (V'_L(q_2 + p_6) - V'_T(q_2 + p_6)) \\
& + \{ (\mathbf{p}_5 \mathbf{p}_6)(-2\delta_{r_4 r_1}\delta_{r_3 r_2} + 5\delta_{r_3 r_1}\delta_{r_4 r_2}) + (\boldsymbol{\sigma} \mathbf{p}_5)_{r_4 r_2} (\boldsymbol{\sigma} \mathbf{p}_6)_{r_3 r_1} \\
& \left. - 2i(\boldsymbol{\sigma}[\mathbf{p}_5 \times \mathbf{p}_6])_{r_4 r_2}\delta_{r_3 r_1} + 2i(\boldsymbol{\sigma}[\mathbf{p}_5 \times \mathbf{p}_6])_{r_3 r_1}\delta_{r_4 r_2} \} V'_T(q_2 + p_6) \right) \\
& \times D_\Delta(p_2 - p_6) D_\Delta(p_1 - p_5) \quad (C.11)
\end{aligned}$$

$$\begin{aligned}
\mathcal{M}_{14} = & i \frac{1}{9} \frac{1}{9} \left(\frac{f^*}{m_\pi} \right)^4 \left(\frac{1}{(\mathbf{q}_2 + \mathbf{p}_6)^2} \{ 2(\mathbf{p}_6(\mathbf{p}_6 + \mathbf{q}_2))\delta_{r_4 r_2} + i(\boldsymbol{\sigma}[\mathbf{p}_6 \times (\mathbf{q}_2 + \mathbf{p}_6)])_{r_4 r_2} \} \right. \\
& \times \{ 2(\mathbf{p}_5(\mathbf{p}_6 + \mathbf{q}_2))\delta_{r_3 r_1} - i(\boldsymbol{\sigma}[\mathbf{p}_5 \times (\mathbf{q}_2 + \mathbf{p}_6)])_{r_3 r_1} \} (V'_L(q_2 + p_6) - V'_T(q_2 + p_6)) \\
& + \{ (\mathbf{p}_5 \mathbf{p}_6)(-2\delta_{r_4 r_1}\delta_{r_3 r_2} + 3\delta_{r_3 r_1}\delta_{r_4 r_2}) - (\boldsymbol{\sigma} \mathbf{p}_5)_{r_4 r_2} (\boldsymbol{\sigma} \mathbf{p}_6)_{r_3 r_1}
\end{aligned}$$

$$\begin{aligned}
& -2i(\boldsymbol{\sigma} [\mathbf{p}_5 \times \mathbf{p}_6])_{r_4 r_2} \delta_{r_3 r_1} - 2i(\boldsymbol{\sigma} [\mathbf{p}_5 \times \mathbf{p}_6])_{r_3 r_1} \delta_{r_4 r_2} \} V'_T(q_2 + p_6) \Big) \\
& \times D_\Delta(p_2 - p_6) D_\Delta(p_3 + p_5) \tag{C.12}
\end{aligned}$$

$$\begin{aligned}
\mathcal{M}_{15} = & i \frac{1}{9} \left(\frac{f^*}{m_\pi} \right)^4 \left(\frac{1}{(\mathbf{q}_2 + \mathbf{p}_6)^2} \{ 2(\mathbf{p}_6(\mathbf{p}_6 + \mathbf{q}_2)) \delta_{r_4 r_2} - i(\boldsymbol{\sigma} [\mathbf{p}_6 \times (\mathbf{q}_2 + \mathbf{p}_6)])_{r_4 r_2} \} \right. \\
& \times \{ 2(\mathbf{p}_5(\mathbf{p}_6 + \mathbf{q}_2)) \delta_{r_3 r_1} + i(\boldsymbol{\sigma} [\mathbf{p}_5 \times (\mathbf{q}_2 + \mathbf{p}_6)])_{r_3 r_1} \} (V'_L(q_2 + p_6) - V'_T(q_2 + p_6)) \\
& + \{ (\mathbf{p}_5 \mathbf{p}_6)(-2\delta_{r_4 r_1} \delta_{r_3 r_2} + 3\delta_{r_3 r_1} \delta_{r_4 r_2}) - (\boldsymbol{\sigma} \mathbf{p}_5)_{r_4 r_2} (\boldsymbol{\sigma} \mathbf{p}_6)_{r_3 r_1} \\
& \left. + 2i(\boldsymbol{\sigma} [\mathbf{p}_5 \times \mathbf{p}_6])_{r_4 r_2} \delta_{r_3 r_1} + 2i(\boldsymbol{\sigma} [\mathbf{p}_5 \times \mathbf{p}_6])_{r_3 r_1} \delta_{r_4 r_2} \} V'_T(q_2 + p_6) \Big) \\
& \times D_\Delta(p_4 + p_6) D_\Delta(p_1 - p_5) \tag{C.13}
\end{aligned}$$

In these expressions p_1, p_2 ($p = (p^0, \mathbf{p})$) are the momenta of the incoming nucleons while p_3, p_4 are the momenta of the outgoing ones; p_5, p_6 are π^- and π^+ momenta respectively and $q_{1(2)}$ denote $p_{3(4)} - p_{1(2)}$. Here $r_3, r_4, r_1, r_2, m = (1, 2)$ are spin indices and a sum in m is understood in Eq. (C.6).

Appendix D

Integrals for the NN wave function

The integrals

$$\begin{aligned}
\mathcal{I}_{ij}(k) &= M \int \frac{d\mathbf{q}}{(2\pi)^3} \frac{g_i(q)g_j(q)}{k^2 - q^2 + i\epsilon} \\
&= -\frac{M}{2\pi^2} V.P. \int dq q^2 \frac{g_i(q)g_j(q)}{q^2 - k^2} - i\frac{\pi}{2} k g_i(k)g_j(k) \quad i, j = 1, 2
\end{aligned} \tag{D.1}$$

appear in the solution of the Schroedinger equation for the scattering problem using the separable potential of Ref. [68] (see Sec. 2.3). They can be evaluated analytically.

Since g_1^2 is a sum of three terms

$$g_1^2(q) = \frac{1}{(q^2 + \beta_{11}^2)^2} + \frac{\gamma_1^2 q^4}{(q^2 + \beta_{12}^2)^4} + \frac{2\gamma_1 q^2}{(q^2 + \beta_{11}^2)(q^2 + \beta_{12}^2)^2}$$

then

$$\mathcal{I}_{11} = \mathcal{I}_{11}^a + \mathcal{I}_{11}^b + \mathcal{I}_{11}^c \tag{D.2}$$

where

$$\mathcal{I}_{11}^a = -\frac{1}{4\pi} \frac{M}{(k^2 + \beta_{11}^2)^2} \left\{ ik + \frac{\beta_{11}^2 - k^2}{2\beta_{11}} \right\} \tag{D.3}$$

$$\mathcal{I}_{11}^b = -\frac{1}{4\pi} \frac{\gamma_1^2 M}{(k^2 + \beta_{12}^2)^4} \left\{ ik^5 + \frac{\beta_{12}^6 + 5\beta_{12}^4 k^2 + 15\beta_{12}^2 k^4 - 5k^6}{16\beta_{12}} \right\} \tag{D.4}$$

$$\begin{aligned}
\mathcal{I}_{11}^c &= -\frac{1}{4\pi} \frac{2\gamma_1 M}{(k^2 + \beta_{11}^2)(k^2 + \beta_{12}^2)^2} \left\{ ik^3 + \frac{\beta_{12}}{2} (\beta_{12}^2 + 3k^2) \right. \\
&\quad \left. - \frac{\beta_{12} + 2\beta_{11}}{2(\beta_{11} + \beta_{12})^2} (k^2 + \beta_{12}^2)^2 \right\}.
\end{aligned} \tag{D.5}$$

Analogously,

$$\begin{aligned} g_1(q)g_2(q) &= \frac{q^2}{(q^2 + \beta_{11}^2)(q^2 + \beta_{21}^2)^2} + \frac{\gamma_1 q^4}{(q^2 + \beta_{12}^2)^2(q^2 + \beta_{21}^2)^2} \\ &+ \frac{\gamma_2 q^4}{(q^2 + \beta_{11}^2)(q^2 + \beta_{22}^2)^3} + \frac{\gamma_1 \gamma_2 q^6}{(q^2 + \beta_{12}^2)^2(q^2 + \beta_{22}^2)^3} \end{aligned}$$

and therefore

$$\mathcal{I}_{12} = \mathcal{I}_{12}^a + \mathcal{I}_{12}^b + \mathcal{I}_{12}^c + \mathcal{I}_{12}^d \quad (\text{D.6})$$

with

$$\begin{aligned} \mathcal{I}_{12}^a &= -\frac{1}{4\pi} \frac{M}{(k^2 + \beta_{11}^2)(k^2 + \beta_{21}^2)^2} \left\{ ik^3 + \frac{\beta_{21}}{2}(\beta_{21}^2 + 3k^2) \right. \\ &\quad \left. - \frac{\beta_{21} + 2\beta_{11}}{2(\beta_{11} + \beta_{21})^2}(k^2 + \beta_{21}^2)^2 \right\} \quad (\text{D.7}) \end{aligned}$$

$$\begin{aligned} \mathcal{I}_{12}^b &= -\frac{1}{4\pi} \frac{\gamma_1 M}{(k^2 + \beta_{12}^2)^2(k^2 + \beta_{21}^2)^2} \left\{ ik^5 + \frac{1}{2(\beta_{12} + \beta_{21})^3} [\beta_{21}^2 - k^2]k^4 \beta_{21}(3\beta_{12} + \beta_{21}) \right. \\ &\quad \left. + \beta_{12}^4(\beta_{21}^2 + k^2)^2 + \beta_{12}^3\beta_{21}k^2(\beta_{21}^2 + 3k^2) + \beta_{12}^2(2\beta_{21}^4k^2 + 7\beta_{21}^2k^4 - k^6)] \right\} \quad (\text{D.8}) \end{aligned}$$

$$\begin{aligned} \mathcal{I}_{12}^c &= -\frac{1}{4\pi} \frac{\gamma_2 M}{(k^2 + \beta_{11}^2)(k^2 + \beta_{22}^2)^3} \left\{ ik^5 + \frac{1}{8(\beta_{11} + \beta_{22})^3} [(3\beta_{11}\beta_{22}k^2 + \beta_{22}^2k^2) \right. \\ &\quad \times (\beta_{22}^4 + 6\beta_{22}^2k^2 - 3k^4) + \beta_{11}^3(3\beta_{22}^5 + 10\beta_{22}^3k^2 + 15\beta_{22}k^4) \\ &\quad \left. + \beta_{11}^2(\beta_{22}^6 + 6\beta_{22}^4k^2 + 21\beta_{22}^2k^4 - 8k^6)] \right\} \quad (\text{D.9}) \end{aligned}$$

$$\begin{aligned} \mathcal{I}_{12}^d &= -\frac{1}{4\pi} \frac{\gamma_1 \gamma_2 M}{(k^2 + \beta_{12}^2)^2(k^2 + \beta_{22}^2)^3} \left\{ ik^7 + \frac{1}{8(\beta_{12} + \beta_{22})^4} [4\beta_{12}^5(\beta_{22}^2 + k^2)^3 \right. \\ &\quad + (4\beta_{12} + \beta_{22})\beta_{22}^2k^4(\beta_{22}^4 + 6\beta_{22}^2k^2 - 3k^4) + 2\beta_{12}^2\beta_{22}k^2(\beta_{22}^6 + 6\beta_{22}^4k^2 + 21\beta_{22}^2k^4 - 8k^6) \\ &\quad + 4\beta_{12}^3k^2(2\beta_{22}^6 + 7\beta_{22}^4k^2 + 12\beta_{22}^2k^4 - k^6) \\ &\quad \left. + \beta_{12}^4(\beta_{22}^7 + 6\beta_{22}^5k^2 + 13\beta_{22}^3k^4 + 16\beta_{22}k^6)] \right\}. \quad (\text{D.10}) \end{aligned}$$

Finally,

$$g_2^2(q) = \frac{q^4}{(q^2 + \beta_{21}^2)^4} + \frac{\gamma_2^2 q^8}{(q^2 + \beta_{22}^2)^6} + \frac{2\gamma_2 q^6}{(q^2 + \beta_{21}^2)^2 (q^2 + \beta_{22}^2)^3}$$

and

$$\mathcal{I}_{22} = \mathcal{I}_{22}^a + \mathcal{I}_{22}^b + \mathcal{I}_{22}^c \quad (\text{D.11})$$

with

$$\mathcal{I}_{22}^a = -\frac{1}{4\pi} \frac{M}{(k^2 + \beta_{21}^2)^4} \left\{ ik^5 + \frac{\beta_{21}^6 + 5\beta_{21}^4 k^2 + 15\beta_{21}^2 k^4 - 5k^6}{16\beta_{21}} \right\} \quad (\text{D.12})$$

$$\begin{aligned} \mathcal{I}_{22}^b = & -\frac{1}{4\pi} \frac{\gamma_2^2 M}{(k^2 + \beta_{22}^2)^6} \left\{ ik^9 + \frac{1}{256\beta_{22}} [7\beta^1 0_{22} + 45\beta_{22}^3 k^2 + 126\beta_{22}^6 k^4 \right. \\ & \left. + 210\beta_{22}^4 k^6 + 315\beta_{22}^2 k^3 - 63k^{10}] \right\} \quad (\text{D.13}) \end{aligned}$$

$$\begin{aligned} \mathcal{I}_{22}^c = & -\frac{1}{4\pi} \frac{2\gamma_2 M}{(k^2 + \beta_{21}^2)^2 (k^2 + \beta_{22}^2)^3} \left\{ ik^7 + \frac{1}{8(\beta_{21} + \beta_{22})^4} [4\beta_{21}^5 (\beta_{22}^2 + k^2)^3 \right. \\ & + (4\beta_{21} + \beta_{22})\beta_{22}^2 k^4 (\beta_{22}^4 + 6\beta_{22}^2 k^2 - 3k^4) + 2\beta_{21}^2 \beta_{22} k^2 (\beta_{22}^6 + 6\beta_{22}^4 k^2 + 21\beta_{22}^2 k^4 - 8k^6) \\ & + 4\beta_{21}^3 k^2 (2\beta_{22}^6 + 7\beta_{22}^4 k^2 + 12\beta_{22}^2 k^4 - k^6) \\ & \left. + \beta_{21}^4 (\beta_{22}^7 + 6\beta_{22}^5 k^2 + 13\beta_{22}^3 k^4 + 16\beta_{22} k^6)] \right\}. \quad (\text{D.14}) \end{aligned}$$

Appendix E

Deuteron wave functions

The following formulae for the s-wave deuteron wave function in momentum space are normalized according to Eq. (3.5).

- Hulthen wave function

The Hulthen wave function [87] is the exact solution for the deuteron problem using the Hulthen potential

$$V(r) = -V_0 \frac{e^{-\mu r}}{1 - e^{-\mu r}} \quad (\text{E.1})$$

and whose parameters are adjusted to fit the observed properties of the deuteron system. Its expression is

$$\tilde{\varphi}_d(k) = \sqrt{8\pi \frac{\alpha\beta(\alpha + \beta)}{(\alpha - \beta)^2}} \left(\frac{1}{\alpha^2 + k^2} - \frac{1}{\beta^2 + k^2} \right), \quad (\text{E.2})$$

with $\alpha = 45$ MeV/c, $\beta = 7\alpha$.

- Bonn and Paris wave functions

The deuteron wave functions obtained for the Paris and Bonn realistic boson exchange potentials have been parameterized with the following ansatz [30, 66]; in coordinate space:

$$\varphi_d(r) = \frac{1}{\sqrt{4\pi}} \frac{u(r)}{r}, \quad u(r) = \sum_{j=1}^n C_j e^{m_j r}, \quad (\text{E.3})$$

and in momentum space

$$\tilde{\varphi}_d(k) = 2\sqrt{\pi} \sum_{j=1}^n C_j \frac{1}{k^2 + m_j^2}, \quad (\text{E.4})$$

where the coefficient C_n is constrained to

$$C_n = - \sum_{j=1}^{n-1} C_j \quad (\text{E.5})$$

in order to satisfy the boundary condition $u(0) = 0$. The masses m_j are chosen to be

$$m_j = \alpha + (j - 1)m_0 \quad (\text{E.6})$$

with $\alpha = (M\epsilon_d)^{1/2} = 0.23 \text{ fm}^{-1}$ (M is the nucleon mass and ϵ_d the deuteron binding energy), and $m_0 = 1(0.9) \text{ fm}^{-1}$ for the Paris (Bonn) solutions. Finally, the list of C_j ($j = 1, n - 1$) values can be found in the original references [30, 66].

Appendix F

Amplitudes for $np \rightarrow d (\pi\pi)^0$

- $N^* \rightarrow N(\pi\pi)_{S-wave}^{T=0}$ mechanism (Fig. 3.1 a)

$$\mathcal{M}_{Rr_1r_2}^{(a)} = i2 \frac{m_\pi^2}{f_\pi^2} \left[c_1^* + c_2^* \frac{E_\pi(2E_0 - E_d - E_\pi)}{m_\pi^2} \right] \sum_{r'_1 r'_2} \left(\frac{1}{2} r'_1 \frac{1}{2} r'_2 \right| 1R \times \left. \right) \times \left\{ 3 \frac{f_{NN\pi}}{m_\pi} \frac{\tilde{f}}{m_\pi} [(\sigma_j)_{r'_1 r_1} (\sigma_l)_{r'_2 r_2} \mathcal{I}^{jl} + (\sigma_j)_{r'_1 r_1} (\sigma_j)_{r'_2 r_2} \mathcal{I}^1] - g_{NN\sigma} g_{N^* N\sigma} \delta_{r'_1 r_1} \delta_{r'_2 r_2} \mathcal{I}^2 \right\} \quad (\text{F.1})$$

with

$$\mathcal{I}^{jl} = \int \frac{d\mathbf{q}}{(2\pi)^3} \tilde{\varphi}_d(\mathbf{P}_2) [V'_L(q) - V'_T(q)] D_{N^*}(p_1 - q) \hat{q}_j \hat{q}_l \quad + \quad (1 \leftrightarrow 2) \quad (\text{F.2})$$

$$\mathcal{I}^1 = \int \frac{d\mathbf{q}}{(2\pi)^3} \tilde{\varphi}_d(\mathbf{P}_2) V'_T(q) D_{N^*}(p_1 - q) \quad + \quad (1 \leftrightarrow 2) \quad (\text{F.2})$$

$$\mathcal{I}^2 = \int \frac{d\mathbf{q}}{(2\pi)^3} \tilde{\varphi}_d(\mathbf{P}_2) D_{T=0}(q) D_{N^*}(p_1 - q) \quad + \quad (1 \leftrightarrow 2)$$

Notice that, when $c_2^* = 0$, the amplitude squared can be factorized out from the phase space integral 3.1. In the case of this mechanism, the previous expressions are valid for both charged ($\pi^+ \pi^-$) and neutral ($\pi^0 \pi^0$) channels.

- $N^* \rightarrow \Delta\pi$ mechanism (Fig. 3.1 b)

$$\mathcal{M}_{Rr_1r_2}^{(b)} = -i \frac{a}{9} \frac{f^*}{m_\pi} \frac{g_{N^*\Delta\pi}}{m_\pi} \sum_{r'_1 r'_2} \left(\frac{1}{2} r'_1 \frac{1}{2} r'_2 \right| 1R \right) \left\{ b \frac{f_{NN\pi}}{m_\pi} \frac{\tilde{f}}{m_\pi} [(\sigma_j)_{mr_1} (\sigma_l)_{r'_2 r_2} \mathcal{I}_{r'_1 m}^{jl} + (\sigma_j)_{mr_1} (\sigma_j)_{r'_2 r_2} \mathcal{I}_{r'_1 m}^1] - g_{NN\sigma} g_{N^* N\sigma} \delta_{mr_1} \delta_{r'_2 r_2} \mathcal{I}_{r'_1 m}^2 \right\} \quad (\text{F.3})$$

with

$$\mathcal{I}_{rm}^\kappa = -2((\mathbf{p}_d + \mathbf{p}_\pi)\mathbf{p}_\pi)\delta_{rm}\mathcal{I}_+^\kappa + i(\boldsymbol{\sigma}[\mathbf{p}_d \times \mathbf{p}_\pi])_{rm}\mathcal{I}_-^\kappa \quad \kappa = (jl), 1, 2 \quad (\text{F.4})$$

and

$$\begin{aligned} \mathcal{I}_\pm^{jl} &= \int \frac{d\mathbf{q}}{(2\pi)^3} \tilde{\varphi}_d(\mathbf{P}_2) [V'_L(q) - V'_T(q)] D_{N^*}(p_1 - q) \times \\ &\quad [cD_\Delta(p_1 - q - p_\pi) \pm dD_\Delta(p_d + p_\pi - q - p_2)] \hat{q}_j \hat{q}_l \\ \mathcal{I}_\pm^{jl}(1 \leftrightarrow 2) &= \int \frac{d\mathbf{q}}{(2\pi)^3} \tilde{\varphi}_d(\mathbf{P}_1) [V'_L(q) - V'_T(q)] D_{N^*}(p_2 - q) \times \\ &\quad [dD_\Delta(p_2 - q - p_\pi) \pm cD_\Delta(p_d + p_\pi - q - p_1)x] \hat{q}_j \hat{q}_l \\ \mathcal{I}_\pm^1 &= \int \frac{d\mathbf{q}}{(2\pi)^3} \tilde{\varphi}_d(\mathbf{P}_2) V'_T(q) D_{N^*}(p_1 - q) \times \\ &\quad [cD_\Delta(p_1 - q - p_\pi) \pm dD_\Delta(p_d + p_\pi - q - p_2)] \quad (\text{F.5}) \\ \mathcal{I}_\pm^1(1 \leftrightarrow 2) &= \int \frac{d\mathbf{q}}{(2\pi)^3} \tilde{\varphi}_d(\mathbf{P}_1) V'_T(q) D_{N^*}(p_2 - q) \times \\ &\quad [dD_\Delta(p_2 - q - p_\pi) \pm cD_\Delta(p_d + p_\pi - q - p_1)] \\ \mathcal{I}^2 &= \int \frac{d\mathbf{q}}{(2\pi)^3} \tilde{\varphi}_d(\mathbf{P}_2) D_{T=0}(q) D_{N^*}(p_1 - q) \times \\ &\quad [eD_\Delta(p_1 - q - p_\pi) \pm fD_\Delta(p_d + p_\pi - q - p_2)] \\ \mathcal{I}^2(1 \leftrightarrow 2) &= \int \frac{d\mathbf{q}}{(2\pi)^3} \tilde{\varphi}_d(\mathbf{P}_1) D_{T=0}(q) D_{N^*}(p_1 - q) \times \\ &\quad [fD_\Delta(p_2 - q - p_\pi) \pm eD_\Delta(p_d + p_\pi - q - p_1)] \end{aligned}$$

The coefficients take the following values:

	a	b	c	d	e	f
$(\pi^+ \pi^-)$	1	1	7	5	1	3
$(\pi^0 \pi^0)$	2	3	1	1	1	1

- $\Delta\Delta$ mechanism (Fig. 3.1 c)

$$\begin{aligned}
\mathcal{M}_{Rr_1r_2}^{(c)} = & i \frac{a}{81} \left(\frac{f^*}{m_\pi} \right)^4 \sum_{r'_1 r'_2} \left(\frac{1}{2} r'_1 \frac{1}{2} r'_2 \middle| 1R \right) \left\{ [2(\mathbf{p}_\pi)_j \delta_{r'_2 r_2} + i \epsilon_{k m j} (\sigma_k)_{r'_2 r_2} (\mathbf{p}_\pi)_m] \times \right. \\
& [-2(\mathbf{p}_\pi + \mathbf{p}_d)_l \delta_{r'_1 r_1} + i \epsilon_{n m l} (\sigma_n)_{r'_1 r_1} (\mathbf{p}_\pi + \mathbf{p}_d)_m] \mathcal{I}^{jl} \\
& + \left. \left[-((\mathbf{p}_\pi + \mathbf{p}_d) \mathbf{p}_\pi) (-2 \delta_{r'_1 r_1} \delta_{r'_2 r_2} + 5 \delta_{r'_1 r_1} \delta_{r'_2 r_2}) - (\boldsymbol{\sigma} (\mathbf{p}_\pi + \mathbf{p}_d))_{r'_2 r_2} (\boldsymbol{\sigma} \mathbf{p}_\pi)_{r'_1 r_1} \right. \right. \\
& \left. \left. - 2i(\boldsymbol{\sigma} [\mathbf{p}_d \times \mathbf{p}_\pi])_{r'_2 r_2} \delta_{r'_1 r_1} + 2i(\boldsymbol{\sigma} [\mathbf{p}_d \times \mathbf{p}_\pi])_{r'_1 r_1} \delta_{r'_2 r_2} \right] \mathcal{I}^1 \right\} + b \times (1 \leftrightarrow 2) \}
\end{aligned} \tag{F.6}$$

with

$$\begin{aligned}
\mathcal{I}^{jl} = & \int \frac{d\mathbf{q}}{(2\pi)^3} \tilde{\varphi}_d(\mathbf{P}_2) [V'_L(q) - V'_T(q)] D_\Delta(p_1 - q) D_\Delta(p_2 + q) \hat{q}_j \hat{q}_l \\
\mathcal{I}^1 = & \int \frac{d\mathbf{q}}{(2\pi)^3} \tilde{\varphi}_d(\mathbf{P}_2) V'_T(q) D_\Delta(p_1 - q) D_\Delta(p_2 + q)
\end{aligned} \tag{F.7}$$

and where a and b take the values

	a	b
$(\pi^+ \pi^-)$	1	11
$(\pi^0 \pi^0)$	6	1

In all these expressions $p_{1(2)} = (E_0, \mathbf{p}_{1(2)})$ is the momentum of the incoming proton (neutron) in CM ($\mathbf{p}_1 = \mathbf{p}_2$); $q_0 = 1/2E_d - E_0$, and $\mathbf{P}_{1(2)} = \mathbf{q} + \mathbf{p}_{1(2)} - \mathbf{p}_d/2$ for the first two mechanisms, while for the third one $\mathbf{P}_{1(2)} = \mathbf{q} + \mathbf{p}_{1(2)} - \mathbf{p}_d/2 - \mathbf{p}_\pi$ where \mathbf{p}_d is the CM deuteron momentum, and \mathbf{p}_π is the momentum of the pion over whose energy the integral in Eq. (3.1) is performed. The presence of integrals over the transferred momentum imply that we will, in general, run into the poles of the meson propagators at $q_p = (q_0^2 - m^2)^{1/2}$. To the present calculation, only the poles on the lightest π propagator will contribute. In this case, the integrals can be evaluated as follows

$$\begin{aligned}
\int \frac{d\mathbf{q}}{(2\pi)^3} f(\mathbf{q}, \dots) \frac{1}{q^2 - m_\pi^2 + i\epsilon} = & V.P. \int \frac{d\mathbf{q}}{(2\pi)^3} f(\mathbf{q}, \dots) \frac{1}{q^2 - m_\pi^2 + i\epsilon} \\
& - i\pi \int \frac{d\mathbf{q}}{(2\pi)^3} f(\mathbf{q}, \dots) \delta(q^2 - m_\pi^2).
\end{aligned} \tag{F.8}$$

Appendix G

Charged current neutrino-nucleon quasielastic scattering

The matrix element of the process $\nu_l(k) + n(p) \rightarrow l^-(k') + p(p')$ is given by

$$\mathcal{M} = \frac{G}{\sqrt{2}} \cos \theta_c l_\mu J^\mu, \quad (\text{G.1})$$

where l_α is the standard V-A leptonic current of Eq. (4.4), and the hadronic current can be written in terms of three vector $F_{1,2,3}^V$, the axial vector F_A and the pseudoscalar F_P form factors

$$\begin{aligned} J^\mu &= \bar{u}(p') A^\mu u(p), \\ A^\mu &= F_1^V(q^2) \gamma^\mu + i F_2^V(q^2) \sigma^{\mu\nu} \frac{q_\nu}{2M} + F_3^V(q^2) q^\mu + F_A(q^2) \gamma^\mu \gamma^5 + F_P(q^2) q^\mu \gamma^5. \end{aligned} \quad (\text{G.2})$$

CVC implies that $F_3^V \equiv 0$. The remaining two vector form factors are related to the isovector electromagnetic ones through the relations

$$F_{1(2)}^V = F_{E(M)}^p - F_{E(M)}^n \quad (\text{G.3})$$

where the index $p(n)$ stands for proton(neutron) and $E(M)$, for electric(magnetic). The proton(neutron) electric and magnetic form factors can be defined as

$$\begin{aligned} G_E^{p(n)} &= F_E^{p(n)} + \frac{q^2}{4M^2} F_M^{p(n)} \\ G_M^{p(n)} &= F_E^{p(n)} + F_M^{p(n)} \end{aligned} \quad (\text{G.4})$$

with $G_E^p(0) = 1$, $G_E^n(0) = 0$, $G_M^p(0) = 1 + \mu_p$ and $G_M^n(0) = \mu_n$ corresponding to proton and neutron charges and magnetic moments. Electron scattering experiments reveal that

G_E^p , G_M^p and G_M^n have the same q^2 dependence, which can be parametrized as

$$\frac{G_E^p(q^2)}{G_E^p(0)} = \frac{G_M^p(q^2)}{G_M^p(0)} = \frac{G_M^n(q^2)}{G_M^n(0)} = \left(1 - \frac{q^2}{M_V^2}\right)^{-2}. \quad (\text{G.5})$$

Also one finds $G_E^n(q^2) = 0$.

Let us now consider the axial vector form factors. One of the contributions to the pseudoscalar form factor comes from the one pion exchange diagram (analogous to the one of Fig. 4.1). Assuming that F_P is dominated by this contribution one gets

$$\frac{F_P(q^2)}{2M} = -2f_\pi \frac{f_{NN\pi}}{m_\pi} \frac{1}{q^2 - m_\pi^2} F_\pi(q^2). \quad (\text{G.6})$$

Then, substituting this result in the axial part of the hadronic current, and applying PCAC one finds

$$F_A(q^2) = 2f_\pi \frac{f_{NN\pi}}{m_\pi} F_\pi(q^2) \quad (\text{G.7})$$

The extrapolation of this relation to $m_\pi \neq 0$ leads to

$$F_P(q^2) = F_A(q^2) \frac{2M}{m_\pi^2 - q^2}. \quad (\text{G.8})$$

Moreover, since $F_\pi(0) \approx F_\pi(m_\pi^2) \equiv 1$

$$F_A(0) \equiv g_A = 2f_\pi \frac{f_{NN\pi}}{m_\pi}. \quad (\text{G.9})$$

We have actually derived the Goldberger-Treiman relation [19], which was introduced in Chapter 1, Eq. (1.38). The q^2 dependence of F_A is generally parametrized in a dipole form

$$\frac{F_A(q^2)}{F_A(0)} = \left(1 - \frac{q^2}{M_A^2}\right)^{-2} \quad (\text{G.10})$$

and the axial dipole mass M_A is determined from the experimental data.

The q^2 distribution reads

$$\frac{d\sigma}{dq^2} = \frac{1}{64\pi} \frac{1}{(s - M^2)^2} G^2 \cos \theta_c L_{\mu\nu} H^{\mu\nu}, \quad (\text{G.11})$$

where $L_{\mu\nu}$ is the standard leptonic tensor defined in Eq. (4.8) and $H^{\mu\nu}$ is

$$H^{\mu\nu} = \text{Tr} \left[(\not{p} + M) \tilde{A}^\mu (\not{p}' + M) A^\nu \right]. \quad (\text{G.12})$$

If the mass of final lepton can be neglected and in the limit of $q^2 = 0$, Eq. G.11 takes the simple form

$$\frac{d\sigma}{dq^2}(q^2 = 0) = ([F_A(0)]^2 + [F_1^V(0)]^2) \frac{1}{2\pi} G^2 \cos^2 \theta_c, \quad (\text{G.13})$$

where $F_1^V(0) = 1$ and $F_A(0) = 1.26$, which was used in Sec. 5.3.

Bibliography

- [1] R. Bilger et al., *Acta Phys. Pol.* 29 (1998) 2987.
- [2] M. Andersson et al., *Acta Phys. Pol.* 29 (1998) 2969.
- [3] F. Belleman et al., [nucl-ex/9812011](#).
- [4] L. Alvarez-Ruso, E. Oset, E. Hernández, *Nucl. Phys. A* 633 (1998) 519.
- [5] E. Hernández, E. Oset, [nucl-th/9808017](#).
- [6] E. Oset, M. J. Vicente Vacas, *Nucl. Phys. A* 446 (1985) 584.
- [7] E. Ferrari, *Nuovo Cimento* 30 (1963) 240.
- [8] L. G. Dakhno et al., *Sov. J. Nucl. Phys.* 37 (1983) 540.
- [9] D. C. Brunt, M. J. Clayton, B. A. Westwood, *Phys. Rev.* 187 (1969) 1856.
- [10] F. Shimizu et al., *Nucl. Phys. A* 386 (1982) 571.
- [11] J. Stepaniak, private communication.
- [12] A. Abdivaliev et al., *Nucl. Phys. B* 168 (1980) 385.
- [13] W. Brodowski et al., *Z. Phys. A* 355 (1996) 5.
- [14] F. Mandl, G. Shaw, *Quantum Field Theory* (Wiley-Interscience, 1984).
- [15] S. Weinberg, *Phys. Rev.* 166 (1968) 1568.
- [16] J. Gasser, M. E. Sainio, A. Švarc, *Nucl. Phys. B* 307 (1988) 779.
- [17] V. Bernard, N. Kaiser, U. G. Meissner, *Int. J. Mod. Phys. E* 4 (1995) 193.
- [18] C. Caso et al., *Eur. Phys. J C* 3 (1998) 1.
- [19] M. L. Goldberger, S. B. Treiman, *Phys. Rev.* 110 (1958) 1178.
- [20] M. G. Olsson, L. Turner, *Phys. Rev. Lett.* 20 (1968) 1127.

- [21] M. F. Jiang, D. S. Koltun, Phys. Rev. C 42 (1990) 2662.
- [22] R. Haag, Phys. Rev. 112 (1958) 669; S. Coleman, J. Wess, B. Zumino, Phys. Rev. 177 (1969) 2239; C. G. Callen, S. Coleman, J. Wess, B. Zumino, Phys. Rev. 177 (1969) 2247.
- [23] J. Schwinger, Phys. Lett. B 24 (1967) 473.
- [24] R. A. Arndt et al., Phys. Rev. D 20 (1979) 651.
- [25] M. G. Olsson, U. G. Meissner, N. Kaiser, V. Bernard, πN Newsletter 10 (1995) 201.
- [26] V. Bernard, N. Kaiser, U. G. Meissner, Nucl. Phys. A 619 (1997) 261.
- [27] V. Bernard, N. Kaiser, U. G. Meissner, Nucl. Phys. A 615 (1997) 483
- [28] R. Koch, Nucl. Phys. A 448 (1986) 707.
- [29] T. E. O. Ericson, W. Weise, Pions and Nuclei (Clarendon Press, Oxford, 1988).
- [30] R. Machleidt, K. Holinde, C. Elster, Phys. Rep. 149 (1987) 1.
- [31] M. B. Johnson et al., Phys. Rev. C 44 (1991) 2480.
- [32] D. Lohse, J. W. Durso, K. Holinde, J. Speth, Nucl. Phys. A 516 (1990) 513; Phys. Lett. B 234 (1990) 235.
- [33] S. Barshay, G. E. Brown, M. Rho, Phys. Rev. Lett. 32 (1974) 787.
- [34] E. Oset, H. Toki, W. Weise, Phys. Rep. 83 (1982) 282.
- [35] L. M. Nath, B. K. Bhattacharyya, Z. Phys. C 5 (1980) 9; M. G. Olsson, E. T. Osypowski, E. H. Monsay, Phys. Rev. D 17 (1978) 2938.
- [36] M. Benmerrouche, R. M. Davidson, N. C. Mukhopadhyay, Phys. Rev. C 39 (1989) 2339.
- [37] D. M. Manley, E. M. Saleski, Phys. Rev. D 45 (1992) 4002.
- [38] G. Höler, πN Newsletter 9 (1993) 1.
- [39] R. A. Arndt, I. I. Strakovsky, R. L. Workman, Phys. Rev. C 56 (1997) 577; Phys. Rev. C 53 (1996) 430
- [40] G. E. Brown, W. Weise, Phys. Rep. 22 (1975) 279.
- [41] F. Bonutti et al., Nucl. Phys. A 638 (1998) 729
- [42] M. B. Johnson, E. R. Siciliano, H. Toki, A. Wirzba, Phys. Rev. Lett. 52 (1984) 593.

- [43] T. S. Jensen, A. F. Miranda, Phys. Rev. C 55 (1997) 1039.
- [44] H. P. Mørch et al., Phys. Rev. Lett. 69 (1992) 1336.
- [45] J. A. Gomez Tejedor, E. Oset, Nucl. Phys. A 571 (1994) 667.
- [46] O. Jaekel et al., Nucl. Phys. A 511 (1990) 733.
- [47] V. Sossi et al., Nucl. Phys. A 548 (1992) 562.
- [48] V. Bernard, N. Kaiser, U. G. Meissner, Nucl. Phys. B 457 (1995) 147.
- [49] <http://pibeta.psi.ch/~pipin/Welcome.html>; E. Frlez, PhD Thesis, Los Alamos National Laboratory (1993) and references therein.
- [50] M. Ericson, T. E. O. Ericson, Ann. of Phys. 36 (1966) 323.
- [51] J. Speth, V. Klemt, J. Wambach, G. E. Brown, Nucl. Phys. A 343 (1980) 382; P. Ring, J. Speth, Nucl. Phys. A 235 (1974) 315.
- [52] A. Arima, Progr. Part. Nucl. Phys. 11 (1984) 53.
- [53] P. Fernández de Córdoba et al., Nucl. Phys. A 586 (1995) 586.
- [54] S. Hirenzaki, P. Fernández de Córdoba, E. Oset, Phys. Rev. C 53 (1996) 277.
- [55] R. D. Amado in Modern three hadron physics, edited by A. W. Thomas (Springer, Berlin, 1997).
- [56] M. G. Olsson, Nucl. Phys. B 78 (1974) 55.
- [57] R. C. Carrasco, E. Oset, Nucl. Phys. A 536 (1992) 445.
- [58] C. Wilkin, [nucl-th/9810047](#); J. Haidenbauer, C. Hanhart, J. Speth, Acta Phys. Polon. B 27 (1996) 2893.
- [59] T. Johansson, Nucl. Phys. A 631 (1998) 331c; H. O. Meyer, Acta Phys. Polon. B 26 (1995) 553; H. Machner et al., Acta Phys. Polon. B 24 (1994) 1555.
- [60] V. Bernard, N. Kaiser, U. G. Meissner, Eur. Phys. J. A 4 (1999) 259.
- [61] A. Sibirtsev, W. Cassing, [nucl-th/9904046](#).
- [62] R. Shyam, U. Mosel, Phys. Lett. B 426 (1998) 1.
- [63] C. Hanhart, K. Nakayama, [nucl-th/9809059](#)
- [64] J. A. Niskanen, [nucl-th/9812029](#)
- [65] M. L. Goldberger, K. M. Watson, Collision Theory (Wiley, 1964).

- [66] M. Lacombe et al., Phys. Rev. C 21 (1980) 861; Phys. Lett. B 101 (1981) 139.
- [67] J. M. Eisenberg, W. Greiner, Microscopic Theory of the Nucleus (North-Holland, 1972).
- [68] L. Mathelitsch, W. Plessas, W. Schweiger, Phys. Rev. C 26 (1982) 65.
- [69] W. Schweiger, W. Plessas, L. P. Kok, H. van Haeringen, Phys. Rev. C 27 (1983) 515.
- [70] V. G. J. Stoks, R. A. M. Klomp, M. C. M Rentmeester, J. J. de Swart, Phys. Rev. C 48 (1993) 792.; <http://nn-online.sci.kun.nl/>
- [71] Y. Yamaguchi, Phys. Rev. 95 (1954) 1628
- [72] J. P. Naisse, Nucl. Phys. A 278 (1977) 506.
- [73] A. Abashian, N. E. Booth, K. M. Crowe, Phys. Rev. Lett. 5 (1960) 258.
- [74] I. Bar-Nir et al., Nucl. Phys. B 54 (1973) 17.
- [75] F. Plouin et al., Nucl. Phys. A 302 (1978) 413.
- [76] J. H. Hall, T. A. Murray, L. Riddiford, Nucl. Phys. B 12 (1969) 573.
- [77] J. Banaigs et al., Nucl. Phys. B 105 (1976) 52.
- [78] C. L. Hollas et al., Phys. Rev. C 25 (1982) 2614.
- [79] C. Bargholtz et al., Phys. Lett. B 398 (1997) 264.
- [80] J. C. Anjos, D. Levy, A. Santoro, Nuovo Cimento 33 A (1976) 23.
- [81] I. Bar-Nir, T. Risser, M. D. Shuster, Nucl. Phys. B 87 (1975) 109.
- [82] C. A. Mosbacher, F. Osterfeld, [nucl-th/9903064](http://arxiv.org/abs/nucl-th/9903064).
- [83] G. Kalbermann, J. M. Eisenberg, Nucl. Phys. A 426 (1984) 599.
- [84] A. Gardestig, G. Faldt, C. Wilkin, [nucl-th/9812004](http://arxiv.org/abs/nucl-th/9812004); Phys. Lett. B 421 (1998) 41
- [85] F. Plouin, P. Fleury, C. Wilkin, Phys. Rev. Lett. 65 (1990) 690.
- [86] L. Alvarez-Ruso, Phys. Lett. B 452 (1999) 207.
- [87] L. Hulthen, M. Sugawara, Handbuch der Physik, vol. 39 (Springer Verlag, Berlin, 1957).
- [88] S. Sawada et al., Nucl. Phys. A 615 (1997) 277.

- [89] Proceedings of the International Workshop on N^* Physics, edited by T.S.H. Lee, W. Roberts (World Scientific, Singapore, 1997); Proceedings of the 7th International Conference on the Structure of Baryons, edited by B. F. Gibson, P. D. Barnes, J. B. McClelland, W. Weise (World Scientific, Singapore, 1996).
- [90] P. Stoler, Phys. Rep. 226 (1993) 103.
- [91] T. Kitagaki et al., Phys. Rev. D 42 (1990) 1331.
- [92] T. Kitagaki et al., Phys. Rev. D 34 (1986) 2554.
- [93] G. M. Radecky et al., Phys. Rev. D 25 (1982) 1161.
- [94] P. Allen, Nucl. Phys. B 176 (1980) 269.
- [95] S. J. Barish et al., Phys. Rev. D 19 (1979) 2521.
- [96] L. A. Ahrens et al., Phys. Rev. D 35 (1987) 785; L. A. Ahrens, Phys. Rev. D 34 (1986) 75.
- [97] M. J. Musolf et al., Phys. Rep. 239 (1994) 1.
- [98] L. M. Nath, K. Schilcher, M. Kretzschmar, Phys. Rev. D 25 (1982) 2300; D. R. T. Jones, S. T. Petcov, Phys. Lett. B 91 (1980) 137.
- [99] V. D. Burkert, in Perspectives in the Structure of Hadronic Systems, edited by M. N. Harakeh et al. (Plenum Press, New York, 1994).
- [100] N. C. Mukhopadhyay et al., Nucl. Phys. A 633 (1998) 481.
- [101] H. W. Hammer, D. Drechsel, Z. Phys. A 353 (1995) 321.
- [102] S. P. Wells et al., TJNAF proposal E-97-104.
- [103] T. R. Hemmert, B. R. Holstein, N. C. Mukhopadhyay, Phys. Rev. D 51 (1995) 158.
- [104] R. M. Davidson, N. C. Mukhopadhyay, R. S. Wittman, Phys. Rev. D 43 (1991) 71; Phys. Rev. Lett. 56 (1986) 804; R. M. Davidson, N. C. Mukhopadhyay, Phys. Rev. D 42 (1990) 20; S. Capstick, G. Karl, Phys. Rev. D 41 (1990) 2767; T. D. Cohen, W. Bronioski, Phys. Rev. D 34 (1986) 3472; J. M. Eisenberg, Phys. Rev. D 28 (1983) 71; N. Isgur, G. Karl, R. Koniuk, Phys. Rev. D 25 (1982) 2394.
- [105] L. Alvarez-Ruso, S. K. Singh, M. J. Vicente, Phys. Rev. C 57 (1998) 2693.
- [106] W. Y. P. Hwang, E. M. Henley, L. S. Kisslinger, Phys. Rev. C 35 (1987) 1359.
- [107] J. Liu, N. C. Mukhopadhyay, L. Zhang, Phys. Rev. C 52 (1995) 158.
- [108] S. L. Adler, Phys. Rev. D 12 (1975) 2644; Ann. Phys. (N.Y.) 50 (1968) 189.

- [109] G. L. Fogli, G. Nardulli, Nucl. Phys. B 160 (1979) 116; P. Zucker, Phys. Rev. D 4 (1971) 3350; J. Bijtebier, Nucl. Phys. B 21 (1970) 158.
- [110] P. A. Schreiner and F. von Hippel, Nucl. Phys. B 58 (1973) 333.
- [111] C. H. Llewellyn Smith, Phys. Rep. 3 (1972) 261.
- [112] S. K. Singh, M. J. Vicente Vacas, E. Oset, Phys. Lett. B 416 (1997) 23.
- [113] R. P. Feynman, M. Gell-Mann, Phys. Rev. 109 (1958) 193.
- [114] Th. Wilbois, P. Wilhelm, H. Arenhovel, Phys. Rev. C 57 (1998) 295; R. Beck, Phys. Rev. Lett. 78 (1997) 606; A. J. Buchmann, E. Hernández, A. Faessler, Phys. Rev. C 55 (1997) 448; O. Hanstein, D. Drechsel, L. Tiator, Phys. Lett. B 385 (1996) 45; M. Benmerouche, N. C. Mukhopadhyay, Phys. Rev. D 46 (1992) 101.
- [115] E. D. Cummings, P. H. Bucksbaum, Weak interactions of leptons and quarks (Cambridge University Press, Cambridge, 1983).
- [116] R. C. E. Devenish, T. S. Eisenschitz, J. G. Korner, Phys. Rev. D 14 (1976) 3063.
- [117] C. Gerhardt, Z. Phys. C 4 (1980) 311.
- [118] Z. Li, V. Burkert and Z. Li, Phys. Rev. D 46 (1992) 70.
- [119] F. Cardarelli et al., Phys. Lett. B 397 (1997) 13; F. Cano, P. González, Phys. Lett. B 431 (1998) 270.
- [120] L. A. Copley, G. Karl, E. Obryk, Phys. Lett. B 29 (1969) 117; F. E. Close, An Introduction to Quarks and Partons (Academic Press, London, 1979), Chap. 7.
- [121] H. J. Weber, Phys. Rev. C 41 (1990) 2783.
- [122] L. Alvarez-Ruso, S. K. Singh, M. J. Vicente, Phys. Rev. C 59 (1999) 3386.
- [123] S. K. Singh, H. Arenhoevel, Z. Phys. A 324 (1986) 347; S. L. Mintz, Phys. Rev. D 13 (1976) 637; R. Tarrach, P. Pascual, Nuovo Cimento A 18 (1973) 760; J. Bernabeu, P. Pascual, Nuovo Cimento A 10 (1972) 61; S. K. Singh, Nucl. Phys. B 36 (1971) 419.
- [124] C. H. Albright, L. S. Liu, Phys. Rev. 78 (1965) B78.
- [125] F. Ravndal, Nuovo Cimento A 18 (1973) 385.
- [126] G. Korner, T. Kobayashi, C. Avilez, Phys. Rev. D 18 (1972) 3178.
- [127] A. Le Yaouanc, Phys. Rev. D 15 (1977) 2447.
- [128] M. Beyer Habilitation Dissertation (University of Rostock, Germany, 1997).

- [129] A. Bartl, K. Wittman, N. Paver, C. Verzegnassi, *Nuovo Cimento A* 45 (1978) 457; A. Bartl, N. Paver, C. Verzegnassi, S. Petrarca, *Lett. Nuovo Cimento* 18 (1977) 588.
- [130] S. J. Barish et al., *Phys. Rev. D* 16 (1977) 3103.
- [131] E. Amaldi, S. Fubini and G. Furlan, *Pion electroproduction*, Vol. 83 of Springer Tracts in Modern Physics (Springer, Berlin, 1977).
- [132] J. C. Nacher and E. Oset, [nucl-th/9804006](https://arxiv.org/abs/nucl-th/9804006).
- [133] L. Elouadrhiri et al., CEBAF Experiment E-94-005.
- [134] R. Guardiola, in *Microscopic Quantum Many Body Theories and their Applications*, edited by J. Navarro, A. Polls (Springer, Berlin, 1998).
- [135] L. Salcedo, PhD Thesis.

Agradecimientos

En primer lugar quisiera agradecer a mis padres por el apoyo que me han dado a lo largo de todos estos años, por haber priorizado mis aspiraciones vocacionales aun en los peores momentos. Ante tanto sacrificio, esta modesta tesis se queda pequeña.

Dar con Eulogio fue una una verdadera suerte. Sin el apoyo que me brindó y la confianza que depositó en mí desde el primer momento, mis deseos de seguir investigando se habrían quedado en eso, en deseos. Sus conocimientos y experiencia han sido fundamentales para llevar adelante este trabajo. Ha puesto mucho de algo que no me sobra: optimismo.

A Manolo le he dado la vara de modo continuo durante estos años con problemas mayores y menores, de física, informática y hasta burocracia. He contado siempre con su colaboración y su disposición en mis innumerables irrupciones en su despacho (incluso cuando tenía que preparar clases). Ni que decir de las muchas ocasiones en que hemos charlado de tantas cosas con alguna cerveza de por medio. Aun ha sabiendas de lo que se van a reir algunos lectores de estos Agradecimientos y arriesgándose a suceder comparaciones no deseadas tengo que decir que Manolo ha sido mucho más que un director de tesis.

Llega el turno a los *brothers in arms*, compañeros de despacho y de departamento, los que ya se han ido (de postdocs o consultores) y los que aun quedan; a todos muchas gracias por haber contribuido a crear un ambiente excelente, que contrasta con el que se respira en otras esferas. Esto no habría sido lo mismo sin Sergio, Eugenio, Marina, Pbueno, el gordo, Gabi, ... y tantos otros, con los que he compartido buenos momentos dentro y fuera del departamento, y Oscar, que nos puso a dar seminarios *for pedestrians* y a comer galletas. No me olvido de los usuarios habituales del *Bierwinkel*: Concha, Nuria, el minino y otros ya mencionados y no repetidos to avoid double counting, ni de la *fracción química*: Ileana, Rosa. También quería agradecer a Cristina y Assum por su compañía en lo que se ha venido a denominar como *aquell agost plujós del 96*, que para mí no lo fue tanto.

Last but not least, I would like to thank my collaborators Pedro, Eli, Singh for their help. I have also benefited from discussions with A. P. Krutenkova, H. Clement, W. Brodowski, C. Wilkin, G. Falldt, A. Gardestig.

